ISAS - INTERNATIONAL SCHOOL FOR ADVANCED STUDIES

BIOPHYSICAL STUDIES ON DNA–DRUG INTERACTION: CHARACTERIZATION OF A RUTHENIUM ANTITUMOR COMPLEX WITH DNA

Thesis Submitted for the Degree of
PhilosophiæDoctor

Candidate: Federico Fogolari

Supervisors: Dr. G. Esposito

Prof. P. Viglino

Academic Year 1991/92

SISSA - SCUOLA INTERNAZIONALE SUPERIORE DI STUDI AVANZATI
TRIESTE
Strada Costiera 11

TRIESTE

BIOPHYSICAL STUDIES ON DNA–DRUG INTERACTION: CHARACTERIZATION OF A RUTHENIUM ANTITUMOR COMPLEX WITH DNA

Thesis Submitted for the Degree of
PhilosophiæDoctor

Candidate: Federico Fogolari

Supervisors: Dr. G. Esposito

Prof. P. Viglino

Academic Year 1991/92

Contents

Foreword

The present thesis consists of three different sections which reflect most of the work I've been doing in the last four years, and the changes in the research interests as well.

The polyelectrolyte section originated from a collaboration with the University of Trieste (prof. G. Manzini, S. Paoletti, F. Quadrifoglio) and is based on the following papers:

– Manzini, G., Xodo, L. E., Fogolari, F., and Quadrifoglio, F., Secondary structure effects on the interaction of different polynucleotides with Ca^{2+}, (1990) Biopolymers **30**, 325-333.

– Paoletti, S., Benegas, J., Cesaro, C., Manzini, G., Fogolari, F., Crescenzi, V., Limiting–laws of polyelectrolyte solutions. Ionic distribution in mixed-valency counterions systems. I: The model. (1991) Biophysical Chemistry, **41**, 73-80.

– Fogolari, F., Manzini, G., Quadrifoglio, F., Polyelectrolytes in mixed salts: Scatchard plots obtained by means of Poisson-Boltzmann calculations, (1992) Biophysical Chemistry, **43**, 213-219.

The NMR section represents work done in collaboration with the C.N.R. of Milano (Prof. L. Zetta, Dr. H. Molinari and Dr. M. Pegna) (SQC–NOESY experiments), with the EMBL of Heidelberg (Dr. A. Pastore and Dr. M. Pfuhl) (discussion of possible 3D experiments) and work done in the University of Udine (Prof. Viglino and Dr. G. Esposito) and is based on the following papers:

– Esposito, G., Fogolari, F., Molinari, H., Pegna M., and Zetta, L., Proton strong coupling in heteronuclear systems. Theoretical and experimental evaluation in quantitative analysis of SQC–NOESY spectra of biopolymers, Journal of Magnetic Resonance, in press (April 1993).

– Fogolari, F., Esposito, G., Cauci S., and Viglino, P., Evaluation of J coupling constants from peak amplitudes in total correlated spectroscopy, Journal of Magnetic Resonance, in press (March 1993).

The last section (DNA-Ruthenium complex) is part of a long term project started in Udine few years ago in collaboration with Dr. S. Cauci and F. Quadrifoglio, and is based on the paper:

– Esposito, G., Cauci, S., Fogolari, F., Alessio, E., Scocchi, M., Quadrifoglio, F., and Viglino, P., NMR structural characterization of the reaction product between d(GpG) and the octahedral antitumor complex *trans*-$RuCl_2(DMSO)_4$, (1992) Biochemistry, **31**, 7094-7103.

Chapter 1

INTRODUCTION

In the last 50 years a great number of drugs, both of syntethic and natural origin have been devised, tested and used in the treatment of tumors. Most of these interact with single steps of cellular differentiation, exerting a toxyc effect on the cell (De Vita et al., 1985). The efficacy of such drugs is judged by the selectivity of the interaction, the presence or absence of side effects and general tolerability. Though such a low–level approach may seem rather crude and simplistic, and higher level concepts are desirable, up to now the only possible therapy is still based on drug interference with specific mechanism of the tumor cell life.

The class of antitumor drugs which interact directly with DNA, binding covalently or not, are particularly appealing to the biophysicist, since a complete description, at the molecular level, of the mechanism of action is possible, and, in turn, it can provide guidelines for the rational design of further and possibly more efficient drugs.

In order to understand ligand–DNA interaction it should be kept in mind that polyelectrolyte effects are likely to affect heavily the process, be the ligand charged or neutral, since the linear charge of DNA is expected to change upon binding with a consequent free energy change, dependent on solvent conditions (Anderson and Record, 1982). Current polyelectrolyte theories can provide a rationale as to the general aspects of the interaction.

However, if a description at the molecular level is required, one has to resort to techniques more suited to the purpose. X–Ray crystallography and NMR spectroscopy have proven to be useful in the last decades, being the information they can give complementary under many respects. The biological and medical aspects of the anticancer therapy will be not treated here, since they are investigated by biologists and physicians with much more suitable tools. The main concerns of this thesis will be focused on:

a) the physical principles which rule the interaction of a polyelectrolyte with a charged ligand, though some of the conclusions can be readily extended to neutral ligands;

b) the detailed theoretical analysis of some existing NMR experiments, in order to gain more information from experimental data, and the design of a novel experimental scheme;

c) the characterization of the three dimensional structure of a specific anti-tumor drug–DNA complex, which is currently under clinical test, and which shows some interesting structural features, compared to other compounds belonging to the same class of drugs.

Chapter 2

POLYELECTROLYTE ASPECTS OF DRUG–DNA INTERACTIONS

It is well known that nucleic acids behave as rather strong polyacids, so that these polymers can be regarded under every respect as highly charged polyelectrolytes. The interaction of this class of macromolecules with small electrolytes as well as with any ligand which bears a net charge, or modifies the linear charge density on the polymer is expected to strongly depend on the solvent ionic conditions. When dealing with charged ligands we must distinguish "territorially"bound molecules from those which are site bound to the polyion. Indeed an uneven distribution is expected to occurr around the polymer which can modulate the experimental observation, as described later.

The different polyelectrolyte theories devised so far have rationalized the observed behaviour on a thermodynamic ground.

An approach proposed by Manning (1969, 1978) has reached widespread popularity, notwithstanding the approximations and simplifications it is based upon, its main advantage being simplicity and physical insight. The polyelectrolyte is modelled here as a linear chain of fixed point charges, which, at sufficiently high density induce counterion condensation. To take into consideration the entropic aspects of binding these counterions are assumed to be condensed in a finite volume around the polyelectrolyte. Minimization of the analytic expression for the free energy gives the fraction of counterions condensed per unit charge on the polymer. A new derivation of the model is given in the following section.

The Poisson–Boltzmann theory combines the Poisson equation relating the electrostatic potential to the local charge density, with the Boltzmann statistical particle distribution in an inhomogeneous potential field. Though the derivation of the equation dates back to the fifties, only recently extimations of the accuracy of the prediction have been performed. This approach suffers mainly from the difficulty of correlating ionic distributions with measurable quantities. In the following a procedure to derive "bound"and "free"concentrations is given.

2.1 MANNING'S MODEL: IONIC DISTRIBUTION IN MIXED VALENCY COUNTERIONS SYSTEMS

Within the framework of counterion condensation (CC) theory of linear polyelectrolytes, the problem of the description of the system in the case of counterions of different valency was already tackled. Both approximate (Manning, 1978) and more exact (Manning, 1984; Friedman and Manning, 1984; Satoh et al., 1988; Riedl et al., 1989) expressions have been reported, and comparison with experimental results was performed (Iwasa, 1977; Record et al., 1978; Paulsen et al., 1988; Manzini et al., 1990). Still, it doesn't appear useless to reconsider the problem and look for new formalisms, especially if aiming at avoiding limited experimental conditions (e. g. excess of one of the counterion species, high ionic strength, etc.).

The scope of this section is to derive the model and to discuss its main features and implications; a detailed comparison with experimental data is still to be performed.

The procedure which will be followed is to write suitable expressions for the different terms contributing to the (excess) free energy of a system consisting of a very dilute solution of a linear polyelectrolyte of known charge density in the presence of variable amounts of counterions of different valency.

Since this model suffers from many approximations and assumptions which will be discussed later, the extension of the model to ligands which can also site bind to the polymer will be not performed. A complete description has been given, for a slightly different model, by Friedman and Manning (1984), including also multiple site exclusion which describes completely, but most probably not much quantitatively, the anticooperative behaviour of the binding curves. The schematization and the assumptions involved in the model, while giving a sound physical explanation of the interaction, are likely to impair any attempt to push too far quantitatively the predictions of the model.

The model

The real polyelectrolyte chain is idealized as a chain of point charges uniformly spaced along a wire, supposed to be of infinite length to neglect end effects. The average distance between the projections of the charges onto the polymer axis is taken as the inter charge space b (expressed in Å, 1 Å= 0.1 nm): the ensuing dimensionless parameter ξ is defined as $\xi = l_B/b$ where l_B is the Bjerrum length (expressed in Å) ($l_B = q^2/\epsilon k_B T$ where q is the proton charge in e.s.u., ϵ is the relative dielectric constant of the solvent, k_B is the Boltzmann constant and T is the temperature). For simplicity, two types of counterions, i and j with valency z_i and z_j, respectively, will be considered taking $z_i = 1$ with no loss of generality. Coions stemming from added simple electrolytes may be present: for simplicity, they will be assumed to be the same for both types of added simple salts. The treatment of the so called "chemical model", as firstly proposed by Manning (1977), will be followed much in the same way as recently reported, e. g. for the derivation of the $\Delta \mathrm{pK}_a(\alpha)$ of linear weak polyacids (Cesàro et al., 1986). The reduced molar (rm) free energy of the system (i. e. the free energy divided by $n_p k_B T$ where n_p is the number of moles of monomeric unit of the polymer) may be written as the sum of two main contributions, a purely electrostatic term, g^{el}, and a rm free energy of mixing of mobile species, g^{mix}.

$$g^{ion} = g^{el} + g^{mix} \tag{2.1.1}$$

The reference state is provided by a solution at the same temperature, pressure and in the solvent) containing the same type and concentration of charges of all kinds including those fixed on the polyelectrolyte, where the latter, however, are assumed to be simple mobile ions instead ("iso–ionic strength condition"). The expression for g^{el} is the "classical"one given by the CC theory:

$$g^{el} = -\xi q_{eff}^2 \ln(1 - \exp(-K_D b)) \tag{2.1.2}$$

where q_{eff} is the net, "effective"charge on each ionized site on the polyelectrolyte and K_D is the reciprocal of the Debye length (i. e. $K_D^2 = \frac{N_{Av}}{1000} 8\pi l_B I$, where $I = \frac{1}{2}\sum_i c_i z_i^2$ with c_i the molar concentration of the ion i of valence z_i). Obviously in the case of no condensation

$$q_{eff} = q_{str} \tag{2.1.3}$$

q_{str} is the value of the fixed charge on the polyion: in what follows it will be assumed equal to unity. In the presence of condensation in systems containing counterions of only one valency z_i, q_{eff} is given by

$$q_{eff} = q_{str}(1 - rz_i) \tag{2.1.4}$$

where r is the (molar) fraction of condensed counterions which will effectively shield a fraction rz_i of fixed charge and whose numerical value stems from the condition of stability of the system at infinite dilution (limiting law condition) (Manning, 1969)

$$r = z_i^{-1}(1 - 1/z_i\xi) \tag{2.1.5}$$

as will be seen clearly in a while.

The derivation of the relevant equations describing the counterion condensation proposed hereafter is much similar to the one given by Manning in (1978), being now not restricted anymore to the case of excess monovalent salts. The condensation will be assumed to be dependent on all the ionic species present in the system, removing in this way the requirement of one excess ionic species. The fraction of condensed counterions, r, is given by:

$$r = r_i + r_j = r(x_i + x_j) \tag{2.1.6}$$

with x_i the ratio of the condensed (denoted by apices b) molar concentration of species i normalized to the total molar concentration of condensed species i. e.

$$x_i = \frac{c_i^b}{c_j^b + c_i^b} \tag{2.1.7}$$

and

$$x_j = 1 - x_i \tag{2.1.8}$$

Equation (2.1.4) will take the form:

$$q_{eff} = q_{str}(1 - rz_i - rz_j) \tag{2.1.9}$$

For the commonly encountered case $z_i = |q_{str}| = 1$ and $z_j = 2$, and making use of eqs. one has:

$$q_{eff} = 1 - r(x_1 + 2(1 - x_1)) = 1 - r(2 - x_1) \tag{2.1.10}$$

In general the final form of g^{el} will then be:

$$g^{el} = -\xi(1 - r(z_j - x_i(z_j - z_i))\ln(1 - \exp(-K_D b)) \tag{2.1.11}$$

For g^{mix} the contributions of the different mobile species to the change of entropy of mixing will be considered:

$$g^{mix} = g_i^{cond} + g_j^{cond} + g_i^{free} + g_j^{free} + g_i^{coions} + g_j^{solv} \tag{2.1.12}$$

The following relations will hold:

$$g_i^{cond} = rx_i \ln \frac{rx_i}{(1 + R_i)V_p C_p} \tag{2.1.13}$$

$$g_j^{cond} = r(1 - x_i) \ln \frac{r(1 - x_i)}{R_j V_p C_p} \tag{2.1.14}$$

$$g_i^{free} = (1 + R_i - rx_i) \ln \frac{(1 + R_i - rx_i)}{1 + R_i(1 - V_p C_p)} \tag{2.1.15}$$

$$g_j^{free} = (R_j - r(1 - x_i)) \ln \frac{(R_j - r(1 - x_i))}{R_j(1 - V_p C_p)} \tag{2.1.16}$$

$$g_i^{coions} = (R_i + z_j R_j) \ln \frac{1}{1 - V_p C_p} \tag{2.1.17}$$

$$g_j^{solv} = r_i + r_j = r \tag{2.1.18}$$

where R_i and R_j stand for the molar ratios between the concentrations of the i–th (e. g. univalent) and j–th (e.g. bivalent) species, respectively, and and that of the polymer in monomeric units; V_p is the molar volume of the condensed phase, expressed in liters per mole of fixed charge.

The system is therefore characterized by the usual variables (temperature, pressure, volume and concentration of solutes), the two independent variables r and x_i and V_p which is a physical parameter of the system whose value is not numerically determined as yet. For the determination of r and x_i it was found convenient to resort to the free energy minimization procedure followed by Manning (1977); according to such established procedure the r– and x_i–derivatives of V_p will be neglected, and the minimization conditions will read:

$$\frac{\partial g^{ion}}{\partial r} = 0 \tag{2.1.19}$$

and

$$\frac{\partial g^{ion}}{\partial x_i} = 0 \tag{2.1.20}$$

The following expression is derived from eqs. (2.1.11)–(2.1.18) by performing the operation of eq. (2.1.19)

$$2\xi(1 - r(z_j - x_i(z_j - z_i)))(z_j - x_i(z_j - z_i))\ln(1 - \exp(-K_D b)) +$$

$$+\frac{(\xi(1 - r(z_j - x_i(z_j - z_i)))^2(x_i(z_i^2 - z_j^2) + z_j^2)K_D b)}{2DEN(\exp(K_D b) - 1)} +$$

$$+x_i \ln \frac{r x_i(1 - V_p C_p)}{(R_i + 1 - r x_i)V_p C_p} +$$

$$+(1 - x_i)\ln \frac{(1 - x_i)r(1 - V_p C_p)}{(R_j - r(1 - x_i)V_p C_p)} + 1 = 0 \tag{2.1.21}$$

where:

$$DEN = 1 + R_i(z_i^2 + z_i) + R_j(z_j^2 + z_j) - r(x_i(z_i^2 - z_j^2) + z_j^2)$$

Upon linearization of the exponential for the condition $K_D b \ll 1$, eq. can be rearranged into the form:

$$2\xi(1 - r(z_j - x_i(z_j - z_i)))(z_j - x_i(z_j - z_i))\ln(K_D b) +$$

$$+\frac{(\xi(1 - r(z_j - x_i(z_j - z_i)))^2(x_i(z_i^2 - z_j^2) + z_j^2))}{2DEN} +$$

$$+x_i \ln \frac{r x_i(1 - V_p C_p)}{(R_i + 1 - r x_i)V_p C_p} +$$

$$+(1 - x_i)\ln \frac{(1 - x_i)r(1 - V_p C_p)}{(R_j - r(1 - x_i)V_p C_p)} + 1 = 0 \tag{2.1.22}$$

Exploring the condition of infinite dilution, much in the same way as in the original "limiting law"treatment (Manning, 1969), it is immediately revealed that the system will be unstable for all r and x_i values not obeying to the following condition:

$$\xi(1 - r(z_j - x_i(z_j - z_i)))(z_j - x_i(z_j - z_i)) = 1 \tag{2.1.23}$$

Equation (2.1.23) implies that, at equilibrium, for the limiting conditions:

$$r = \frac{1}{z_i x_i + z_j(1-x_i)} \left(1 - \frac{1}{\xi(z_i x_i + z_j(1-x_i))}\right) \tag{2.1.24}$$

It can be easily verified that, at equilibrium, reduces to eq. (2.1.5) for the two extreme cases of purely monovalent ($x_i = 1$) and purely divalent counterions ($x_j = 1$). Similarly eq. (2.1.20) leads to:

$$2\xi(1 - r(z_j - x_i(z_j - z_i)))(z_j - z_i)\ln(1 - \exp(-K_D b)) +$$

$$+\frac{(\xi(1 - r(z_j - x_i(z_j - z_i)))^2((z_i^2 - z_j^2) + z_j^2)K_D b)}{2DEN(\exp(K_D b) - 1)} +$$

$$+\ln\frac{x_i(R_j - r(1-x_i))}{(1-x_i)(R_i + 1 - r x_i)} = 0 \tag{2.1.25}$$

The system at equilibrium is then uniquely determined, regarding the two variables r and x_i, by the simultaneous solution of eqs. (2.1.24) and (2.1.25). Once the values of r and x_i (which are not functionally dependent on V_p) have been calculated, the value of the parameter V_p can be determined from the numerical solution of eq. (2.1.22).

Before proceeding further on commenting the results, it seems convenient to present some remarks on the procedure followed hitherto:

(i) the system has been schematized as a chain of point charges uniformly spaced along a wire, surrounded by a "condensation volume"assumed to exist sharply distinct from the bulk volume. The volume excluded by the polymer is neglected as well as the discreteness of the charges;

(ii) the condensation volume is assumed to be, to a large extent, independent of the variables of the system, and finite in the limit of infinite dilution, which is, strictly speaking, true only when the system is viewed under a Debye length scale, as proven by Gueron and Weisbuch (1980);

(iii) eqs. (2.1.24) and (2.1.25) which are derived under limiting conditions are assumed to hold true also at finite concentrations of the polymer.

Results and discussion

For practical reasons, the more frequently encountered case of a mixture of mono– and divalent counterions (i. e. $z_i = 1$ and $z_j = 2$) will be considered in the following calculations.

The dependence of r, r_1 and r_2 on x_1 is reported in Figure 2.1.1 for $\xi = 1.5$.

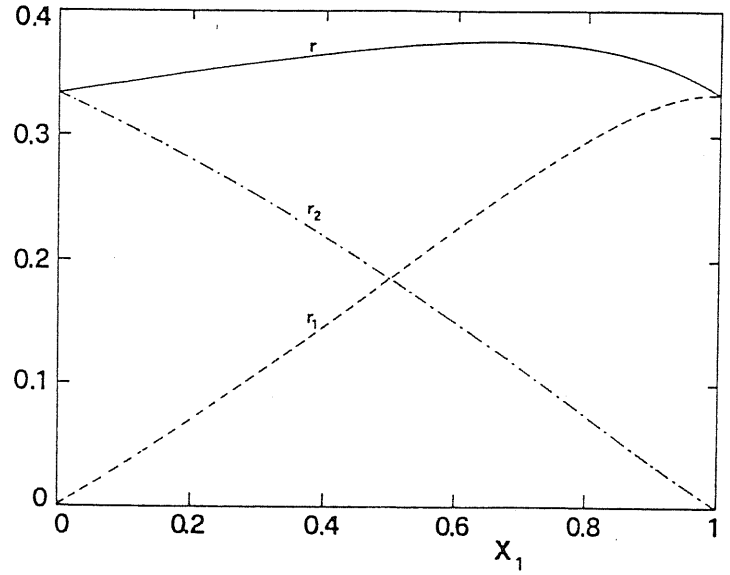

Figure 2.1.1 Dependence of r (solid line), r_1 (broken line) and r_2 (dashed line) on x_1 for ξ=1.5, according to eq. (2.1.24).

The plot, which is the graphical representation of eq. (2.1.24) is independent of the composition variables c_p, R_i and R_j, etc. Clearly non–linear relations hold among those quantities which render non-obvious any prediction. Such a behaviour is even more clearly shown by the curves of Figure 2.1.2 which display r, r_1 and r_2 as a function of x_1 for $\xi = 1$.

The last case reveals a striking behaviour: the fraction of condensed monovalent counterions, r_1, attains the value of zero as predicted by the original CC theory only for the limiting condition of the "one type of counterion"case, i. e. $x_1 = 1$ (and $R_2 = 0$, "pure monovalent"), and for $x_1 = 0$ ("pure divalent"). For all finite values of R_2 the value of r_1 is non–zero, indicating that the condensation of

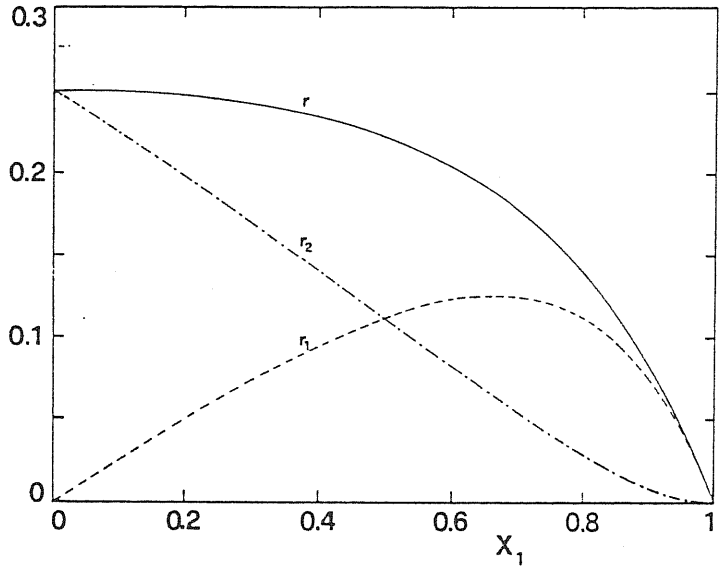

Figure 2.1.2 Dependence of r (solid line), r_1 (broken line) and r_2 (dashed line) on x_1 for ξ=1, according to eq. (2.1.24).

divalent ions, which is required anyway by CC theory for $\xi > 0.5$, also induces the condensation of monovalent ions. This result is illustrated by the plots given in Figures 2.1.3 and 2.1.4, showing the dependence on ξ of r, r_1, r_2 and x_1 for the experimentally interesting cases of excess monovalent salt, and equal concentrations of mono– and divalent salts, respectively.

The plots for the extreme case of excess divalent counterions (not shown) reduce to those predicted by the original CC theory, under the same assumptions, inasmuch as all condensed counterions are divalent.

Generally, the functional dependence of r, r_1 and r_2 on ξ will in turn depend on the complicate interplay of c_p, R_1 and R_2 values given by eqs. (2.1.24) and (2.1.25). However, the most intersting feature of the model is that there is the presence of a unique value of ξ, ξ_{crit}, marking the onset of the condensation of *all* counterions. The numerical value of ξ_{crit} does in turn depend on the chemical composition of the system (i. e. c_p, R_1, R_2), varying continuosly from $\xi = 1$ for the "pure monovalent"case to $\xi = 0.5$ for the "pure divalent"system.

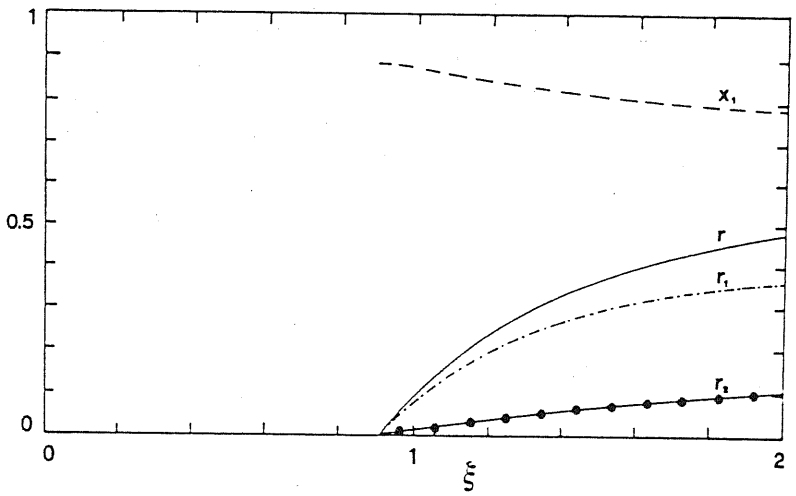

Figure 2.1.3 Dependence of x_1 (broken line), r (solid line), r_1 (dashed line) and r_2 (filled circles line) on ξ for C_p=0.0001 M, R_1=100 and R_2=1.

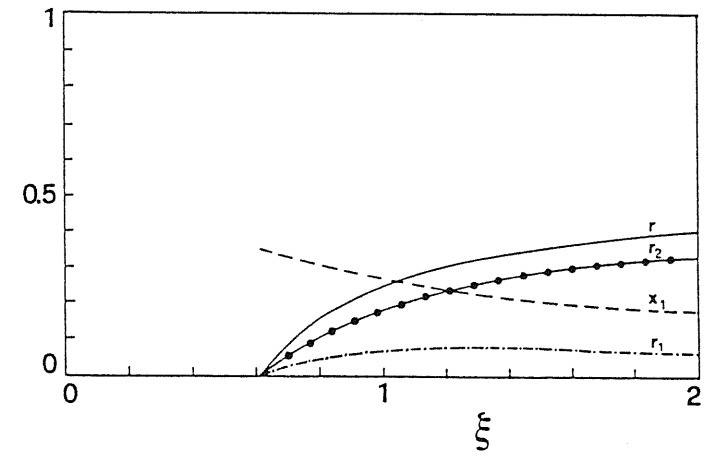

Figure 2.1.4 Dependence of x_1 (broken line), r (solid line), r_1 (dashed line) and r_2 (filled circles line) on ξ for C_p=0.0001 M, R_1=R_2=10.

The plot of Figure 2.1.5 helps to visualize the interesting effect of the "induced condensation"of monovalent ions by the presence of divalent ions (i. e. $R_2 > 0$). As can be seen r_2 always increases with R_2: the increase is monotonous, reaching the limiting value $r_2 = r = 1/2(1 - (2\xi)^{-1})$ for $R_2 \to \infty$.

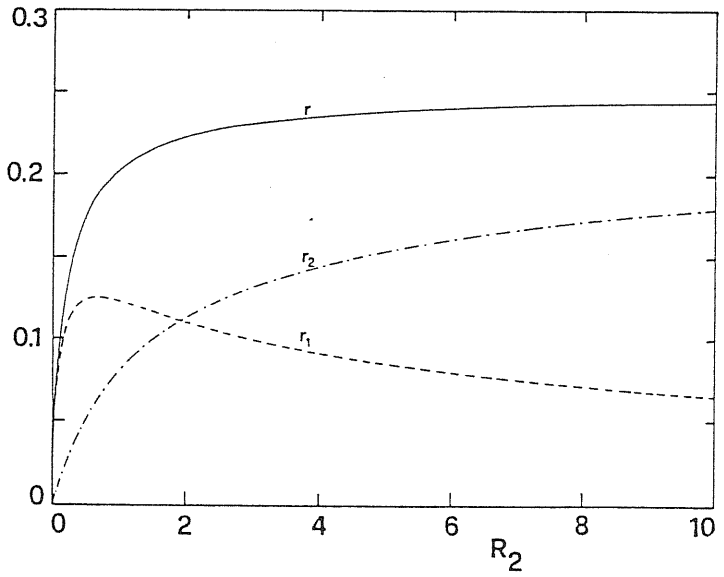

Figure 2.1.5 Dependence of r (solid line), r_1 (broken line) and r_2 (dashed line) on R_2 for ξ=1 , C_p=0.0001 and R_1=10.

A sharp increase with a maximum is shown by r_1 for small values of R_2, followed by a monotonous decrease, which may be more readily understood on an intuitive basis. For the given conditions and for the sample case $R_2 = 0.5$ (i. e. R_2 much higher than the r_2 value predicted by Manning's limiting law, $r_2 = 0.25$), the model predicts that the r_2 fraction is as low as 0.05 whereas r_1 is 0.124. Therefore, monovalent counterions not only condense for $\xi = 1$, but, for this particular case, they account for 70% of the total number of condensed ions! (Similar behaviour is found for ξ values ranging from 0.5 to 1).

Concepts like "competition"between i–valent and j–valent ions, which are widely spread in the scientific literature may conveniently be addressed by considering the relative extent of "binding"(i. e. condensation) of the species for given boundary conditions. The value of the fraction of condensed divalent ions, r_2, has

been the master variable in the Scatchard plots which have been calculated and reported in Figures 2.1.6 to 2.1.9 for monovalent/divalent mixtures and for different experimental conditions. In the plots the ordinate is K_2 ($K_2 = r_2/((R_2 - r_2)c_p)$) and the abscissa is r_2. For $\xi = 4.2$, i. e. for the charge density of B–DNA, Figure 2.1.6 shows that for low r_2 values the affinity of the chain for a divalent ion is rather high, but it rapidly decreases upon increasing the amount of bound ions.

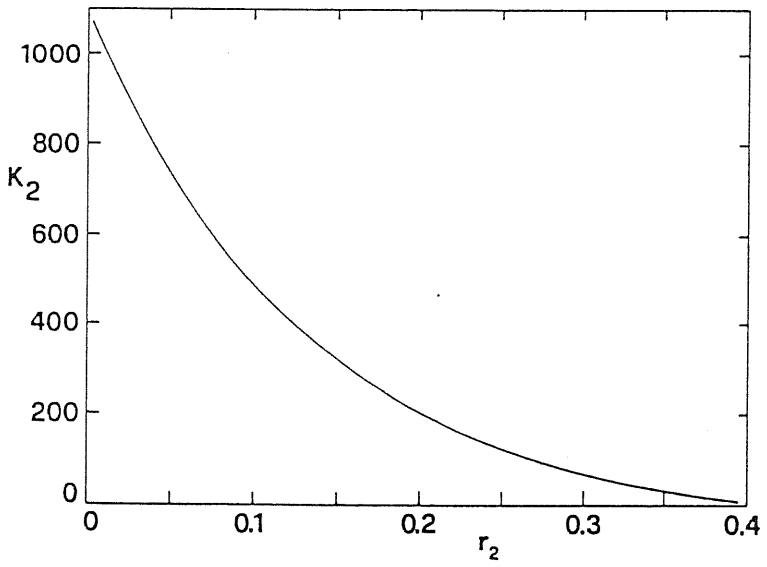

Figure 2.1.6 Scatchard plot (K_2=$r_2/((R_2-r_2)c_p)$ vs. r_2) for ξ=4.2, C_p=0.001 M and R_1=50.

Such a behaviour could be interpreted as a "negative cooperativity"or anti–cooperativity but it is nevertheless the simple outcome of the interplay of electrostatic interactions between ions of different valency. Similarly (and still for $\xi = 4.2$), in Figure 2.1.7 the higher level of binding of divalent ions in the presence of a lower concentration of the monovalent ones shows that interionic competition has to appear in polyelectrolyte systems simply as a result of the role of the entropy of mixing without the need to invoke any "specific"interaction.

The results of Figure 2.1.8, obtained for $\xi = 2$, confirm the above mentioned trend, but with a smaller effect due to the reduced electrostatic interaction.

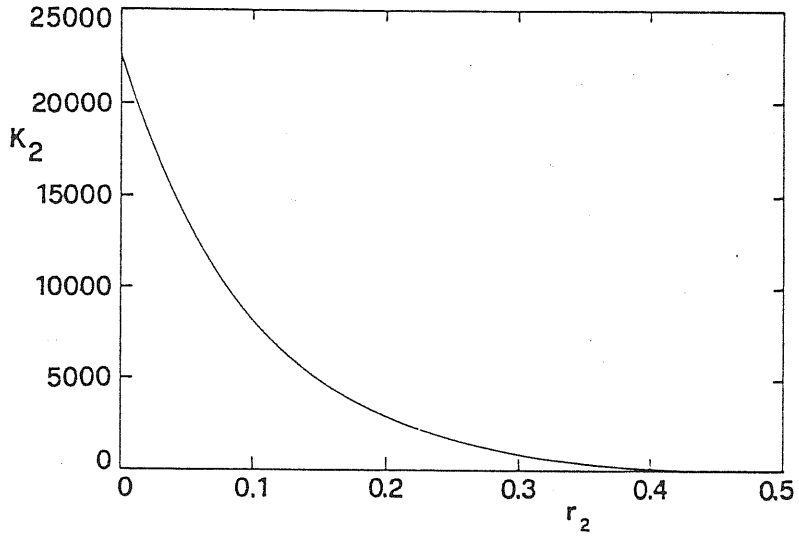

Figure 2.1.7 Scatchard plot ($K_2=r_2/((R_2-r_2)c_p)$ vs. r_2) for ξ=4.2, C_p=0.001 M and R_1=10.

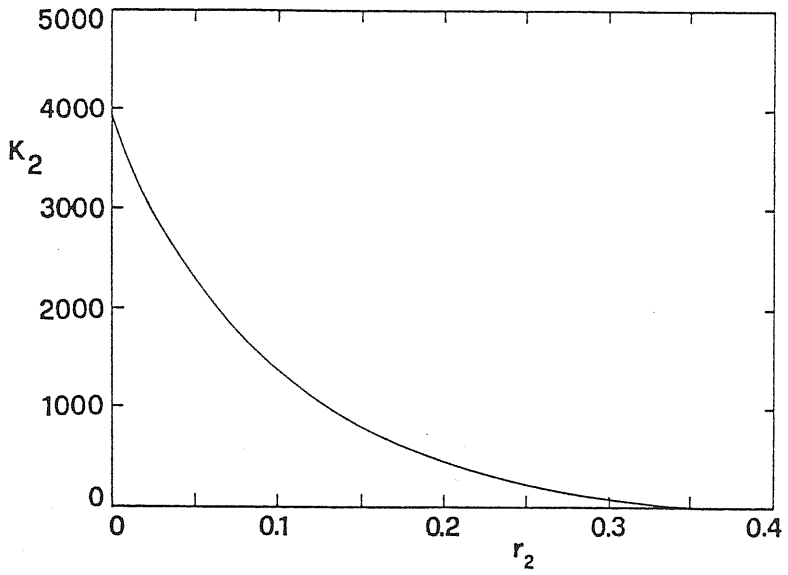

Figure 2.1.8 Scatchard plot ($K_2=r_2/((R_2-r_2)c_p)$ vs. r_2) for ξ=2, C_p=0.001 M and R_1=10.

Even lower binding levels are reported in Figure 2.1.9 for $\xi = 1$; in this case,

however, a new effect comes into play, that is: a marked *positive* cooperativity is shown at low binding levels, which was totally undetectable in the curves calculated for higher values of the linear charge density.

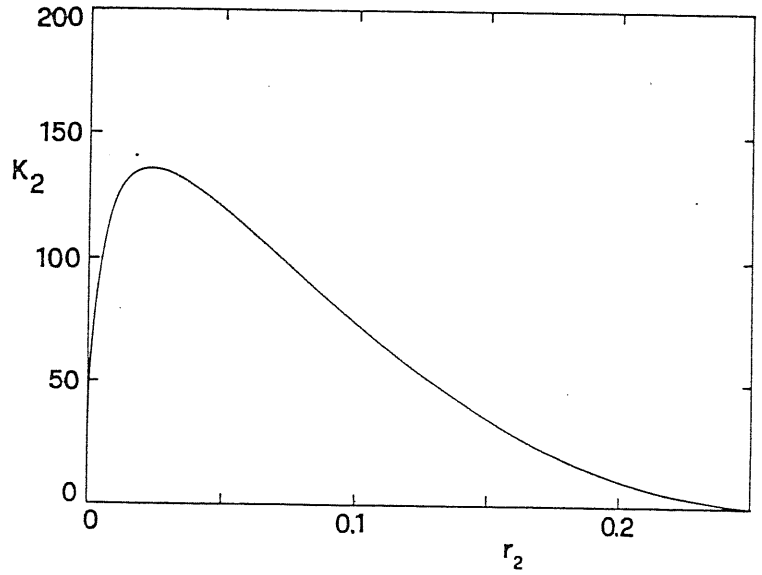

Figure 2.1.9 Scatchard plot ($K_2=r_2/((R_2-r_2)c_p)$ vs. r_2) for $\xi=1$, $C_p=0.001$ M and $R_1=50$.

This result is clearly much more striking than the former ones: no a priori argument might have suggested that, for small values of ξ and low binding levels, the polymer affinity for the more charged ions would be rather low and that further binding would increase an "intrinsic"affinity in a rather marked (positive) cooperative way.

The apparent oddity of the previous result obviously makes it even more compelling to resort to the calculation of experimental quantities to test the theoretical predictions. An extensive comparison between the predictions of the present approach and the experimental data is beyond the scope of this section; still, to derive some indication from the experimental literature was necessary to assess the general trend of the theoretical predictions. It was already known that careful determinations of the single–ion activity coefficient of Cu(II) ions ($\gamma_{Cu^{2+}}$) in the presence of different carboxylates in various conditions all have shown the presence

of a behavior of ($\gamma_{Cu^{2+}}$) strongly similar to the positive cooperativity of Figure 2.1.8. This has prompted us to derive the proper expression for γ_j from the free energy expression of eqs.

$$\ln \gamma_j = \frac{-\xi(1 - r(z_j - x_i(z_j - z_i)))^2 K_D b z_j^2}{2(\exp(K_D b) - 1)DEN} + \ln \frac{R_j - r(1 - x_i)}{R_j(1 - V_p C_p)} \qquad (2.1.26)$$

The calculated curves of γ_2 for given system conditions are reported in Figure 2.1.10. The "positive cooperativity"behavior of the Scatchard plot of Figure 2.1.8 has found an exact counterpart in the behavior of $\gamma_2(R_2)$.

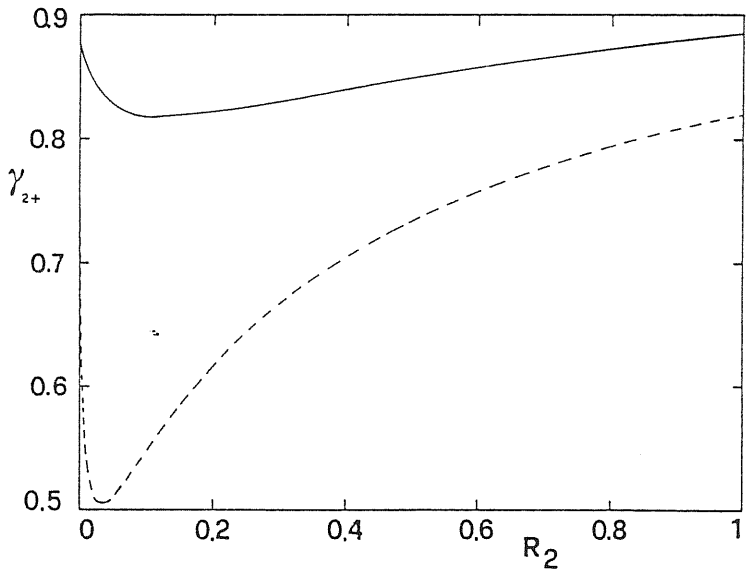

Figure 2.1.10 Dependence of the activity coefficient of divalent counterions (eq. (2.1.26)) on R_2 for ξ=1. C_p=0.001 M, R_1=10 (upper curve) and C_p=0.0001 M, R_1=10 (lower curve).

Changes in the experimental conditions (e. g. polymer concentration, ionic strength, etc.) qualitatively affect the calculated curves in the same way as the experimental ones (Reisenhofer et al., 1984). The approach presented above to polyelectrolyte theory, correct some inconsistencies existing in the original presentation by Manning (1978), but follows basically the same guidelines. It can be therefore extended readily to the case where site–binding and not only counterion condensation is observed in the very same way Friedman and Manning (1984) did

for the original theory. This will not be done here and the reader is referred to their detailed work.

2.2 – POLYELECTROLYTES IN MIXED SALTS: SCATCHARD PLOTS OBTAINED BY MEANS OF POISSON–BOLTZMANN CALCULATIONS

Introduction

The application of Poisson–Boltzmann (P–B) equation to the polyelectrolytes has been known for a long time (Alfrey et al., 1951; Fuoss et al., 1951; Katchalsky, 1971) although only in the last decade an explicit evaluation of the approximations involved has been put forward (Fixman, 1979; Ramanathan and Woodbury, 1982). It is generally acknowledged that the P–B equation is a valid tool to study polyelectrolytes. The solution of this equation provides information on the spatial behaviour of the electrostatic potential and therefore on the spatial distribution of the ions around the polymer. In most cases this property cannot be experimentally investigated. Indeed the quantities usually available from experiments are the concentrations of "bound" and "free" ions where a "bound" and a "free" state have to be defined (and are often defined by the experimental procedure).

In the past years a physically based schematization which has proved useful in understanding the behaviour of polyelectrolytes has been proposed by Manning (1978) (see previous chapter). In his model the two above mentioned states are postulated to exist sharply distinct. This assumption has raised several criticisms among researchers, since such a clearcut separation of "free"and "bound"states is not predicted by the P–B theory. Nevertheless Manning's model allowed to compare experimental "binding"data with theoretical predictions.

Within the frame of P–B theory measurable quantities as the activity coefficients of the counterions in the presence of the polyelectrolyte and in the presence or absence of added salts have been compared with the results of the calculations. In particular the cell model (vide infra) firstly proposed by Alfrey et al. (1951) and Fuoss et al. (1951) was often employed and the quantities measured in solution were compared in several cases with the analogous quantities calculated from the model at the cell surface. However useful concepts that rely on the existence of two different molecular states, like that of binding constant, appear to fall present-

ly outside the P–B theory. In spite of what *is not* free ion concentration, be it site binding, condensation, P–B accumulation, etc.), it should be noted that the outcome of experiments like equilibrium dialysis, potentiometry, dye indicators, etc. can always be expressed operatively (independently of their physical counterparts at the molecular level) in terms of "free"ion concentration (what is directly measured) and of its difference from the total concentration employed, i. e. the apparent "bound"concentration.

The aims of the present chapter are:

(i) to give a definition of these quantities, i. e. the "free"and "bound"ion concentrations, in the limiting case of infinite dilution, within the framework of P–B theory;

(ii) to see how far this definition can be retained also at finite concentrations of the polymer;

(iii) to calculate the extent of binding according to this definition (divalent cations, for which a large amount of experimental data are available, will be used as a test case) in the presence of monovalent supporting salts for different values of salts concentrations, polyelectrolyte reduced charge density and radius;

(iiii) investigate, within this framework, the polyelectrolyte effects on site–binding.

Theory

The P–B approach to polyelectrolytes problem has been the subject of several research papers (Alfrey et al., 1951; Fuoss et al., 1951; Katchalsky, 1971; Gueron and Weisbuch, 1980) We will summarize only the basic theory here.

The polyelectrolyte is modelled as an infinite uniformly charged cylinder. We will consider explicitly the case where a uni–univalent (A^+ and B^-) supporting salt, a biuni–divalent (C^{2+} and B^-) salt and a negatively charged polyelectrolyte are present. We can write the Poisson equation for the electrostatic potential U (the changes of the dielectric constant of water (ϵ) around the cylinder are not taken into account):

$$\nabla^2 U = \frac{-4\pi}{\epsilon} \sum_i \rho_i \qquad \text{in c.g.s. units} \tag{2.2.1}$$

(where ρ_i is the charge density due to the i–th ionic species) and the Boltzmann equation for the distribution of any ionic species under the limiting condition of infinite dilution of the polymer:

$$\rho_i = \frac{N_{Av}}{1000} c_i^{\infty} z_i q \exp(\frac{-z_i q U}{kT}) \tag{2.2.2}$$

where c_i^{∞} is the molar concentration of the i–th species at an infinite distance from the cylinder (in the following we will write for simplicity c_1 instead of c_1^{∞}, since we are not interested in the distribution of the monovalent counterions around the polyelectrolyte). Substituting the second equation into the first one we get the so–called P–B equation which can be further specified, in the present case, introducing the following reduced quantities:

$$\psi = \frac{qU}{kT} \tag{2.2.3a}$$

$$x = k_D r = (\frac{8\pi q^2}{\epsilon kT} \frac{N_{Av}}{1000} c_1)^{\frac{1}{2}} r \tag{2.2.3b}$$

$$R = \frac{c_2^{\infty}}{c_1} \tag{2.2.3c}$$

so that the P–B equation becomes:

$$\psi'' = \frac{-\psi'}{x} + \sinh\psi + R[\exp(\psi) - \exp(-2\psi)] \tag{2.2.4}$$

The boundary conditions are given by the electric field at the surface of the polymer:

$$\psi'(x_0) = \frac{2\xi}{x_0} \tag{2.2.4a}$$

where x_0 is the reduced radius of the cylinder (i.e. $x_0 = k_D r_0$), and

$$\xi = \frac{q^2}{\epsilon kTb} \tag{2.2.4b}$$

and by the request that the potential becomes 0 at infinite distance from the polymer:

$$\psi \longrightarrow 0 \qquad \text{as} \qquad x_0 \longrightarrow \infty \tag{2.2.5}$$

The P–B equation can be solved numerically (the Runge–Kutta–Nyström fourth order method was actually used, Kreyszig (1972)) by a trial and error procedure. A

tentative value for the potential at the polymer surface is chosen, then the solution is computed at increasing distances until either the potential or its derivative changes sign, then the starting value is set to be halfway between the last two trial values which exhibited opposite divergencies. This procedure is applied until the new starting value differs from the old one by less than one hundred thousandth of its value. The integration step size is decreased until no further changes are found in the solution. A strict convergence criterion has the advantage that the region where the integration procedure stops is already in the range where both (the exact) ψ and ψ' are close to 0, since we do not expect a slight modification of the starting value to bring up a large variation at the point of zero–crossing.

Once the solution is obtained a natural way to define the "bound" concentration of divalent counterions per polymer charge is to take the integral of its excess with respect to c_2^∞ over the (infinite) volume pertaining to a monomer:

$$\frac{c_2^b}{c_p} = \frac{N_{Av}}{1000}\int_{r_0}^{\infty} 2\pi r c_2^\infty(\exp(-2\psi)-1)b\,dr \qquad (2.2.6)$$

In practice, since in the presence of finite ionic strength the solution decays rather fastly, it is necessary to take the integral up to few Debye lengths. The integration procedure usually stops between 4 and 6 Debye lengths and the value of ψ is 0 within few hundredths. (Remember the asymptotic behaviour of the solution:

$$\psi \longrightarrow \frac{\exp(-cx)}{\sqrt{x}}; \qquad c \geq 1 \qquad \text{as} \qquad x \longrightarrow \infty \qquad (2.2.7)$$

Obviously, in the most natural way under the same limiting conditions the "free" concentration is assumed to be the bulk concentration. It is worth to comment on the above definitions. When we consider the cell model in the limit $D \longrightarrow \infty$ (D is the radius of the cell) the perturbation effect on the local concentration due to the polymer is negligible over most of the cell volume. The concentration of the divalent counterion would be c_2^∞ over the whole volume except for a very limited portion of it around the polyelectrolyte where the electrostatic potential fastly decays to zero. When $D \longrightarrow \infty$ any measurement would sample therefore regions where c_2 is equal to c_2^∞. However, the total number of divalent counterions present in the cell pertaining to a single monomer would be different from:

$$\frac{N_{Av}}{1000}\int_{r_0}^{D} 2\pi r c_2^\infty b\,dr \qquad (2.2.8)$$

being equal to:

$$\frac{N_{Av}}{1000}\int_{r_0}^{D} 2\pi r c_2^{\infty}(\exp(-2\psi))b\mathrm{d}r \qquad (2.2.9)$$

While both these quantities diverge as $D \longrightarrow \infty$ their difference remains finite and is defined in eq. (2.2.6) as (c_2^b/c_p) since the same difference expresses the number of apparently bound counterions per unit charge. Though not assuming two real different states these definitions are able to match exactly under this limiting condition what would be measured as "free"and "bound"concentrations in several experiments like equilibrium dialysis, or potentiometric measurements, in the absence of any hypothesis on the process involved. For the sake of clarity we have compared in a pictorial way the present definitions with those of Manning in Figure 2.2.1.

With these definitions we can calculate points in a Scatchard plot for several different situations. Scatchard variables (Cantor and Schimmel, 1980) are defined, as usual, in the following way:

$$\frac{c_2^b}{c_p} = r_2 \qquad \frac{r_2}{c_2^f} = K_2 \qquad (2.2.10)$$

A plot of K_2 vs. r_2 leads to a straightforward visualization of the extent and of the possible cooperativity of the interaction.

Results and discussion

We have extensively calculated Scatchard plots for various values of ξ, r_0 and c_1 at 25 °C; we show here only few of these plots (Figure 2.2.2) while we give an exhaustive table (Table 2.2.I) of values of K_2^0, i.e. the value of K_2 for $r_2 = 0$.

The dependence of this constant on ξ and r_0 is illustrated in Figures 2.2.3 and 2.2.4; as can be easily gleaned by the figures K_2^0 does not depend too heavily on these parameters therefore we suspect that the often observed change of affinity following intramolecular conformational transitions involving only minor changes in the radius and reduced charge of the polymer (as is the case, for instance, of the B–Z transition in DNA) cannot be explained within this approach.

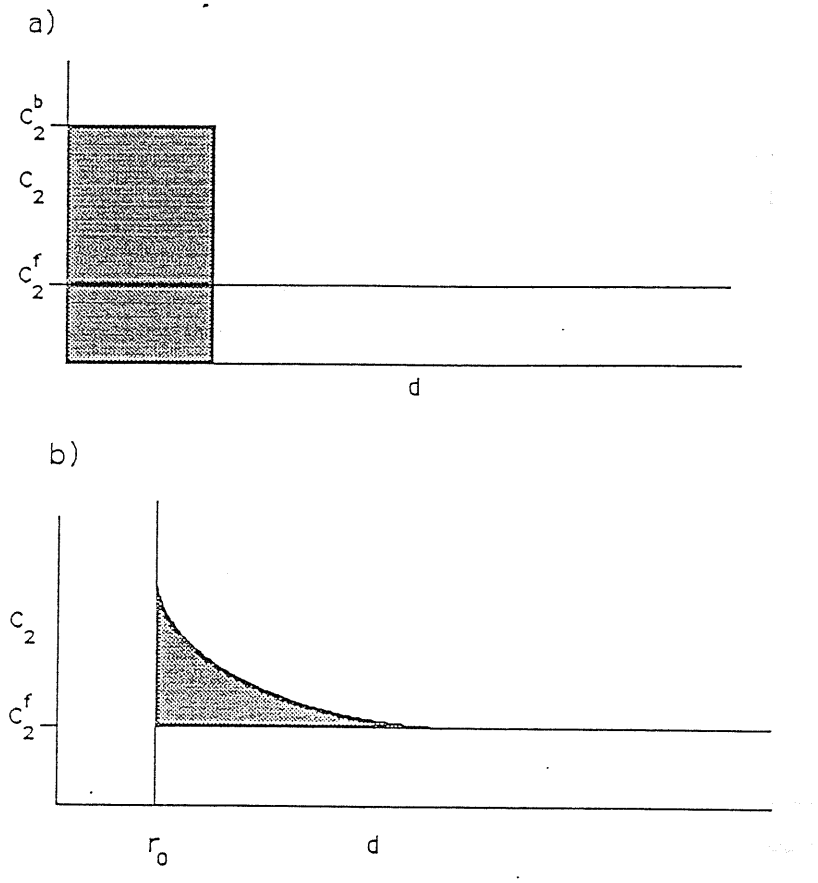

Figure 2.2.1 Pictorial representation of (a) Manning's definition of "free"divalent counterion concentration and (b) the present one. c_2 is plotted against d which is the distance from the polymer. In both cases the integral (over the whole volume competing to one monomer) represents the number of "bound"ions per unit charge on the polymer.

This does not mean that the mere electrostatics cannot account for the transition since, as already mentioned the global free energy change (including monovalent counterions and coions contributions) should be calculated. There is instead a marked dependency on the ionic strength and the equation given by Manning (1978),

$$\frac{\mathrm{d}\log K_2}{\mathrm{d}\log c_1} = -2 \tag{2.2.11}$$

in the present case, describes very well the results obtained for high values of

ξ	$r_0 = 5$	$r_0 = 6$	$r_0 = 8$	$r_0 = 10$	$r_0 = 11$	c_1
1	24.20	22.13	19.48	17.76	17.19	0.1
1	105.8	94.63	80.87	72.27	69.08	0.0316
1	495.8	434.1	357.3	311.1	294.3	0.01
1	2493.2	2142.5	1699.0	1438.0	1344.3	0.0032
1	13470	11300	8658.7	7126.1	6579.6	0.001
1	367174	315768	244049	198132	181129	0.0001
2	72.48	58.48	43.31	35.10	32.34	0.1
2	488.4	379.2	259.9	199.8	179.4	0.0316
2	3673.0	2761.9	1795.2	1308.7	1148.0	0.01
2	29949	22039	13735	9661	8341.8	0.0032
2	255756	185654	112939	77284	66008	0.001
2	$1.95{\cdot}10^7$	$1.40{\cdot}10^7$	8340282	5600920	4731378	0.0001
3	182.7	137.8	90.66	67.46	59.83	0.1
3	1501.2	1099.0	684.5	482.0	417.2	0.0316
3	13196	9487.6	5696.2	3875.7	3299.1	0.01
3	121260	86164	50609	33756	28410	0.0032
3	1136665	803650	466139	306630	256661	0.001
3	$1.17{\cdot}10^8$	$7.95\cdot10^7$	$4.37{\cdot}10^7$	$2.79{\cdot}10^7$	$2.31{\cdot}10^7$	0.0001
4	371.6	271.4	168.4	118.6	102.7	0.1
4	3324.4	2375.4	1416.3	960.2	816.1	0.0316
4	30891	21863	12761	8451.2	7103.0	0.01
4	295853	207938	119737	78305	65442	0.0032
4	2862643	2003492	1145063	743612	618806	0.001
4	$3.57{\cdot}10^8$	$2.33{\cdot}10^8$	$1.22\cdot10^8$	$7.56{\cdot}10^7$	$6.19{\cdot}10^7$	0.0001
5	647.3	464.8	279.2	190.7	162.7	0.1
5	6034.4	4272.4	2492.2	1655.7	1392.1	0.0316
5	57599	40476	23295	15241	12729	0.01
5	560498	392485	224036	145220	120868	0.0032
5	5512631	3843783	2180080	1406133	1167827	0.001
5	$7.99{\cdot}10^8$	$5.11{\cdot}10^8$	$2.58{\cdot}10^8$	$1.56{\cdot}10^8$	$1.26{\cdot}10^8$	0.0001

Table 3.2.I Values of the constant K_2^0 as a function of the reduced charge density ξ, radius (in Å) and molar concentration of the supporting salt.

ξ (Figure 2.2.5). However, care must be used since K_2^0, which, in Manning's approach, dependent only on ξ, is found to depend also on r_0 and is different from Manning's calculated values for cases like B–DNA ($\xi = 4.2$ and $r_0 = 10$ Å), Z–DNA ($\xi = 3.9$ and $r_0 = 9$Å) and A–RNA ($\xi = 5.1$ and $r_0 = 11$ Å).

Moreover a straightforward manipulation of the formulae leads to the following

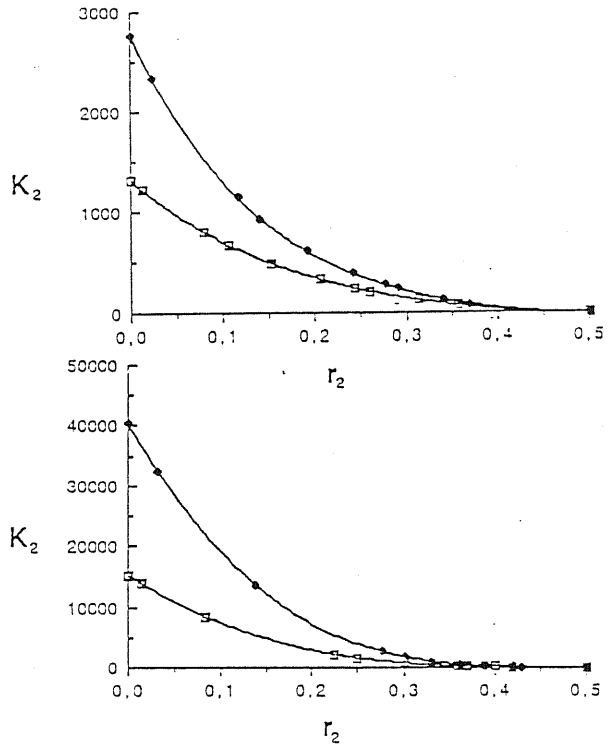

Figure 2.2.2 Scatchard plots obtained for c_1=0.01 M and ξ=2 (top) and ξ=5 (bottom). The higher curves refer to r_0=6 Åand the lower ones to r_0=10 Å.

"scaling" equations for the Scatchard variables:

$$r_2 = f(R, \xi, x_0) \qquad (2.2.12a)$$

$$K_2 = \frac{1}{c_1} g(R, \xi, x_0) \qquad (2.2.12b)$$

Though we will discuss in a while the retainability of the results under non–limiting conditions, it is worth being mentioned that the predicted absolute levels of binding agree satisfactorily with experimental data obtained previously in our laboratory (Ruggiero et al., 1987; Manzini et al., 1990; see Figure 2.2.6).

We have discussed so far the limiting case of infinite dilution; we are left with three questions. First of all, how does a finite concentration of the polyelectrolyte affect the solution, i. e. which is the effect of moving the boundary condition from infinity to a finite distance corresponding to the radius of a cell enclosing the polyelectrolyte. The answer is straightforward: nothing will happen as long as the cell radius is maintained in a range where the PB equation solution is sufficiently close to 0, i. e. at least 4 or 5 Debye lengths away from the center of

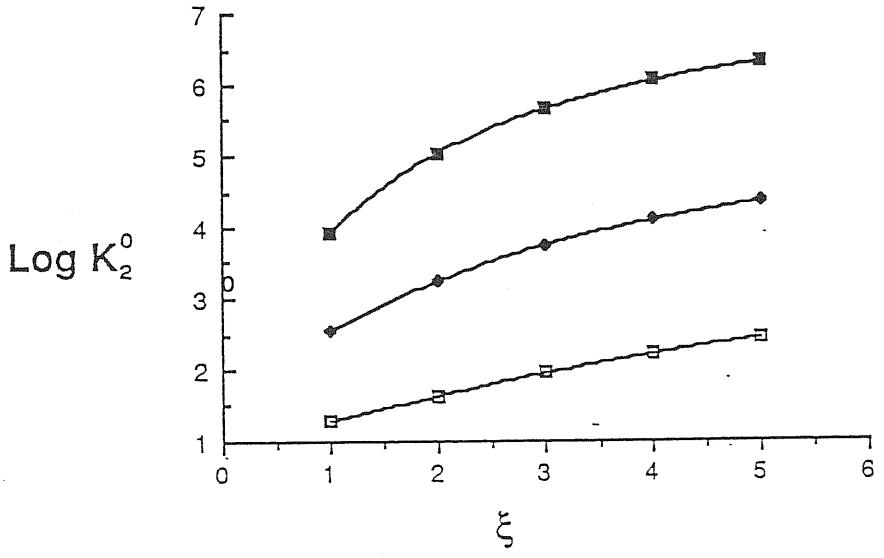

Figure 2.2.3 The decimal logarithm of the constant K_2^0 plotted against the reduced charged density ξ for the case of r_0=8 Åand, starting from the lower curve, c_1=0.1 M, c_1=0.01 M and c_1=0.001M.

the cylinder (for the case of B–DNA this corresponds roughly to concentrations in the range of 20 mM at 10 mM ionic strength). The second and more subtle point regards the adherence of the formal definition of "bound" and "free" counterion concentrations to the experimentally obtainable quantities and this has to do with the experimental procedure used. In cases where a measure of free ions involves sampling regions not too near to the polyelectrolyte, as for equilibrium dyalisis and potentiometric measurements, this adherence is fulfilled. On the contrary this is not the case of quadrupolar N.M.R. measurements where a more restrictive definition of "bound" ions has to be used (and has actually been used (Bleam et al., 1983; Braunlin et al. 1987)). However, we think that having a reference for the extent of binding due to the electrostatics can help in discriminating among different types of interaction.

The third question left is what kind of free energy is associated to the (equilibrium) constant K_2. We can imagine to have two baths (I and II) containing only mixed salts with the same concentration of AB but with an excess concentration of CB_2 on side I. We can measure a ΔG for the divalent cation, neglecting

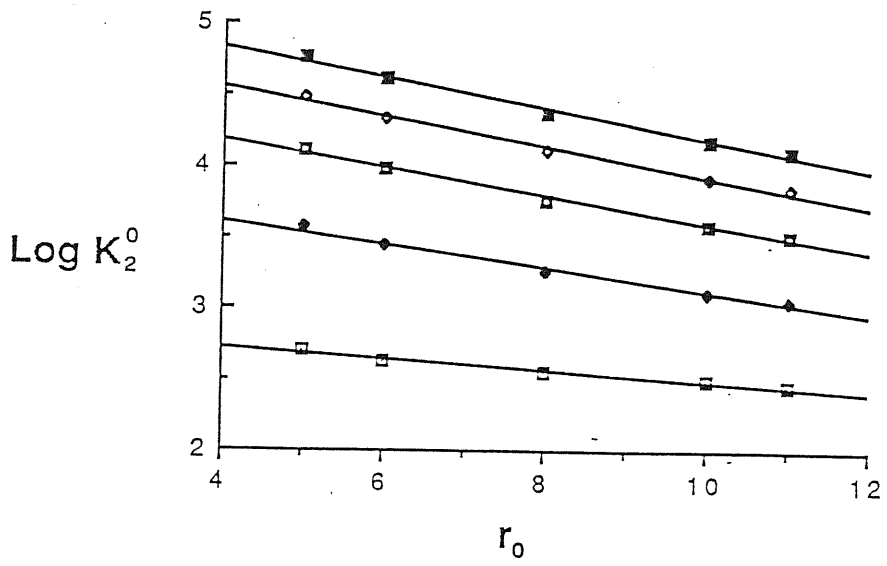

Figure 2.2.4 The decimal logarithm of the constant K_2^0 plotted against the radius of the polymer for different reduced charged densities (ξ is 1,2,3,4 and 5 starting from the lower curve) and for the case of c_1=0.01 M.

activity coefficients, through the usual equation:

$$\Delta G = -RT\ln\frac{c_2^I}{c_2^{II}} \tag{2.2.13}$$

We add now the charged polymer into bath I at a concentraton c_p such that what has been defined as free divalent concentration is equal to c_2^{II}. If we measure ΔG we find it equal to 0 so that we can recast the previous expression in terms of K_2 and c_p:

$$\Delta G = -RT\ln(1 + K_2 c_p) \tag{2.2.14}$$

and, since for most experimental situations $K_2 c_p \gg 1$, we can also write:

$$\Delta G = -RT\ln(K_2 c_p) \tag{2.2.15}$$

It is now clear that we can associate to K_2 the free energy change for one mole of divalent cation in the interaction with one monomole of polymer in the process described above.

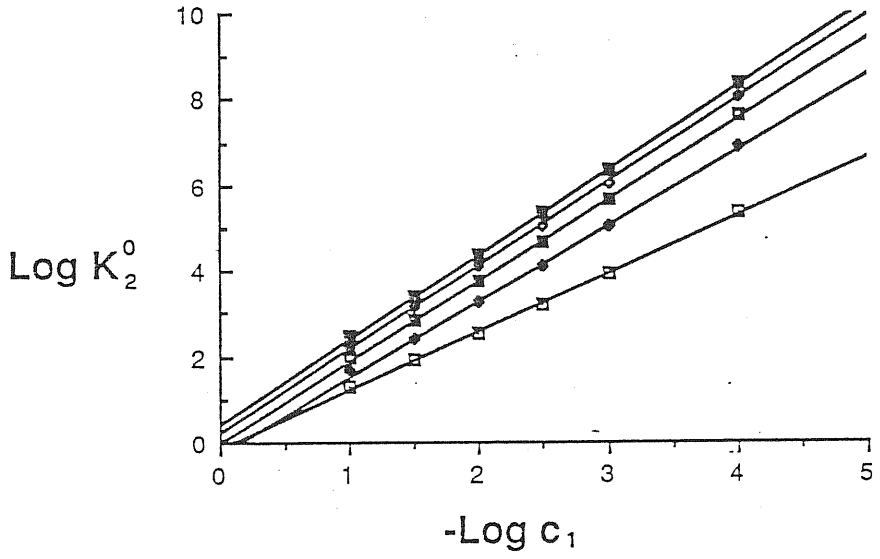

Figure 2.2.5 The decimal logarithm of the constant K_2^0 plotted against the decimal logarithm of c_1 for different reduced charged densities (ξ is 1,2,3,4 and 5 starting from the lower curve) and for the case of r_0=8 Å.

It should be remembered, anyway, that, in trying to explain or predict conformational transitions, melting or temperature and salts dependence of 1these processes the global free energy change should be calculated.

From Table 3.2.I, values of the K_2^0 at different temperatures, and therefore values of the entropy and enthalpy of the process described above, can be extracted after suitable interpolation, since changing the temperature amounts to change ξ and x_0.

The approach to the polyelectrolyte–counterion interaction described in the present section aims to be the PB analogue of Manning's solution to the same problem (Manning, 1978). Unfortunately, opposite to that case, no analitycal formula is available so numerical interpolation of the values reported in Table 3.2.I is necessary.

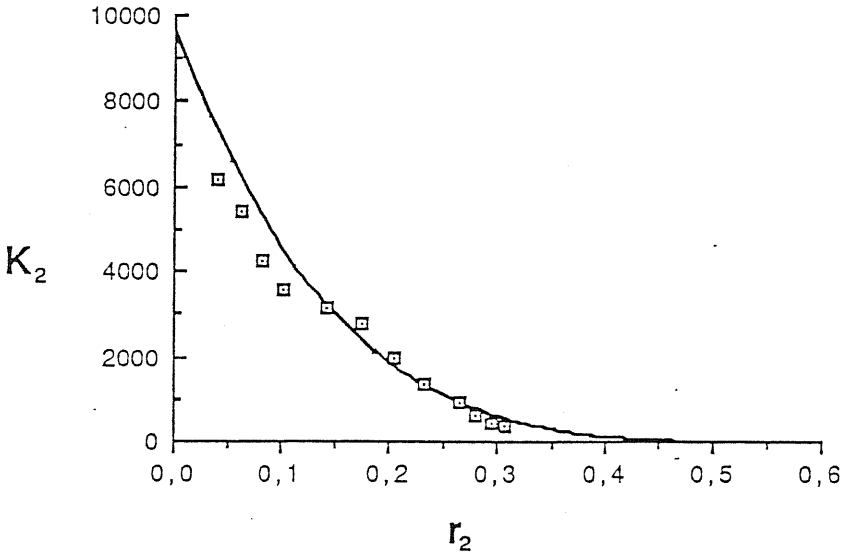

Figure 2.2.6 Experimental data (filled circles) (taken after Manzini et al. (1990)) for the Calcium induced B–Z transition in poly(dG–dm^5C) in the presence of NaCl 0.01 M vs. calculated points (squares) and interpolated Scatchard curve for B–DNA (ξ=4.2 and r_0=10 Å. The analogous curve for Z–DNA, almost completely overlapping the other one, is not shown.

Extensive investigation on the binding of calcium ions by differently structured DNA's had been performed earlier (Manzini et al., 1990). Fair agreement between experimental data and theoretical predictions (see also the data reported in Manning (1978)) which holds over a large range of ξ and ionic strength, proves that this treatment may be useful in common experimental situations.

Polyelectrolyte effects on site–binding within P–B framework

The previous methods and considerations will be here extended to the case where also site–binding is present. Possible structural modifications of the polymer will be not considered here since their effectiveness is limited in the P–B approach. For instance any process leading to unwinding, or to a structural transition, is expected to alter simultaneously the charge density and the average radius of the polymer, resulting in opposite partly compensating effect on the level of binding (see for instance Figure 2.2.6).

P–B theory give, as seen above, the ionic species distribution around the polyion. The concentrations at the surface of the polymer may be unrealistically high, being equal to $c_i^{\infty} \exp(-\psi(x_0))$. Though the quantitative details should be regarded with some care, due to the approximations involved in this mean field approach, the concentrations experienced by the binding sites on the polymer, i. e. the concentrations at the surface of the polymer, should deeply affect the apparent binding constants, which deal, on the contrary with bulk concentrations (i. e. c_i^{∞}). These ideas are not new, since Gueron and Weisbuch (1980) proposed this approach to site–binding, taking into consideration the CIV (concentration in the immediate vicinity of the polyion) as the effective concentration as to the binding equilibrium. The choice of surface concentrations, instead of more judicious choices, such as the average concentration within a cutoff radius, has the advantage to make site–binding readily incorporable in the formalism (also the radius of the model cylinder can be always chosen as to take into account the steric hindrance of the ligands). Upon binding the linear charge density of the polyelectrolyte is reduced and the ion distributions rearrange accordingly. We will consider here the most general case, including multiple site exclusion, using a formalism consistent with the one used by Friedman and Manning (1984) (for a detailed discussion of the phenomena described by the present approach the reader is referred to their paper).

Consider a ligand L bearing a charge Mq (q is the proton charge), which can bind sites on the polymer whose net charge is Jq, excluding from further binding n sites. L may be for instance a charged drug, which may intercalate a couple of base pairs or bind to the posphates of DNA; the number of sites on the polymer and their charge should be considered accordingly to the mechanism of action of the ligand. Following the treatment given by Mc Ghee and von Hippel (1974), in the absence of any electrostatic effect, we can derive the equilibrium equation:

$$\frac{\theta_L}{[L]} = K_0(1 - n\theta_L)\left(\frac{1 - n\theta_L}{1 - (n-1)\theta_L}\right)^{n-1} \qquad (2.2.16)$$

where θ_L is the ratio of bound to total sites, K_0 is the site affinity constant and $[L]$ is the concentration of the ligand at the surface of the polymer (i. e. the "free"ligand concentration experienced by the sites). The above equation must be satisfied together with the P–B equation for the distribution of the ions around

the polymer (the boundary conditions must be changed according to the effective linear charge density of the polymer $\xi_{eff} = \xi_{str}(1 - \frac{M}{J}\theta_L)$:

$$\psi'' = \frac{-\psi'}{x} + \sinh\psi + R[\exp(\psi) - \exp(-2\psi)] \qquad (2.2.17a)$$

$$\psi'(x_0) = \frac{2\xi_{eff}}{x_0} \qquad (2.2.17b)$$

$$\psi \longrightarrow 0 \qquad \text{as} \qquad x_0 \longrightarrow \infty \qquad (2.2.17c)$$

Eqs. 2.2.16 and 2.2.17 univoquely determine the function $\psi(x)$ and the level of binding θ_L.

We have derived the system of equations (2.2.16)–(2.2.17) using simple considerations, we want to show in the following that the same equations are consistent with the free energy minimization of the system, and, therefore, correctly describe the equilibrium state of the system. The free energy of the system may be split in different contributions: an electrostatic term G^{el} (which include the mobile and fixed charges, taking into account also those site–bound on the polymer surface, a term describing the entropy of mixing for both the mobile species G^{mix} and the solvent G^{solv}, which are all described as free energy density integrals over the space, and finally, a discrete term accounting for the free energy of site–binding G^{sb} (assuming no electrostatic interactions). The latter one, in the presence of multiple site exclusion, is not a simple function of the concentrations, and will not be derived here. It should be well borne in mind that, in the absence of electrostatic effects, which are accounted for by G^{el}, minimization of G^{sb} with respect to θ_L leads to eq. (2.2.16). Since all of the forces which lead to site–binding are ultimately of electrostatic nature, the previous statement must be regarded with some care. Indeed we can define the additional electrostatic term as the solvent ionic conditions dependent part of the complex energy, which can be operatively reduced to zero by increasing the ionic strength.

$$G = G^{el} + G^{mix} + G^{solv} + G^{sb} \qquad (2.2.18)$$

The above expression for the free energy must be minimized with respect to both the function $\psi(r)$, which determines the local concentrations of the solutes, and the level of binding θ_L i. e.:

$$\frac{\delta G}{\delta\psi(r)} = 0 \qquad (2.2.19a)$$

and

$$\frac{\partial G}{\partial \theta_L} = 0 \qquad (2.2.19b)$$

An explicit expression for the different terms normalized by $n_p k_B T$, to make notation consistent with the formalism of the previous sections, is given hereafter:

$$g^{el} = \frac{1}{2}\left[\int \frac{N_{Av}}{1000} c_i^{\infty} z_i q \exp(-z_i q\psi(r))\psi 2\pi r b \mathrm{d}r + q(1 - \frac{M}{J}\theta_L)\psi(r_0)\right] \qquad (2.2.20)$$

$$g^{mix} = \int \frac{N_{Av}}{1000} c_i^{\infty} \exp(-z_i q\psi(r)) \ln(\exp(-z_i q\psi(r)))2\pi r b \mathrm{d}r \qquad (2.2.21)$$

$$g^{solv} = \int \frac{N_{Av}}{1000} c_i^{\infty} \exp(-z_i q\psi(r))\psi 2\pi r b \mathrm{d}r \qquad (2.2.22)$$

g^{el} and g^{mix} may be rewritten, alternatively, in terms of the mobile and fixed charge densities, ρ_m and ρ_f, respectively, where the latter includes the site bound charged ligand as well, or in terms of the elctrostatic field:

$$g^{el} = \frac{1}{2}\int (\rho_m\psi + \rho_f\psi)2\pi r b \mathrm{d}r = \frac{\epsilon k_B T}{8\pi q^2}\int (\nabla\psi)^2 2\pi r b \mathrm{d}r \qquad (2.2.23)$$

$$g^{mix} = -\int \rho_m \psi 2\pi r b \mathrm{d}r \qquad (2.2.24)$$

With such notations the terms g^{el}, g^{mix} and g^{solv} may be grouped together:

$$g^{el} + g^{mix} + g^{solv} = \int \left(-\frac{\epsilon k_B T}{8\pi q^2}(\nabla\psi)^2 + \rho_f\psi\right) +$$

$$+ \int \frac{N_{Av}}{1000} c_i^{\infty} \exp(-z_i q\psi(r))\psi 2\pi r b \mathrm{d}r \qquad (2.2.25)$$

.

Since g^{sb} does not depend on $\psi(r)$, functional minimization of the global free energy (equation (2.2.19a)) amounts to minimization of the integral (2.2.25), which in turn implies the P–B equation, as shown for a simpler case by the work of Sharp and Honig (1991), the only difference is that now the relevant parameter for the boundary conditions is not ξ, but $\xi_{eff} = \xi(1 - \frac{M}{J}\theta_L)$, due to the charge of the site bound ligand.

Eq. (2.2.19b) leads to the usual Mc Ghee–Von Hippel formula, when the free concentration is replaced by the concentration at the surface of the polymer, as can

be seen from the factor $\exp(-z_L\psi(x_0))$ multiplying the bulk ligand concentration. As can be immediately seen, the apparent affinity constant for the ligand site interaction, is magnified by a factor $\exp(-z_L\psi(x_0))$ with respect to the absence of polyelectrolyte effects, when the bulk concentrations are the same.

In order to calculate the exact value of $\psi(x_0)$ for a given system, one can plot $\psi(x_0)$ versus θ_L (assuming fixed the bulk ion concentrations and the structural value of ξ) using alternatively the Mc Ghee–Von Hippel formula, after suitable rearrangement, and the P–B equation (remember that $\psi(x_0)$ depends on θ_L through the boundary conditions which contain the effective linear charge density ξ_{eff}). The value of $\psi(x_0)$ at the crossing of the two curves is then the only one satisfying eqs. (2.2.19). Values of $\psi(x_0)$ may be computed explicitly or derived from previous works. Gueron and Weisbuch (1980) have however reported that, for various linear charge densities, the concentration of monovalent salts at the surface of a charged cylinder is almost independent of the ionic strength condition, within commonly used ranges. More complex situations, which may be described by the formalism developed in the present section, are still to be investigated.

Moreover the set of eqs. (2.2.20)–(2.2.22) permits a straightforward comparison between P–B and Manning's theories, and may probably set on a thermodynamically correct ground the limits of applicability of Manning's theory.

Chapter 3

NUCLEAR MAGNETIC RESONANCE EXPERIMENTS

3.1 BASIC THEORY OF NUCLEAR MAGNETIC RESONANCE

Nuclear Magnetic Resonance (N.M.R.) is a phenomenon associated with nuclei possessing angular momentum and magnetic moment. (A comprehensive review on the physical principles of N.M.R. can be found in the book of Abragam (1961), for more recent developments an excellent text has been published by Ernst et al. (1990) and a very good book dealing with N.M.R. of proteins and nucleic acids is the one by Wüthrich (1986))

a) Classical treatment – Consider a system with angular momentum $\vec{L} = \hbar\vec{I}$ (where $\hbar$ is as usual the planck's constant divided by 2π and $\vec{I}$ is an a–dimensional vector assuming integer or semi–integer values) and associated magnetic moment $\vec{M} = \gamma\vec{L}$, (where γ is the gyromagnetic ratio). The classical equation for this system is

$$\frac{d\vec{L}}{dt} = \gamma\vec{L} \times \vec{H} \tag{3.1.1}$$

and if we turn to a reference frame rotating with frequency $-\omega$ (the minus sign means left–hand rotation) around axis $\vec{k}$, then the same equation holds with $\vec{H}$ replaced by $\vec{H}_{eff} = (\vec{H}_{rot} - \frac{\omega}{\gamma}\vec{k})$, where $\vec{H}_{rot}$ is the magnetic field expressed in the rotating frame coordinates. Two cases are interesting:

1) $\vec{H} = H_0\vec{k}$ (static field) $\vec{M}$ precesses in the laboratory frame with (resonance) frequency $-\omega_0\vec{k} = -\gamma\vec{H}_0$ around $\vec{k}$;

2) $\vec{H} = H_0\vec{k} - H_1(\vec{i}\cos\omega_0 t - \vec{j}\sin\omega_0 t)$ (static plus externally applied oscillating field) where $|\omega_0| = |\gamma\vec{H}_0|$. In the frame rotating at the resonance frequency $-\omega_0$ along $\vec{k}$ only a static field $-H_1\vec{i}'$ is left and the magnetization precesses around $\vec{i}'$ with frequency $\omega_1 = \gamma\vec{H}_1$. If the rotating field is applied for a time t_p the angle $\omega_1 t_p$ is called the flip angle of the pulse.

b) Quantum mechanical treatment – In the Heisenberg representation we

have

$$\frac{\hbar}{i}\frac{d\vec{I}}{dt} = [\mathbf{H}, \vec{I}] = [\gamma\hbar\vec{H}\vec{I}, \vec{I}] = \gamma\hbar\vec{I} \times \vec{H} \tag{3.1.2}$$

so the expectation value for $\vec{I}$ follows the classical equation. If we have a statistical ensemble of spins we must turn to a density matrix treatment (Fano, 1957). If every system can be described by a wave function $|\psi >= \sum_m a_m|\psi_m >$ we call density operator the operator having the following matrix elements:

$$\sigma_{mm'} =< \psi_m|\sigma|\psi_{m'} >= \overline{a_m a^*_{m'}} \tag{3.1.3}$$

where the bar indicate the ensemble average. If we chose an orthonormal basis O_i (i.e. $\mathrm{Tr}(O_i^\dagger O_j) = \delta_{ij}$) then the coefficients c_i of the density operator expansion in this basis will be simply the expectation value of the corresponding basis operator:

$$< O_k >= Tr(O_k^\dagger\sigma) = Tr(\sum_i O_k^\dagger c_i O_i) = \sum_i c_i\delta_{ik} = c_k \tag{3.1.4}$$

Therefore it is useful to have among the basis operators also the observables or the "coherence"we are interested in. Every non zero off–diagonal element of the density matrix reflects a coherence in the phases of the coefficients of the single system wave function expansion.

It is worthwhile at this point to introduce the concept of "phase cycling"(Bain, 1984; Bodenhausen et al., 1984) . In general we can expand the density matrix in components corresponding to p–quantum coherences:

$$\sigma = \sum_p \sigma^p \tag{3.1.5}$$

(we call p–quantum coherences the coherent superposition of states differing in their m_z quantum number by $\Delta m_z = p$). Suppose we have a unitary transformation U (it can be brought about by a sequence of pulses) such that : $\sigma^{p'} = U\sigma^p U^{-1}$. If we change the phase of U obtaining $U' = \exp(-i\sum_i I_{iz}\phi)U\exp(i\sum_i I_{iz}\phi)$ (this amounts to rotating the space around $\vec{k}$ by an angle ϕ) we get $U'\sigma^p U'^{-1} = \sigma^{p'}\exp[i(p-p')\phi]$. By summing the signals from experiments performed with different pulse phases we can get rid of the unwanted coherences. Since we can expand the density matrix in p–quantum coherence terms at every step of the

experiment we can also follow the coherence pathway of every term of the final density matrix (keeping in mind that only single quantum coherences like I_x or I_y can be measured). The process of changing the phase of the pulse sequence (or of part of it) and summing the relative signals is referred to as "phase cycling".

Useful further effects derive from:

a) the direct interaction with the electrons surrounding the nucleus – In the presence of an applied field the Larmor precession of the induced orbital magnetic moment of the electrons creates a diamagnetic field at the nucleus while the distortion of the electron wave functions produces a second field opposite in sign to the previous one. Since both are proportional to the primary field applied H_0, the effective field at the nucleus will be $H_0(1-\sigma)$. σ is called the chemical shift. Although its explicit calculation is not straightforward we can assign regions of the spectrum to specific types of atoms (for instance amide protons have always chemical shifts different from methyl protons)

b) the indirect interactions among the nuclei mediated by the electrons – If we consider the second order terms in the perturbative expansion of the Hamiltonian of the nuclei and the electrons of one molecule, assuming isotropic molecular tumbling, we get an Hamiltonian of the following type

$$\mathrm{H}_{12} = J_{12}\vec{I}_1\vec{I}_2 \tag{3.1.6}$$

where J_{12} could be in principle calculated, but this would require the knowledge of all the excited states of the molecule. The coupling constant J_{12} can be, in some cases, empirically connected to the dihedral angles involving the coupled atoms through so–called "Karplus–type"relations (for biological applications see Wütrich (1986) and Altona (1982)).

c) the direct through space dipolar coupling with other nuclei and with the lattice – As a consequence of the random character of this kind of interactions all the effects can be taken into account by means of a relaxation matrix for the expectation values of the magnetization (Solomon, 1955). We can get expressions for T_1 and T_2 (respectively the longitudinal and trasversal relaxation rates) and for the cross–relaxation rates assuming isotropic tumbling, no mechanisms of relaxation other than dipolar coupling and unlike spins. The time evolution of the magnetization M_z toward its equilibrium value M_z^0 can be described by the

following equations:

$$\frac{d\vec{M}_z}{dt} = -R\vec{M}_z \tag{3.1.7}$$

where

$$\vec{M}_z = \begin{pmatrix} M_{1z} - M_{1z}^0 \\ M_{2z} - M_{2z}^0 \\ \vdots \\ M_{nz} - M_{nz}^0 \end{pmatrix} \tag{3.1.8}$$

and the coefficients of R (the relaxation matrix) are:

$$R_{ii} = \sum_{j \neq i} q_{ij}(J(\omega_i - \omega_j) + 3J(\omega_i) + 6J(\omega_i + \omega_j)) \tag{3.1.9}$$

$$R_{ij} = q_{ij}(J(\omega_i - \omega_j) - 6J(\omega_i + \omega_j)) \tag{3.1.10}$$

with $q_{ij} = \frac{\gamma_i^2 \gamma_j^2 \hbar^2}{10}$. In the assumption of a single exponential correlation function the spectral density is a very simple function of the rotational correlation time τ_c:

$$J(\omega) = \frac{\tau_c}{1 + \omega^2 \tau_c^2} \tag{3.1.11}$$

Additional relaxation rates to be included in the above formulae are due to interaction with the lattice and can be computed as a function of the intensity and decay constant τ_0 of the random fluctuating field experienced, according to expressions:

$$\frac{1}{T_1} = 2\gamma^2 \overline{H}_{tr}^2 \left(\frac{\tau_0}{1 + \omega_0^2 \tau_0^2}\right) \qquad \text{for longitudinal magnetization} \tag{3.1.12}$$

and

$$\frac{1}{T_2} = \gamma^2 \left(\overline{H}_{long}^2 \tau_0 + \overline{H}_{tr}^2 \frac{\tau_0}{1 + \omega_0^2 \tau_0^2}\right) \qquad \text{for transversal magnetization} \tag{3.1.13}$$

NMR experiments

It is worthwhile to summarize here the basic schemes of NMR experiments. The most simple experiment one can do is a one dimensional (1D) Fourier Transform (FT) NMR experiment. We must allow the system to reach its equilibrium

state inside a magnetic field (this may take a variable time, according to the relaxation time of the sample), then we apply an oscillating field to rotate longitudinal magnetization into transversal magnetization. The free precession of the latter in a coil will induce an oscillating current, $s(t)$, which can be recorded and Fourier transformed. Since the system contains spins with (possibly) different chemical shifts, all of these will be represented by a peak in the frequency spectrum of $s(t)$.

A 2D FT NMR experiment is basically the straightforward extension of the above described 1D experiment. Whereas a function of the time domain $s(t)$ is transformed to give a spectrum in the frequency domain, in the 2D experiments a signal depending on two time intervals $s(t_1, t_2)$ is converted in a 2D frequency spectrum. The basic scheme of a 2D–experiment is given in fig. 3.1.1.

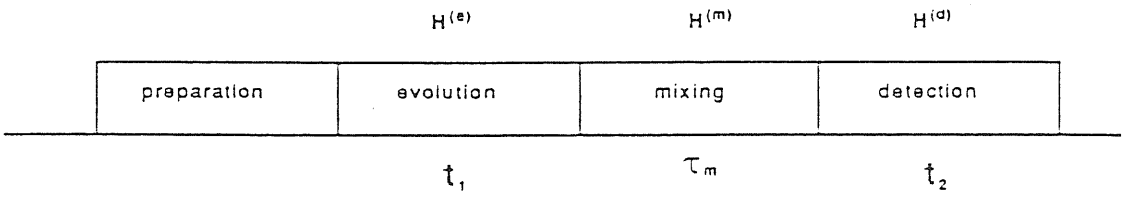

Figure 3.1.1 Basic scheme for a 2D FT N.M.R. experiments: H indicates the Hamiltonian governing the time evolution.

We can divide an ideal 2D N.M.R. experiment in four periods of time. Although these can be of different nature and also overlapping we can understand the principles of the experiment following this scheme.

1) The preparation period is devoted to create a coherent non–equilibrium state of the spin system (for instance a non selective $\frac{\pi}{2}$ pulse could suffice to this purpose). Then magnetization (which was parallel to the main field) is brought into a transversal plane.

2) During the evolution period the system evolves under the Hamiltonian H^e (in the simplest case this could be the free precession Hamiltonian). The duration of this period t_1 is incremented from an experiment to another, so that memory of the evolution will be kept in the ω_1 frequencies.

3) The mixing period is designed to let the system evolve under the Hamiltonian bearing the information we want to get from the experiment (for instance a

TOCSY Hamiltonian giving information on J coupling). The mixing time is really the core of the experiment since magnetization which has acquired, during period 2, ω_1 "labelling"can be exchanged and acquire in the following evolution step a different precession frequency.

4) During the detection period the system evolves under the Hamiltonian $\mathbf{H}^d$ (for instance again the free precession Hamiltonian) and the transverse magnetization is recorded as a function of t_2.

After 2D Fourier Transform a 2D frequency spectrum is obtained. Following the discussion above, the off diagonal peaks in such spectrum, are related to the exchange of magnetization among nuclei with different chemical shifts, while diagonal peaks are representative of unexchanged magnetization.

The above considerations need not be restricted to just two dimensions, indeed one can introduce three or more time variables in the experiments, which can be Fourier transformed to give 3– (or n–) dimensional spectra. In the following a possible scheme for a three dimensional experiment will be discussed. The whole variety of experiments which have been used will not be discussed in the present thesis, since a detailed treatment may be found in the book of Ernst et al. (1990). Only the total correlation spectroscopy (TOCSY) and the possible extension to the heteronuclear correlation spectroscopy via Single Quantum Coherence (SQC–spectroscopy) experimental schemes will be described, being the information that can be gained from this class of experiments still not fully explored.

TOCSY

Before discussing this experiment it is useful to introduce the average Hamiltonian theory (Haeberlen and Waugh, 1968; Ernst et al., 1990). The starting question is the following: can we replace the actual time dependent Hamiltonian $\mathbf{H}(t)$ with some kind of average evolution operator? The answer is yes if we are interested only in the state of the system at a certain time t_c disregarding the way the system has come to this state and if the requirement that $U(t_c) = \mathbf{1}$ is fulfilled. We can show this and compute explicitly the average Hamiltonian. Suppose a piecewise constant Hamiltonian, the evolution operator can be written in

the following way (we are only interested in the time t_c):

$$U(t_c) = \exp(-i\mathbf{H}_n t_n) \ldots \exp(-i\mathbf{H}_1 t_1) \tag{3.1.14}$$

where Hamiltonians are expressed for simplicity in $\hbar$ units. If we remember the Baker–Campbell–Hausdorff relation:

$$\exp(A)\exp(B) = \exp((B+A) + \frac{1}{2}([B,A]) + \frac{1}{12}([B,[B,A]] + [[B,A],A]) + \ldots \tag{3.1.15}$$

we can write the evolution operator at t_c using an "average"Hamiltonian

$$U(t_c) = \exp(-i\overline{\mathbf{H}}t_c) \tag{3.1.16}$$

$\overline{\mathbf{H}}$ can be computed making use of the following expansion:

$$\overline{\mathbf{H}} = \overline{\mathbf{H}}^0 + \overline{\mathbf{H}}^1 + \ldots \tag{3.1.17}$$

where:

$$\overline{\mathbf{H}}^0 = \frac{1}{t_c}(\mathbf{H}_1 t_1 + \mathbf{H}_2 t_2 + \ldots) \tag{3.1.18}$$

$$\overline{\mathbf{H}}^1 = \frac{i}{2t_c}([\mathbf{H}_2 t_2, \mathbf{H}_1 t_1] + [\mathbf{H}_3 t_3, \mathbf{H}_1 t_1] + \ldots) \tag{3.1.19}$$

$$\vdots$$

We can neglect higher order terms if $\|\mathbf{H}_i t_i\| \ll 1$. Usually the time dependent Hamiltonian (produced for instance by a sequence of pulses) does not fulfill this requirement so that we have to transfer the time dependence on the static Hamiltonian. We can do this using a reference system "toggling"around with the time dependent Hamiltonian where the previous static Hamiltonian has become time dependent without losing the feature of being "weak". In a more formal way we start with an Hamiltonian of the type:

$$\mathbf{H}(t) = \mathbf{H}_0 + \mathbf{H}_1(t) \tag{3.1.20}$$

whose corresponding evolution operator is:

$$U(t) = \mathbf{T}\exp[-i\int_0^t (\mathbf{H}_0 + \mathbf{H}_1(t'))]dt' \tag{3.1.21}$$

where $\mathbf{T}$ is the Dyson time–ordering operator. We want to separate the static and time dependent Hamiltonian by writing the evolution operator as a product

$$U(t) = U_1(t)U_0(t) \tag{3.1.22}$$

with

$$U_1(t) = \mathbf{T}\exp(-i\int_0^t \mathbf{H}_1(t_1)dt_1) \tag{3.1.23}$$

$$U_0(t) = \mathbf{T}\exp(-i\int_0^t \tilde{\mathbf{H}}_0(t_1)dt_1) \tag{3.1.24}$$

and

$$\tilde{\mathbf{H}}_0(t_1) = U_1^{-1}(t_1)\mathbf{H}_0U_1(t_1) \tag{3.1.25}$$

Suppose that $U_1(t_c) = \mathbf{1}$, than we can write explicitly the first terms of the average Hamiltonian expansion:

$$\overline{\mathbf{H}}_0^0 = \frac{1}{t_c}\int_0^{t_c} \tilde{\mathbf{H}}_0(t_1)dt_1 \tag{3.1.26}$$

$$\overline{\mathbf{H}}_0^1 = \frac{-i}{2t_c}\int_0^{t_c} dt_2 \int_0^{t_2} dt_1[\tilde{\mathbf{H}}_0(t_2), \tilde{\mathbf{H}}_0(t_1)] \tag{3.1.27}$$

$$\vdots$$

With this result we can discuss the TOCSY experiment starting from what is called an ideal TOCSY Hamiltonian:

$$\mathbf{H} = \sum_{ij} \frac{1}{2} J_{ij}\vec{I}_i\vec{I}_j \tag{3.1.28}$$

In order to reach such an effective we should be able to suppress the chemical shift terms in the actual Hamiltonian (i.e. $\mathbf{H}_{c.s.} = \sum_i \Delta\omega_i I_{iz}$). Average Hamiltonian theory offers the tool to design the pulse sequences to achieve the so called "isotropic mixing"condition eq. (3.1.28).

The evolution of the system under such Hamiltonian is not really straightforward to be calculated. Analytical formulas are available only for a limited class of cases. The evocative name of "collective spin modes"(Braunschweiler and Ernst, 1983) doesn't give any clue to extend the considerations made on the very simple two–spin system. Numerical calculations were performed for the amino–acid

spin systems (Cavanagh et al., 1990) assuming definite values of the J coupling constants.

The symmetry properties of the Hamiltonian can however suggest the general features of the TOCSY experiments, and determine the situations in which an analytical solution is possible. For instance the invariance of the Hamiltonian with respect to rotations, implies that all the components of the total angular momentum are constants of the motion, i. e. that any transfer among the spins represents a net exchange of magnetization. Moreover the eigenvalues of the Hamiltonian depend only on the total angular momentum, and not on the single components. The transfer at time t among two spins i and j may be defined as the expectation value of I_{zj} at time t when the initial density matrix was I_{zi}. The transfer is expressed by:

$$< I_{zj} >= \mathrm{Tr}(I_{zj} \exp \frac{-i\mathrm{Ht}}{\hbar} I_{zi} \exp \frac{i\mathrm{Ht}}{\hbar}) \qquad (3.1.29)$$

where, to perform the trace, we can choose the vector eigenbasis of the Hamiltonian. Invariance with respect to time–reversal implies that the transfer is symmetrical in the time (due to the properties of transformation of both the density matrix and the observable), i. e. it can be expressed as a sum of cosine terms. However, since the quantitative information is not directly available, we want just to discuss the appearance of the spectra obtained. All the peaks are in pure 2D absorption mode and the information they bear depends mainly on the length of the mixing period:

1) for a short τ_{mix} only direct connectivities will appear and the topology of the spectrum will be the same as that of a COSY spectrum,

2) for a long τ_{mix}, in the most favorable cases all the resonances belonging to the same spin system are connected by a crosspeak. The usefulness of this feature is appearent if we think that every amino–acid constitutes an autonomous spin–system.

Heteronuclear Single Quantum Coherence (SQC) experiments

The introduction of time variables, other than the acquisition time allows for the observation of nuclei different from the one directly observed without the need

of a specific probe. Moreover it is possible to exploit the sensitivity of one nucleus to improve the observation of another one. Some basic sensitivity considerations will be reminded here.

For any 2D experiment the signal to noise ratio is proportional to $\gamma_{exc}\gamma_{obs}^{\frac{3}{2}}B_0^{\frac{3}{2}}$ where subscripts *exc* and *obs* refer to the excited and the directly observed nucleus, respectively (Ernst et al., 1990). Therefore efficient schemes exploiting the high gyromagnetic ratio of the proton may be devised to observe much lower sensitive nuclei like carbon and nitrogen. Among all the schemes conceivable for heteronuclear 2D NMR spectra, those involving heteronuclear coherence transfer seem to be the most efficient ones (Ernst et al., 1990)

Such schemes encompass basically five steps, namely:

1 – starting proton excitation;

2 – heteronuclear polarization transfer;

3 – labelling of relevant coherences with heteronuclear frequencies;

4 – polarization backtransfer;

5 – proton observation. Between period 4 and 5, we may let proton spins interact via a suitable Hamiltonian in order to observe proton – proton interactions as well.

A particular scheme will be discussed here, much following the presentation of Molinari et al. (1992), and in the next sections. The pulse sequence is depicted in Figure 3.3.1, and represents the SQC version of the Heteronuclear Multiple Quantum Coherence (HMQC) proposed by Shon and Opella (1989) to exploit the additional spreading of resonances in the heteronuclear axis. t_m is designed to let NOE's develop. In the final spectrum not only so called "auto peaks"(i. e. peaks at the frequency of scalarly coupled X– and H– nuclei) but also "cross peaks"among X–nuclei and non–coupled H–nuclei, will be present as a result of homonuclear transfer during mixing time.

Due to the lack of a symmetry plane, resolution improves in heteronuclear 2D spectra. To fully exploit the resolution available one should properly choose the heteronuclear magnetization transfer scheme in order to reduce relaxation during t_1. For instance ^{15}N–SQC experiments offer improved resolution compared to analogous HMQC schemes (Bax et al., 1990; Norwood et al., 1990). In fact the ^{1}H–^{1}H dipolar contribution to the HMQC transverse relaxation is larger than the

heteronuclear counterpart to the ^{15}N–SQC (antiphase) relaxation rate, and the unresolved J splittings are absent in the F_1 dimension of the SQC spectra.

For ^{13}C the heteronuclear dipolar contribution is much larger however, the presence of J couplings in the F_1 dimension reduces largely any possible advantage in the use of MQC experiments.

The two OverBodenhausen INEPT steps flanking t_1 evolution in Figure 3.3.1, are a very efficient choice for two reasons: 1) their duration is shorter compared to alternative schemes (INEPT or DEPT); 2) the efficiency of transfer does not depend on the multiplicity of the spins coupled to the heteronucleus.

The evolution of the density matrix up to the mixing time may be followed using the standard product operator formalism (assuming I_k directly coupled to spin S and no other homocoupling for spin I_k):

$$I_{kz} \xrightarrow{\frac{\pi}{2}I_x} -I_{ky} \xrightarrow{\Delta-\pi_x-\Delta} -2I_{kx}S_z \xrightarrow{\frac{\pi}{2}(I_y+S_x)} -2I_{kz}S_y \xrightarrow{\frac{t_1}{2}-(\pi I_x)-\frac{t_1}{2}}$$

$$2I_{kz}S_y\cos(\omega_S t_1) \xrightarrow{(\frac{\pi}{2})_x} -2I_{ky}S_z\cos(\omega_S t_1) \xrightarrow{\Delta-\pi_x-\Delta} I_{kx}\cos(\omega_S t_1) \xrightarrow{\frac{\pi}{2}I_y} -I_{kz}\cos(\omega_S t_1) \tag{3.1.30}$$

When homonuclear coupling ($J_{kl}I_{kz}I_{lz}$) is present as well, also other coherences will develop so that the density matrix at the starting of the mixing time will be:

$$I_{kz}\cos(\omega_S t_1)\cos(\frac{\pi J_{kl}}{2J_{kS}}) + -2I_{ky}I_{lx}\cos(\omega_S t_1)\sin(\frac{\pi J_{kl}}{2J_{kS}}) -$$

$$2I_{ky}S_x\sin(\omega_S t_1)\cos(\frac{\pi J_{kl}}{2J_{kS}}) - 4I_{ky}S_xI_{lx}\sin(\omega_S t_1)\sin(\frac{\pi J_{kl}}{2J_{kS}}) \tag{3.1.31}$$

The experiment is designed to select only the first term of eq. (3.1.31). The two rightmost terms can be neglected since they do not give rise to any observable magnetization, while the second term may give rise to antiphase observable components (which are anyway expected to be small due to the factor $\sin(\frac{\pi J_{kl}}{2J_{kS}}$ ranging from 0.05 to 0.25 for typical values of the couplings). The z–magnetization at the starting of the mixing time may be let exchange under suitable Hamiltonian, the most simple case would involve no additional pulse scheme in the mixing time, with the spins interacting through dipolar coupling, but ROESY or TOCSY schemes would be devisable as well.

It can be easily seen that the resulting 2D spectrum is just a projection of a 3D heteronuclear analogous experiment.

3.2 PROTON STRONG COUPLING IN HETERONUCLEAR SYSTEMS : THEORETICAL AND EXPERIMENTAL EVALUATION IN QUANTITATIVE ANALYSIS OF SQC–NOESY SPECTRA OF BIOPOLYMERS

In a recent report Molinari et al. (1992) investigated the application of the cross/auto–peak volume ratio method to interproton distance calculation (Bodenhausen and Ernst, 1982; Macura et al., 1986; Esposito and Pastore, 1988; Wagner, 1990) in ^{1}H detected NOE–relayed heteronuclear correlation spectroscopy via single quantum coherence (SQC), briefly referred to as SQC–NOESY (Wagner, 1990; Bax et al., 1990; Norwood et al., 1990).

In spite of the inherent limitations due to the low natural abundance of many heterospins, heteronuclear SQC–NOESY spectroscopy, compared to conventional homonuclear NOESY, also shows interesting features that may prove advantageous in structural NMR work.

Indeed the heteronuclear chemical shift dispersion in ω_1, in conjunction with the lack of a symmetry plane, generally increases the resolution of proton dipolar connectivity maps, often removing overlap in complex spectra such as those of biopolymers. As a result, not only cross–peaks (from proton–proton NOE), but also auto–peaks (from proton–heteronucleus J coupling) become amenable to quantitation in SQC–NOESY spectra. This makes the evaluation of interproton distances feasible, either through the approximate approach entailing the knowledge of auto–peak intensities (Bodenhausen and Ernst, 1982; Macura et al., 1986; Esposito and Pastore, 1988), or the complete relaxation matrix treatment (Keepers and James, 1984), provided all the dipolarly coupled protons are attached to the heteronucleus observed in ω_1 and the differences in relaxation rates of the coherences evolving in t_1 are properly accounted for.

Molinari et al. (1992) drew attention to the onset of proton strong scalar coupling effects in heteronuclear spin systems when:

$$|(\omega_I \pm \pi J_{IS}) - \omega_{I'}| \leq 20\pi J_{II'} \qquad (3.2.1)$$

where I and I' are protons (scalarly and possibly dipolarly coupled) and S the heterospin (coupled to I only). In more simple words, negligibly small (but already

present) strong coupling effects are enhanced by the proper resonance frequency pattern of heteronuclear coupled I spins.

The specific problems arising in quantitative analysis of ^1H–^{13}C SQC–NOESY spectra as a consequence of eq. (3.2.1), were examined in detail for the aromatic connectivities of bovine pancreatic trypsin inhibitor (BPTI), a well characterized protein (Wagner and Wüthrich, 1982). However intensity deviations due to strong coupling in SQC–NOESY experiments may arise for any class of proton resonances in crowded biopolymer spectra.

Although proper spin configurations exhibiting such features may occur for many heteronuclear systems, the strong coupling perturbations should be of practical relevance in ^1H–^{13}C systems. The peculiarities of the spin system configuration fulfilling condition (3.2.1) were earlier pointed out by Bolton and Bodenhausen (1979) and Garbow et al. (1982). More recently the topic of proton strong coupling in ^1H–^{13}C HOESY spectra has been addressed by Kövér and Batta (1987) and Muhandiram and McClung (1988).

In this section we wish to provide a formal description of the phenomenon in SQC–NOESY spectra and try to evaluate the extent of expected intensity deviations.

Theory

The sequence we deal with is sketched in Figure 3.2.1. It encompasses two INEPT Overbodenhausen type (Morris and Freeman, 1979; Bodenhausen and Ruben, 1980) polarization transfer steps, flanking t_1 heteronuclear chemical shift evolution, to select magnetization of those protons directly attached to the heteronucleus.

Then a homonuclear dipolar exchange step follows during which the heteronuclear labelled proton longitudinal magnetizations cross–relax to nearby nuclei. When condition (3.2.1) applies, the coherences of type $S_\alpha I_\beta$ $(\alpha, \beta = x, y, z)$ will undergo oscillatory transfer to $S_\alpha I'_\beta$ coherences, without the need of any pulse perturbation. Thus the INEPT transfers, as well as the t_1 precession step, will no longer be effective in sorting out only antiphase or transverse components of the proton spin directly coupled to the heteronucleus S.

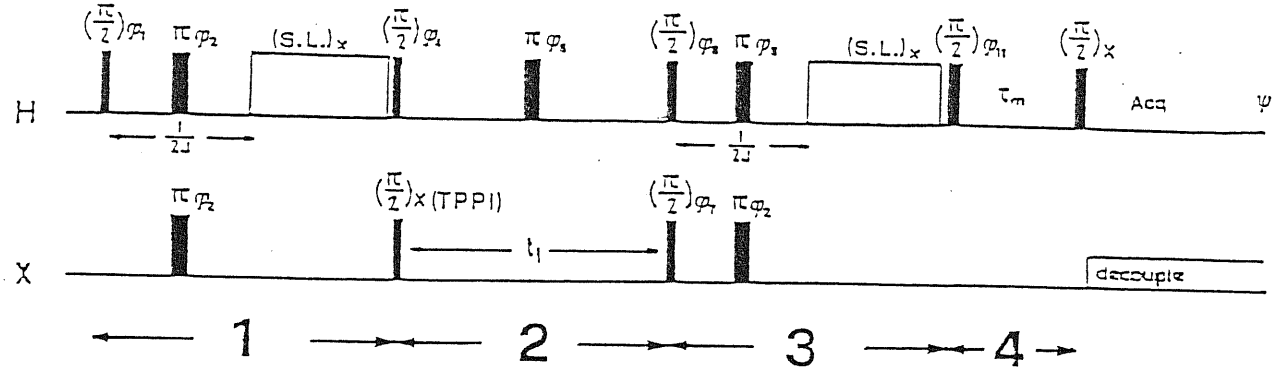

Figure 3.2.1 ^{1}H–X SQC–NOESY pulse sequence. ϕ_1=x,$-x$; ϕ_2=x,$-x$; ϕ_4=y,$-y$; ϕ_6=ϕ_7=x,$-x$; ϕ_8=x,y,$-x$,$-y$; ϕ_{11}=ϕ_8+$\pi/2$; ψ=$(x,-x,-x,x)_{64}$ $(-x,x,x,-x)_{64}$. All explicit phase cycles, except for the receiver, are performed independently giving a 128 step cycle.

Of course when the proton spin system is inherently strongly coupled, i.e. in practice when $|\omega_I - \omega_{I'}| < 20\pi J_{II'}$, an additional oscillatory transfer is expected to also operate during the homonuclear dipolar exchange interval (t_m) and the acquisition time (t_2). Further intensity perturbation will ensue, but we shall not be concerned here with this type of process, that is also expected in ordinary homonuclear NOESY experiments and can be fully accounted for using the theoretical treatment outlined by Kay et al. (1986b). Suffice it to say that the important consequence of the absence of oscillatory transfers during t_m and t_2 is that dipolar exchanges will take place unperturbed, which should make the quantitative estimation of homonuclear cross–relaxation rates simpler.

Formal description

When the isotropic scalar coupling term $2\pi J_{II'}\mathrm{II}'$ must be included in the Hamiltonian, the latter can no longer be factorized in terms of Zeeman and weak scalar coupling propagators.

Following Braunschweiler and Ernst (1984), one should look for an appropriate orthogonal operator basis possessing recursive commutation properties with all the terms of the Hamiltonian, but no simple analytical basis exists when strong coupling and Zeeman evolution are simultaneously involved in systems with more

than two non–equivalent nuclei.

In fact, when condition (3.2.1) holds, the Hamiltonian governing the evolution of the three 1/2 spin system $\{I, I', S\}$ can be written as:

$$H = H_0 + H_1 \tag{3.2.2a}$$

with

$$H_0 = S_z\omega_S + c^+S_z \qquad H_1 = aA + b^+\Delta_z \tag{3.2.2b}$$

where

$$a = 2\pi J_{II'} \qquad b^{\pm} = (\Delta\omega_I \pm 2\pi J_{IS}S_z) \qquad c^{\pm} = (\Sigma\omega_I \pm 2\pi J_{IS}S_z)$$

$$A = \mathrm{II}' = \Sigma_{\alpha=x,y,z}(I_\alpha I'_\alpha) \qquad \Sigma_\alpha = \frac{1}{2}(I_\alpha + I'_\alpha) \qquad \Delta_\alpha = \frac{1}{2}(I_\alpha - I'_\alpha)(\alpha = x,y,z)$$

$$\Sigma\omega_I = (\omega_I + \omega_{I'}) \qquad \Delta\omega_I = (\omega_I - \omega_{I'}) \tag{3.2.3a}$$

Throughout the calculation we shall also make use of the additional definitions:

$$\Pi^{\pm}_{\alpha\beta} = \frac{1}{2}(I_\alpha I'_\beta \pm I_\beta I'_\alpha) \qquad M^{\pm}_{\alpha\beta} = \frac{1}{2}(I_\alpha I'_\alpha \pm I_\beta I'_\beta) \qquad (\alpha,\beta = x,y,z) \tag{3.2.3b}$$

The above definitions (and, hence, the following calculations) assume that only nucleus I is coupled to the heteronucleus S. Introduction of an additional I' heteronuclear coupling is immaterial in ^{1}H–^{13}C systems at natural abundance, as well as in any systems with rare heterospin, unless both the inequivalent I and I' hydrogens are bound to the same heteroatom S. However, for our purposes, this situation is of no concern (see Experimental test section).

Going back to eqs. (3.2.2a) and (3.2.2b), commutation relationships hold:

$$[H_0, A] = [H_0, \Delta_z] = [H_0, H] = 0$$

but

$$[H_1, A] \neq [H_1, \Delta_z] \neq 0$$

which implies that strong coupling and Zeeman evolution cannot be treated separately, whatever the selected operator basis.

Nonetheless the effects of heteronuclear coherence mediated strong proton coupling can be estimated using a mixed analytical–numerical procedure.

Thus it is convenient to split the evolution of the system perturbed by the sequence of Figure 3.2.1 into four periods, i.e.:

1. preparation Overbodenhausen step;
2. t_1 evolution step;
3. recovery retro–Overbodenhausen step;
4. dipolar evolution step.

The starting $\frac{\pi}{2}$ pulse rotates only I and I' equilibrium longitudinal magnetizations. The density operator undergoes the transformation:

$$\sigma(0) = 2\Sigma_z + S_z \overset{\frac{\pi}{2}(I_x+I'_x)}{\longrightarrow} -2\Sigma_y + S_z = \sigma(1) \tag{3.2.4}$$

During period 1, $\sigma(1)$ evolution takes place under the action of H (eqs. 3.2.2) and of the hard pulse operator $L_x = (I_x + I'_x + S_x)$. Formally, by introducing π_x rotated Hamiltonians, indicated by underlined symbols, e.g. $\underline{\mathrm{H}}$, the tranformation can be arranged as:

$$\sigma(2) = \exp(-i\pi \mathbf{L}_x) exp(-i\underline{\mathbf{H}}t/2) exp(-i\mathbf{H}t/2)\sigma(1) \tag{3.2.5}$$

where $t = \frac{1}{2J_{IS}}$ and, analogous to definitions (3.2.2), we have:

$$\underline{H} = \underline{H}_0 + \underline{H}_1 \tag{3.2.6a}$$

$$\underline{H}_0 = -S_z\omega_S - c^-\Sigma_z \qquad \underline{H}_1 = aA - b^-\Delta_z \tag{3.2.6b}$$

Here and throughout the text, commutation superoperators are indicated by bold face symbols of corresponding operators.

Exploiting the additional commutators:

$$[\underline{H}_0, \underline{H}] = [\underline{H}_0, H] = 0$$

transformation (3.2.5) can be factorized as:

$$\sigma(2) = \exp(-i\pi \mathbf{L}_x) \exp[-i(\underline{\mathbf{H}}_0 + \mathbf{H}_0)\frac{t}{2}] \exp(-i\underline{\mathbf{H}}_1 \frac{t}{2}) exp(-i\mathbf{H}_1 \frac{t}{2})\sigma(1) \tag{3.2.7}$$

with $(\underline{\mathbf{H}}_0 + \mathbf{H}_0)\frac{t}{2} = 2\pi J_{IS} S_z \Sigma_z t$ accounting for the refocusing of proton Zeeman evolution.

The remaining terms in $\underline{H}_1$ and H_1 cannot be collected because A and Δ_z do not commute with the whole Hamiltonian. Subsequent calculations can be carried out resorting to numerical evaluation.

For this purpose, it is useful to factorize the S-dependence in the density matrix and consider the evolutions of the parts containing the projectors ($|\alpha><\alpha|_S$) and ($|\beta><\beta|_S$) separately. The manipulation allows us to assign the explicit numerical value $\pm\frac{1}{2}$ to S_z, whenever encountered (as in $b^{\pm}$ or $c^{\pm}$), and restrict the Liouville space to the I, I' operators space. By considering all the possible sequential commutators of A and Δ_z with Σ_y and Δ_y, one can easily perceive that any transformation brought about by the superoperators $\underline{\mathbf{H}}_1$ and $\mathbf{H}_1$, always moves within the same Liouville subspaces, viz. within those spanned by the bases $\lambda_1 = \{\Sigma_y, \Delta_x, \Pi^-_{zy}, \Pi^+_{zx}\}$ $\lambda_2 = \{\Sigma_x, \Delta_y, \Pi^-_{zx}, \Pi^+_{zy}\}$. In other words, these subspaces are eigenspaces of $\underline{\mathbf{H}}_1$ and $\mathbf{H}_1$.

This prompts one to express $\underline{\mathbf{H}}_1$ and $\mathbf{H}_1$ as matrix superoperators operating onto vectors in the bases λ_1 and λ_2, with elements given by the constants a and $\frac{b^+}{2}$, e.g.

$$(\mathbf{H}_1) = (a\mathbf{A} + b^+\Delta_z) = i \begin{pmatrix} 0 & \frac{b^+}{2} & 0 & 0 \\ -\frac{b^+}{2} & 0 & a & 0 \\ 0 & -a & 0 & -\frac{b^+}{2} \\ 0 & 0 & \frac{b^+}{2} & 0 \end{pmatrix} \tag{3.2.8}$$

where the matrix element $\frac{b^+}{2}$ itself includes the operator S_z through its proper numerical value. Therefore, for instance, the far right term of eq. (3.2.7) can be written as:

$$\ldots \exp(-i\mathbf{H}_1\frac{t}{2})\sigma(1) =$$

$$\ldots S_z + \exp(-i\mathbf{H}_1\frac{t}{2}) \begin{pmatrix} -2 \\ 0 \\ 0 \\ 0 \end{pmatrix} \otimes (|\alpha><\alpha|_S + |\beta><\beta|_S) \tag{3.2.9}$$

in which $-2\Sigma_y$ is expressed as the corresponding vector in the λ_1 basis multiplied by the S unity operator, $\mathbf{1}_S$. The same procedure applies, of course, also to the term $\exp(-i\underline{\mathbf{H}}_1\frac{t}{2})$ of eq. (3.2.7).

The calculation is carried out by solving the eigenvalue problem of the matrix exponential and separately evaluating the corresponding terms with $|\alpha><\alpha|_S$ and $|\beta><\beta|_S$, having set S_z (in $\frac{b^+}{2}$) as $+1/2$ and $-1/2$, respectively.

Once the two exponentials in $\underline{\mathbf{H}}_1$ and $\mathbf{H}_1$ of eq. (3.2.7) are computed, the resulting terms in $|\alpha><\alpha|_S$ and $|\beta><\beta|_S$ are recast in terms of the more familiar $\mathbf{1}_S$ and S_z, according to:

$$c_1|\alpha><\alpha|_S + c_2|\beta><\beta|_S = \frac{(c_1+c_2)}{2}\mathbf{1}_S + \frac{(c_1-c_2)}{2}2S_z$$

where c_1 and c_2 are coefficients. Then we let $2\pi J_{IS}S_z\Sigma_z t$ and πL_x operate on the result with the usual expansion formula.

The results obtained for $\Delta\omega_I = \pi J_{IS}$ and $\frac{J_{II'}}{J_{IS}} = 0.06$ (i.e. for a typical $\frac{J_{HH}}{J_{HC}}$ ratio with the average direct J_{HC} value of 130–140 Hz) are listed in Table 3.2.I. The computations were performed using a C written routine with a VGX 320 Silicon Graphics computer.

Only part of the listed coherences will survive after the proton purging pulse following free evolution of period 1 (Table 3.2.I). Among these we only focus on those not negligibly small terms that will acquire the ω_S frequency labelling during t_1, i.e.$-2S_z(m_1\Sigma_x + m_2\Delta_x) \simeq -2S_z(\Sigma_x + \Delta_x)$, henceforth referred to as $\sigma(2')$.

Coherences such as $4S_z\Pi^-_{zx}$ and $4S_z\Pi^-_{zy}$, that would be labelled in t_1, are not included in $\sigma(2')$ because of the effects of the purging pulse. Under $\frac{\pi}{2}(I_x + I'_x)$ rotation, the former coherence would develop into a double quantum term that could be filtered out by phase cycling. The latter would be left unchanged because $[S_z\Pi^-_{zy}, \Sigma_x] = 0$. However a 2–4 ms proton purging pulse cannot be viewed as a sequence of $\frac{\pi}{2}(I_x + I'_x)$ discrete pulses, because of the unavoidable RF inhomogeneity, leading in practice to coherence loss. The role of proton purging pulses in inverse detected heteronuclear correlation via SQC was recently addressed by Tate et al. (1982), who obtained a more conspicuous improvement of the spectral S/N ratio from experiments with purging pulse at the end of the retro–INEPT transfer (period 3). Besides the obvious improvement in solvent suppression, expected when purging is applied as close as possible to acquisition time, the better performance of the period 3 purging pulse should be ascribed also to the transverse relaxation

Period	Starting Density	Final Density
1	$\sigma(1)= -2\Sigma_y + S_z$	$\sigma(2)= -2\Sigma_x S_z \cdot m_1 - 2\Delta_x S_z \cdot m_2 +$ $+ 4\Pi_{zx}^- S_z \cdot m_3 + 4\Pi_{zy}^- S_z \cdot m_4 +$ + other terms
2	$\sigma(2")= -2S_y(\Sigma_z+\Delta_z)$	$\sigma(3)= 2\Sigma_z S_y \cdot m_1 + 2\Delta_z S_y \cdot m_2 +$ + other terms
3	$\sigma(3')= -2S_z(\Sigma_y+\Delta_y)$	$\sigma(4)= -\Sigma_x \cdot m_1 - \Delta_x \cdot m_2 +$ $+ 2\Pi_{zx}^+ \cdot m_3 + 2\Pi_{zx}^- \cdot m_4 +$ + other terms

Period	m_1	m_2	m_3	m_4
1	1.000	0.993	0.014	0.099
2*	t_1-dependent	t_1-dependent		
3	0.997	0.985	0.004	0.025

*when all the theoretically expected frequency components from $\sigma(3)$ elements are considered, a null $I \rightarrow I'$ transfer is obtained, irrespective of $\Delta\omega_I$ and $J_{II'}/J_{IS}$ ratio (see text).

Table 3.2.I Evolution of the relevant density terms of the heteronuclear $\{I,I',S\}$ spin system ($I=S=\frac{1}{2}$) throughout SQC-NOESY experiment. F_1 frequency labelling factors are omitted. $\Delta\omega_I=\pi J_{IS}$; $J_{II'}/J_{IS}=0.06$.

rate of the preserved coherence (T_2^{-1} of proton transverse magnetization $< T_2^{-1}$ of proton antiphase coherence (Bax et al., 1990)).

The same calculation procedure used for period 1 was employed also for period 3, with the proper set of starting coherences (Table 3.2.I), chosen such that i) exhibit ω_S labelling in t_1; ii) be single quantum; iii) evolve into detectable components.

Inspection of Table 3.2.I shows that proton strong coupling introduces only

very small changes in the coefficients of the relevant coherences emerging from steps 1 and 3, at least for $\frac{J_{II'}}{J_{IS}} = 0.06$. At the same time, the extent of "unexpected"coherences created during those periods is rather limited and should be removed by the purging pulses or (for residual detectable components from $\Pi_{zx}^{\pm}$) should lead to dispersive antiphase magnetization, with null contribution to volumes of both auto and NOE–relayed cross–peaks (when digitization is sufficient).

This result is not unexpected as the oscillatory net magnetization transfer due to isotropic coupling is allowed to take place only for short delays compared to $J_{II'}^{-1}$, such as those of periods 1 and 3 ($\frac{1}{2J_{IS}}$), with partial cancellation of the net transfer due to the πL_x pulse bisecting both intervals (vide infra).

The main contribution of the proton strong coupling due to condition (3.2.1) in SQC–NOESY spectra is actually accumulated throughout t_1 evolution.

Following the simultaneous ($\frac{\pi}{2}$) pulse pair closing period 1, $\sigma(2')$ is conveyed into $\sigma(2'') = -2S_y(\Delta_z + \Sigma_z)$. Calculations could be performed in the same way as outlined for periods 1 and 3, with a difference due to the midpoint π pulse, applied now only to I and I' spins. Analogously to eq. (3.2.7), we can write eq. (3.2.10) as:

$$\sigma(3) = \exp(-i\pi 2\mathbf{S}_x)\exp(-i\mathbf{S}_z\omega_S t_1)\exp(-i\underline{\mathbf{H}}_1'\frac{t_1}{2})\exp(-i\mathbf{H}_1\frac{t_1}{2})\sigma(2'') \quad (3.2.10)$$

where $\underline{H}_0' = S_z\omega_S - c^+S_z$ and $\underline{H}_1' = aA - b^+\Delta_z$, and $S_z\omega_S t_1 = (H_0' + H_0)\frac{t_1}{2}$ accounts for the heteronuclear decoupling due to the midpoint π proton pulse.

J_{IS} refocusing at the end of each t_1 interval, however, will not suppress the net transfer that occurred throughout, between protons obeying condition (3.2.1). In this respect, it is worth noting the difference between the two half–evolutions in period 2 and in periods 1 and 3. The midpoint inversion pulse of periods 1 and 3 reverses the heteronuclear spin population difference too, thus affecting the primary factor responsible for the proton strong coupling, i.e. the precession frequency difference between I and I' coherences. On the other hand, t_1 midpoint inversion only applies to protons where strong coupling (by definition invariant to any inversion because $[\mathbf{II}', \Sigma_\alpha] = 0$) develops solely from S spin antiphase coherences, i.e. coherences that are invariant to the proton Zeeman Hamiltonian.

Following on the calculations from eq. (3.2.10), according to the procedure described above, we are faced with the evaluation of the effect of S_z, included

in coefficients b^+ (see eqs. 3.2.3), onto $\sigma(2'')$ elements. In fact $\sigma(2'')$ no longer contains only projectors on the eigenstates of S_z, i.e. $[S_z, \sigma(2'')] \neq 0$, which rules out any possibility of expressing S_z by means of a "numerical operator", as we did before. Nevertheless, it can be shown again that $\sigma(2'')$ evolves within a very limited eigenspace of $\underline{H}_1$ and H_1, namely the one spanned by the basis $\lambda_3 = \{S_y\Delta_z, S_y\Pi^-_{xy}, S_x(\frac{1}{4} + I_zI'_z), S_yM^+_{xy}\}$ (see eqs. (3.2.3)). The calculation can be thus performed with explicit account for the S–dependence of the density operator and finally completed with the application of the heteronuclear Zeeman and πI_x terms (eq. (3.2.10)).

Examination of the resulting coherences reveals that the most significant effects are obtained for $S_y\Sigma_z$ and $S_y\Delta_z$. Their 'imbalance' reflects the transfer between I and I' because:

$$2S_y(m\Sigma_z + n\Delta_z) = 2S_yI_z \tag{3.2.11}$$

only when $m = n = 1$. Since in our case $m = 1$ anyway, imbalance arises because n, which has acquired a dependence on t_1, is now $\neq 1$. By definition m and n, the switching coefficients between the "collective"basis defined in eqs. 3.2.3 and the Cartesian spin product operator basis (Braunschweiler and Ernst, 1983), are not unitary when coherence evolution can no longer be factorized in single spin density terms. Therefore, somehow pictorially, this departure from unity has been referred to as imbalance.

Figure 3.2.2 shows the overall amount of $S_y\Delta_z$ coherence at the end of t_1, i.e. the extent of S_z/Δ_z imbalance, as a function of $\Delta\omega_I$, obtained for $\frac{J_{II'}}{J_{IS}} = 0.06$. Minimum, i.e. maximum imbalance, occurs when $\Delta\omega_I$ is slightly larger than πJ_{IS}, corresponding to a negligible effect for $J_{IS} = 0$ (the relative curve is also reported in Figure 3.2.2 for comparison). Conversely, the presence of a heteronuclear splitting appears quite effective in reducing S_z/Δ_z imbalance for very small $\Delta\omega_I$, when compared with the results obtained for $J_{IS} = 0$.

The curves of Figure 3.2.2 were calculated for t_1=15 ms, a realistic value for SQC–NOESY experiments on unenriched samples. In order to evaluate the actual experimental intensity developing during t_1 from heteronuclear splitting magnification of proton strong coupling effects, diagonalization of matrix exponentials in eq. (3.2.10) should be performed for the different frequency components of the relevant coherences.

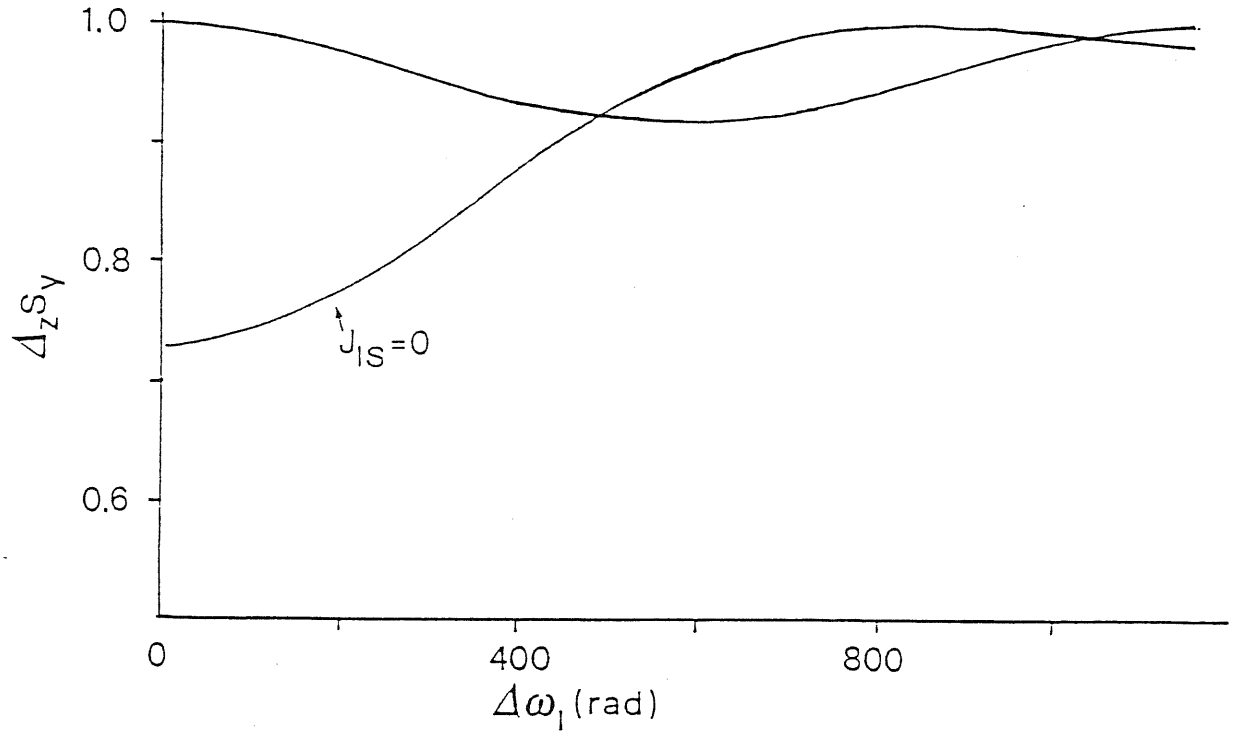

Figure 3.2.2 Extent of S_z/Δ_z coherence imbalance (eq. (3.2.11)) evolving during t_1, as a function of $\Delta\omega_I$, obtained for $J_{II'}/J_{IS}$=0.06 and t_1=15 ms. Minimum, i.e. maximum imbalance, occurs when $\Delta\omega_I$ is slightly larger than πJ_{IS}, corresponding to a negligible effect for J_{IS}=0 (the relative curve is also reported for comparison).

In principle, irrespective of t_1 and $\Delta\omega_I$, a null overall integral is expected for the $I \rightarrow I'$ transfer from S_z/Δ_z imbalance growing during t_1, because at $t_1 = 0$ the transfer is zero. This is actually verified in our calculation by summing the SQC–NOESY intensities of all the theoretically observable frequency components, other than I auto–peak, within the $I--I'$ system. This zero–integral theoretical pattern spans a wide frequency range in F_1 (of the order of $2[J_{IS} + \frac{\Delta\omega_I}{2\pi}]Hz$). However, its intensity distribution is rather uneven because the largest component always occurs at (ω_S, ω_I) frequency, i.e. the cross–peak frequency (except for $\Delta\omega_I = \pi J_{IS}$), whereas the remaining (not vanishing) components are more or less spread in F_1, depending on $\Delta\omega_I$ (or $J_{II'}$ if $2\pi J_{II'} > \Delta\omega_I$). When $\Delta\omega_I = \pi J_{IS}$, the

overall $I \rightarrow I'$ transfer intensity is concentrated in three components, the largest at (ω_S, ω'_I) frequency, symmetrically flanked by two smaller ones, of opposite sign, spaced by $2\pi J_{II'}$. For $\frac{J_{II'}}{J_{IS}} = 0.06$, depending on $\Delta\omega_I$, the component at (ω_S, ω'_I) frequency ranges from 0 to 7% of the total $(I + I')$ observable magnetization.

At the ordinary t_1 underdigitization level of SQC–NOESY experiments, a precise quantitation of the intensities is hindered by the inherent limits of the corresponding low resolution spectrum. As a result, integration of the I' cross–peak will be biased by the large intensity component, in practice often the only appreciable one, leading to a non–zero value, even when the contributions coming from the INEPT steps are really negligible. At the same time the I auto–peak integral will correspondingly be underestimated by the amount the cross–peak integral deviates from zero.

Experimental test

An experimental test of the quantitative predictions of Table 3.2.I and Figure 3.2.2 is presented.

Figure 3.2.3a depicts the aromatic region of a ^{1}H–^{13}C SQC–NOESY spectrum of BPTI obtained with $t_m = 5\mu$s at 11.76 T. Examination of the contour plot reveals the presence of some correlations expected from the detailed assignment reported by Wagner et al. (1987). In spite of the heteronuclear spreading, most of the cross–peaks are too close to their parent auto–peak to safely estimate volumes (see for instance the cluster including F22 and F4 correlations).

As a rule, quantitation of homonuclear cross–relaxation in 2D ^{1}H–^{13}C SQC–NOESY spectra, requires resolution of I and I' resonances on both proton and heteronuclear frequency scales, which imposes their direct coupling to distinct heterospins.

Resolved connectivities are observed in Figure 3.2.3a only for Y10 3,5H–2,6H, F33 4H–3,5H, Y21 3,5H–2,6H, and, at lower contour levels, for Y35 2H–3H and Y35 6H–5H (see Figure 3.2.3 caption for nomenclature); our concern will be focussed accordingly.

In view of the tumbling rate of the molecule ($\approx$ 3 ns (Molinari et al., 1992)),

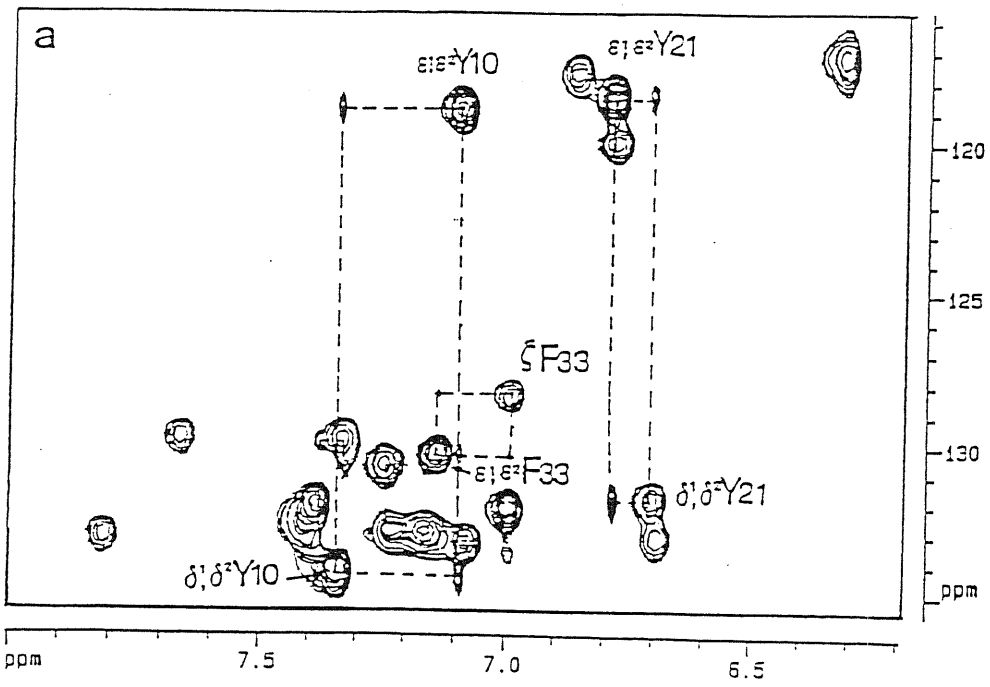

Figure 3.2.3a See caption Figure 3.2.3b

connectivities due to dipolar exchange can hardly show up at the short t_m employed. However, some incoherent transfers may occur due to chemical exchange processes, such as ring flipping of suitable rate. Among the residues giving rise to resolved connectivities, only Y35 exhibits a slow ring flipping motion (50 s^{-1} at 309 K (Wagner et al., 1987). Therefore, excluding the correlations from Y35 (actually due to a mixed strong–coupling/chemical exchange mechanism (Wagner et al., 1987; Molinari et al., 1992)), the remaining resolved ones must arise from coherent transfers between J coupled protons.

Contrary to conventional homonuclear NOESY, in a ^{1}H–^{13}C SQC–NOESY experiment it is not necessary to bother about ZQ interference because the proton antiphase terms, transferred into ZQ coherences by the mixing pulse preceding tm, evolve with an additional $\sin(\pi J_{II'}/2J_{IS})$ attenuation and are further reduced by the purging pulse at the end of the retro–INEPT transfer (period 3). Therefore a SQC–NOESY experiment with $t_m \simeq 0$, besides chemical exchange transfers,

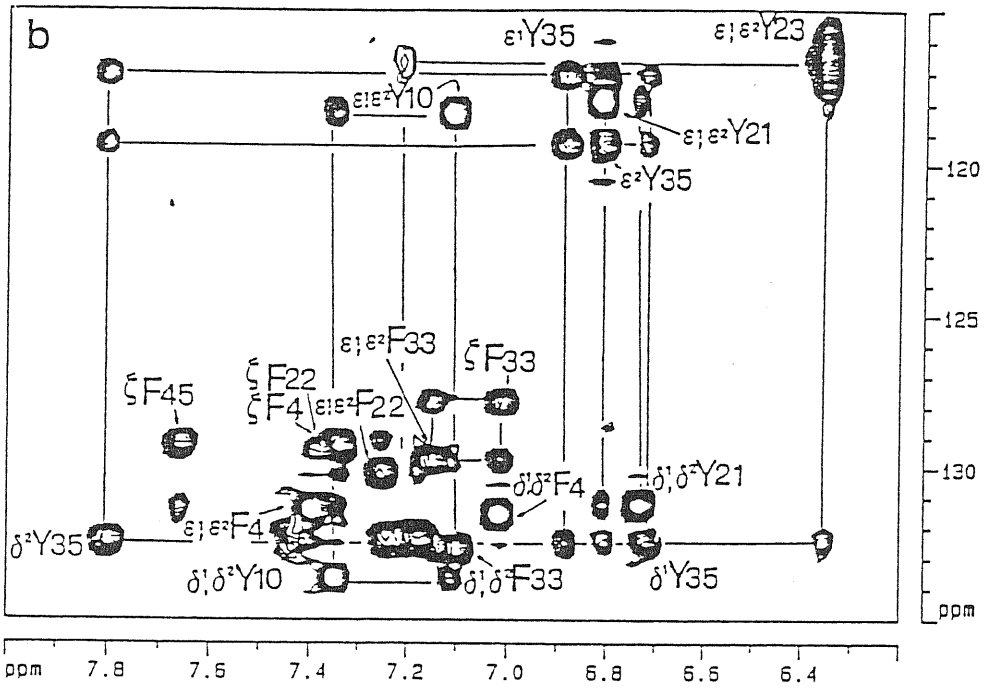

Figure 3.2.3b ^{1}H–^{13}C SQC–NOESY spectrum of 14 mM BPTI (Aprotinin, Fluka, Buchs, Switzerland), pH^{*} = 4.6 (pH^{*} is the uncorrected pHmeter reading). Pure phase spectra were acquired at 309 K with t_m=5 ms (a) and 100 ms (b) on a Bruker AM500 spectrometer, operating at 500 and 125 MHz for ^{1}H and ^{13}C, respectively. The acquisition was performed without spinning the sample tube (5 mm). Delays of periods 1 and 3 (Figure 3.2.1) were adjusted on an average heteronuclear direct coupling of 143 Hz and the purging pulses were set to 3.5 ms. GARP1 (Shaka et al., 1985) was employed as a decoupling sequence using a ^{13}C $\frac{\pi}{2}$ pulse of 44.5 ms. Acquisition time was 0.141 s in t_2 and 7.5 ms in t_1 and 640 transients were collected for each t_1 increment. Sweep widths were set to 7262 and 20833 Hz in t_2 and t_1, respectively, and quadrature detection in t_1 was achieved by TPPI (Drobny et al., 1979). The experimental data were weighted using a squared sine–bell function shifted by $\frac{\pi}{3}$ in both dimensions and zero filling was performed in t_1, to end up with a 2K×1K matrix. Assignments are reported according to Wagner et al. (1987), using the aminoacid single letter code and the IUPAC–IUB Greek code designation for carbons (IUPAC–IUB commission, 1970). In the text we avoided reporting the IUPAC–IUB naming scheme for each single aromatic proton and used numerals instead, i.e. $C\delta_1H$=2H, $C\epsilon_1H$=3H, $C\zeta H$=4H, $C\epsilon_2H$=5H, $C\delta_2H$=6H. Dashed lines in (a) indicate the resolved connectivities arising from proton strong coupling magnified by heteronuclear splitting.

should display only coherent transfers due to proton strong coupling.

Assuming $J_{HC} = 130 \div 160$ Hz and $J_{HH} = 7 \div 8$ Hz, Y21 connectivities arise from inherent strong coupling ($\Delta\omega_I = 0.08$ ppm, i.e. 40 Hz at 500 MHz, between 2,6H and 3,5H), whereas Y10 cross-peaks ($\Delta\omega_I = 0.23$ ppm, i.e. 115 Hz at 500 MHz) are due to strong coupling enhanced by heteronuclear splitting (condition (3.2.1)). An intermediate situation is observed for F33 connectivities. Although the separation between 4H and 3,5H meets condition (3.2.1) ($\Delta\omega_I = 0.14$ ppm), further transfers should take place during tm and t2 within the whole spin system because of the small $\Delta\omega$ between 3,5 and 2,6 proton pairs (0.06 ppm).

The relative intensities of some of these J connectivities, with respect to the corresponding auto-peak and total system (auto+cross) intensities , are listed in Table 3.2.II. The precision of the values reported is limited by the actual F_1 resolution of the experiment (t_1=7.5 ms), a typical one for unenriched samples of medium-sized macromolecules. Volume values are thus representative of the effects detectable in real instances.

		t_m = 5 μs		t_m = 100 ms			
Pair	Δω	cp/ap	cp/(cp+ap)	cp/ap	τ_c	[cp/ap]	[τ_c]
Y10 2,6/3,5	0.23	4.55	4.35	13.2	5.4_3	7.84	3.2_6
Y10 3,5/2,6	"	4.55	4.35				
Y21 3,5/2,6	0.08	13.8	11.5	12.5	5.1_9		
F33 3,5/4	0.14	2.15	2.05	18.7	7.7_6		

Table 3.2.II Cross-peak (cp) / auto-peak (ap) volume ratios (%) of resolved vicinal aromatic connectivities in ^{1}H-^{13}C SQC-NOESY spectra of BPTI at different mixing times. For t_m=5μs the corresponding fractional intensity percentages are listed. The specific $\Delta\omega$ values (ppm) for the corresponding proton pairs are also reported (Wagner et al., 1987).

Yet the extent of strong coupling transfer observed for Y10 agrees quite satisfac-

torily with the theoretical value of $\approx 3.5\%$ expected for the specific $\Delta\omega_I$ and the experimental resolution conditions.

In a typical SQC–NOESY spectrum (i.e. with $t_m \gg 5\mu s$) the volumes of auto and cross–peaks can be corrected for the strong coupling contributions coming from condition (3.2.1). Table 3.2.II reports the volumes of Y10, Y21 and F33 aromatic vicinal connectivities, measured in ^1H–^{13}C SQC–NOESY of BPTI with $t_m = 100\mu s$ (Fig. 3.2.3b). The remaining acquisition parameters were left unchanged with respect to the experiment carried out with $t_m = 5$ ms.

The separation of adjacent aromatic protons is 0.248 nm. By imposing this distance and using the cross/auto–peak volume ratio method to back calculate the local tc (Molinari et al., 1992), one obtains 5.43 ns for Y10, 5.19 ns for Y21 and 7.76 ns for F33. These values, albeit reasonable in principle, are rather different from the average $\tau_c = 3.0$ ns calculated for the whole molecule (Molinari et al., 1992).

As Y21 and F33 are known to be affected by extra contributions coming from inherent strong coupling, we can safely attempt an approximate correction only for Y10. By subtracting from the cross–peak and adding to the auto–peak the strong coupling coherent transfer fractional intensity, measured at $t_m \approx 0$ (i.e. cp/(cp+ap) in Table 3.2.II), we obtain $\tau_c = 3.26$ ns, a figure much closer to the average molecular τ_c.

Specific interproton separations can thus be recalculated with this value. Table 3.2.III shows some distance data obtained for Y10 aromatic hydrogens using the mean molecular τ_c and the local calibration τ_c values, calculated without and with correction for strong coupling effects. No major improvement is obtained in the latter case with respect to the separations estimated with the overall molecular τ_c.

As expected, the actual value of the side chain local τ_c may bear some relevance in approximate distance evaluation only when it is found significantly shorter than the overall molecular counterpart. The deviations from X–ray separations reported in Table 3.2.III should most likely arise from the assumption of isotropic spectral density function, as well as from spin diffusion.

At variance, corrections for strong coupling effects may prove important with backbone reference proton pairs when extracting the molecular tumbling rate.

	X-ray	τ_c=3.0ns a)	τ_c=5.4$_3$ns b)	τ_c=3.2$_6$ns c)
Y10 2,6-Y10α	0.251	0.26$_4$	0.29$_2$	0.26$_8$
Y10 2,6-Y10β	0.242	0.23$_2$	0.25$_7$	0.23$_5$
Y10 3,5-R39β	0.278	0.20$_6$	0.22$_8$	0.20$_9$

a) mean molecular τ_c

b) local τ_c without correction for strong coupling

c) local τ_c with correction for strong coupling

Table 3.2.III Interproton distances (nm) from BPTI Y10 aromatic connectivities.

Improving the overall τ_c accuracy should avoid systematic errors in subsequent calculations.

It must be stressed here that, strictly speaking, the strong coupling contribution from condition (3.2.1) should be accounted for not only with the connectivity of the strongly coupled pair. A corrected auto–peak intensity should in practice be used for NOE calculations involving cross–peaks from "external"nuclei, i.e. not belonging to the strongly coupled system, when the width of the whole auto–peak pattern is likely to exceed F_1 integration limits.

Conclusions

^{1}H detected heteronuclear correlation spectra may be affected by second order anomalies due to proton strong scalar coupling originating either from inherently strong coupled ^{1}H spins or from ^{1}H resonance proximity determined by heteronuclear couplings.

In ^{1}H–^{13}C SQC–NOESY quantitative analysis any strong coupling contribution of the latter type can be computed using the specific parameters of the system under investigation in the procedure described here. This is because heteronuclear splitting magnified strong coupling is no longer effective during t_m and t_2, when any relevant evolution concerns only proton longitudinal and transverse magnetizations.

At variance, when the proton system is inherently strong coupled, the

isotropic coupling effects also extend throughout t_m and t_2 and can be fully accounted for using the treatment reported by Kay et al. (1986b). However, according to these authors, a generalized assessment of the NOE intensity deviations is rather hard, because of the number of variables involved (e.g. correlation times, internuclear distances, spin system type, etc.) (Kay et al. 1986a,b).

Thus practical recipes for correcting amplitudes of ^{1}H–^{13}C SQC–NOESY connectivities can only apply for strong coupling effects elicited due to heteronuclear splittings. Relaxation can be neglected as long as the overall durations of INEPT and t_1 intervals remain limited, which is usually the case with unenriched samples of medium sized macromolecules.

Assuming $\frac{J_{II'}}{J_{IS}} = 0.06$, a correction amounting to 0–7% of the auto and cross–peak volume sum should be applied to the connectivities of the strongly coupled pair, depending on $\Delta\omega_I$. These conclusions apply only to natural abundance or slightly enriched ($\leq 10\%$) samples.

3.3 EVALUATION OF J COUPLING CONSTANTS FROM PEAK AMPLITUDES OF TOTAL CORRELATION SPECTRA

Introduction

Total correlated spectroscopy (TOCSY)(Braunschweiler and Ernst, 1983; Bax and Davis, 1985) has become a very widely used tool among NMR spectroscopists. Scalar coupling information from 2D or multidimensional spectra is employed to identify isolated spin systems and to establish direct and indirect couplings among nuclei, which is a necessary step in virtually every resonance assignment strategy. In practice, it is necessary to design an appropriate pulse sequence during which the spin systems experience an average Hamiltonian (Haeberlen and Waugh, 1968) where only scalar couplings are retained, being the Zeeman terms averaged to zero.

Compared to other kind of experiments aiming at unravelling scalar coupling networks (like Correlated Spectroscopy (COSY)(Aue et al., 1976) and Relayed Coherence Transfer Spectroscopy (RCT)(Eich et al., 1982; Bolton and Bodenhausen, 1982), TOCSY has several advantages, well known to experimentalists. Sensitivity for instance improves in TOCSY spectra due to the in–phase pattern of cross–peaks, as opposed to the antiphase character of the corresponding connectivities in COSY–like spectra that may lead to mutual cancellation of positive and negative lobes within a single or among different cross–peaks. Also a number of ambiguities, persisting even after combined analysis of COSY–like and RCT maps, can often be removed with TOCSY, where connectivity families spanning most or the whole spin system are not unusual. This, besides improving the exploitation of the available resolution space, also makes TOCSY maps very valuable for automatic pattern recognition.

The net coherence transfer versus a null overall cross–peak volume in COSY–like schemes represents another interesting feature of TOCSY, only very seldom addressed in the literature.

Explicit calculation of the time development of the magnetization under isotropic mixing Hamiltonian requires the diagonalization of rather large matrices even for small spin systems, and this is probably the main reason why the quan-

titative information buried in TOCSY spectra is not usually exploited in order to get structural information.

For the most simple case of two coupled spins (Braunschweiler and Ernst, 1983), and for larger systems with proper symmetry properties, analytical solutions and discussions of the suitable theoretical tools are found in the literature (Chandrakumar and Subramamnian, 1985; Chandrakumar, 1987; Visalakshi and Chandrakumar, 1987).

Very recently detailed calculations on biopolymer residues have been published by Cavanagh et al. (1990), together with an exhaustive discussion of the phenomenon. Since the evolution of the magnetization under isotropic mixing can be predicted and comparison with experimental data can be performed, one may think to exploit TOCSY spectra to obtain J coupling constants via minimization of a suitable error function. Such a function most probably possesses several local minima so that a starting guess, not too far from the real values, should be required by any iterative simulation procedure.

In the following we describe some approximations that may serve the purpose and a numerical algorithm we have implemented on our computer and successfully used. An experimental test has also been performed on two model compounds which may be representative of real life situations.

Materials and methods

All NMR experiments were performed at 298 K with a Bruker AM 500 spectrometer operating at 500.13 and 125.76 MHz for proton and carbon, respectively. 2D spectra were collected with quadrature detection in both time dimensions, using the TPPI procedure for t_1 (Drobny et al., 1979).

The complex *trans*–$RuCl(DMSO)_2(H_2O)\{d(GpG)\}$ (in the present notation DMSO stands for dimethylsulfoxide) was obtained by reaction of dinucleotide d(GpG) with *trans*–$RuCl_2(DMSO)_4$. The synthesis of the reactants and the conditions of complexation reaction have been described earlier (Esposito et al., 1992).

The HPLC purified complex was liophylized and dissolved in D_2O (CIL, Cambridge U.K.) at a concentration $\sim$ 1.5 mM and pH (uncorrected) = 5.5.

2D TOCSY spectra (Müller and Ernst, 1979) were obtained with the pulse

scheme proposed by Rance (1987). A single RF source was employed for pulses and spin–lock mixing with a constant γB_2 (8.3 kHz). Spin–lock was accomplished through a WALTZ16 train (Shaka et al., 1983) lasting 11.6, 23.1, 46.2 and 92.5 ms in the different experiments.

Acquisition times were 51.2 and 204.8 ms in t_1 and t_2, respectively and 64 transients were collected for each t_1 increment. A relaxation delay of 1.6 s was always allowed during which the residual HOD resonance was saturated. The size of the experimental matrices (512 $\times$ 2K in t_1 and t_2, respectively) was enlarged to 4K $\times$ 4K points before filtering (square sinebell shifted by $\pi/2$) and transforming.

Biotin (Fluka, Buchs, Switzerland) spectra were obtained by a 0.19 M solution in DMSO d_6 (Aldrich, Milwaukee, WI, U.S.A.). Homonuclear TOCSY experiments were performed either using the Rance sequence (Rance, 1987), with a WALTZ16 mixing lasting 13.7 ms, or the scheme due to Bax and Davis (1985), with a MLEV17 spin–lock 11.4 ms long (including two sandwitching trim pulses of 1ms). In both experiments the decoupler was employed as RF source with $\gamma B_2 = 7.0$ kHz. Acquisition times were 64 and 256 ms in t_1 and t_2, respectively and the relaxation delay was 2.5 s. Matrix sizes and processing protocols were the same as described above. Natural abundance ^{13}C–correlated ^1H–detected relayed TOCSY experiments were performed using the sequence proposed by Otting and Wüthrich (1988). It selects single quantum heteronuclear coherences for t_1 evolution and hence is shortly referred to as ^{13}C–^1H SQC–TOCSY. The delays for the two Overbodenhausen steps (Bodenhausen and Ruben, 1988) flanking t_1 evolution were tuned on an average $^{13}C - {}^1H$ coupling of 135.9 Hz (Hikura and Hikichi, 1987) and heteronuclear decoupling was accomplished during detection by means of the GARP sequence (Shaka et al., 1983), using a reduced power for ^{13}C pulses ($\pi/2 = 104$ μs). The MLEV17 spin–lock was performed with the same conditions of power and duration as the corresponding homonuclear experiments, except for the first purging pulse (2ms). Thus the total mixing time amounted to 12.4 ms. An additional purging pulse (2ms) was also applied at the end of the first Overbodenhausen step to suppress ^{12}C bound proton coherences as suggested by Otting and Wüthrich (1988). Acquisition times were 19 and 256 ms in t_1 and t_2, respectively, with 2.5 s relaxation delay and 128 transients for each t_1 increment. The overall matrix size was 380 $\times$ 2K (t_1 and t_2, respectively), zero–filled to 2K $\times$

2K (reals) prior to weighting (square sinebell shifted by $\pi/2$ in both dimensions) and transforming.

Baseplane distortions were always removed by linear prediction of the first point in t_1 and t_2 (Marion and Bax, 1989) and the baseline was corrected in F_2 by means of a 9^{th} degree polynomial function. Processing and peak volume measurements were performed on a Silicon Graphics 4D320 VGX station using the Hare Research Inc. (Bothell, WA, U.S.A.) software.

Theory

We will consider the most general spin system evolving under ideal isotropic mixing, i.e. neglecting any other possible term in the Hamiltonian, like Zeeman contribution or relaxation effects. The time evolution of the density matrix ρ is described by the Liouville–Von Neumann equation:

$$(i\hbar)\frac{d\rho}{dt} = [H, \rho(t)] \tag{3.3.1}$$

where, in the present case $H = \sum 2\pi J_{ij}\mathbf{I}_i\mathbf{I}_j$, for a system consisting of n 1/2 spins with scalar couplings J_{ij}. Successive differentiation of this equation leads to express the n–th order derivatives of $\rho(t)$, with respect to the time, as iterative commutators of H with ρ. In general we have:

$$(i\hbar)^n\frac{d^n\rho}{dt^n} = \underbrace{[H,[H,\ldots[H,\rho(t)]\ldots]]}_{n-times} \tag{3.3.2}$$

We may exploit these relationships to understand the net coherence transfer occurring during TOCSY mixing time. In particular a Taylor expansion of $\rho(t)$ evidentiates the relayed character of the coherence transfer among not directly coupled spins. Density matrix at time t may be expressed as follows:

$$\rho(t) = \rho(0) + (t/i\hbar)[H,\rho(0)] + 1/2!(t/i\hbar)^2[H[H,\rho(0)]] + \ldots \tag{3.3.3}$$

Each term of $\rho(t)$, in particular the observables, may be split in zero, first, ..., n–th order contributions, being each n–th order term related to the (n−1)–th order terms. To make this relationship clear we may write the n–th order term of $\rho(t)$ as

$$1/n!\rho^n(t) \tag{3.3.4}$$

with

$$\rho^n(t) = (t/i\hbar)^n \underbrace{[\mathrm{H},[\mathrm{H},\ldots[\mathrm{H},\rho(0)]\ldots]]}_{n-times} \tag{3.3.5}$$

where $\rho^n(t)$ can be expanded in any orthonormal basis set of the Liouville space $\{B_i\}$, e. g.

$$\rho^n(t) = (t/i\hbar)^n \sum c_i B_i \tag{3.3.6}$$

Then

$$\rho^{n+1}(t) = (t/i\hbar)[H,\rho^n(t)] = (t/i\hbar)^{n+1} \sum c_i [H,B_i] \tag{3.3.7}$$

Therefore any term B_i at any step of the expansion will produce a term $[H,B_i]$ at the following step. In this way the time development of each term of $\rho(t)$ may be traced back through the expansion. Choosing appropriate units, in the most simple case of a two spin system, where the following equalities hold:

$$\rho(0) = I_{1z} \tag{3.3.8}$$

$$\rho^1(0) = 2\pi J_{12} t(I_{1x}I_{2y} - I_{1y}I_{2x}) \tag{3.3.9}$$

$$\rho^2(0) = -I_{1z}(2\pi J_{12}t)^2/2 + I_{2z}(2\pi J_{12}t)^2/2 \tag{3.3.10}$$

we would then say that the net magnetization transfer from spin 1 to spin 2 proceeds via ($I_{1x}I_{2y}$ - $I_{1y}I_{2x}$) coherence.

NMR spectroscopists are probably familiar with a similar approach in the analysis of NOESY spectra, where the expansion of the exponential of the relaxation superoperator is useful in two respects: i) it allows for approximate calculations and ii) it leads to an understanding of "spin diffusion"and related non–trivial effects as the change of sign of second order NOESY peaks for small molecules (Neuhaus and Williamson, 1989). There are however some relevant differences, due to the coherent character of the transfer in TOCSY, which will be rendered explicit later. We have computed the Taylor expansion of $\rho(t)$ up to the fourth order term, starting from $\rho(0) = I_{wz}$, with w generic spin identifier, for the most general case where $H = \sum 2\pi J_{ij}\mathbf{I}_i\mathbf{I}_j$. Therefore we will only be concerned with z–axis (where z direction may be chosen according to the experimental conditions) single spin magnetization terms which eventually can be observed (Table 3.3.I).

$$
\begin{aligned}
\rho^0 = \rho(0) &= I_{wz} \\
\rho^1 &= \sum_k a_{wk}\Pi_{wk} \\
\rho^2 &= -\sum_k a_{wk}^2\Delta_{wk} + \sum_{j\neq k\neq w} a_{wk}a_{wj}(I_{jz}\mathrm{I}_w\mathrm{I}_k - I_{wz}\mathrm{I}_j\mathrm{I}_k) + \\
&\quad + \sum_{j\neq k\neq w} a_{wk}a_{kj}(I_{kz}\mathrm{I}_w\mathrm{I}_j - I_{jz}\mathrm{I}_w\mathrm{I}_k) \\
\rho^3 &= -\sum_{j,k} a_{wk}^2 a_{wj}\Pi_{wj}/2 + \sum_{j,k} a_{wk}^2 a_{kj}\Pi_{kj}/2 \\
&\quad + \sum_{j\neq k\neq w} (2a_{wk}a_{wj}^2 - a_{wk}^2 a_{wj} - a_{wk}^2 a_{kj} - a_{wk}a_{wj}a_{kj})\Pi_{jk} + \\
&\quad + \sum_{j\neq k\neq w} (-2a_{wk}a_{wj}^2 - a_{wk}a_{kj}^2 + 2a_{wk}a_{wj}a_{kj})\Pi_{wk} + \\
&\quad + \sum_{j\neq k\neq w} (a_{wk}a_{wj}a_{kj} + a_{wk}^2 a_{wj} + a_{wk}^2 a_{kj} - 2a_{wk}a_{kj}^2)\Pi_{jw} + \\
&\quad + \text{other non observable terms} \\
\rho^4 &= \sum_{j,k} a_{wk}^2 a_{wj}^2\Delta_{wj}/2 - \sum_{j,k} a_{wk}^2 a_{kj}^2\Delta_{kj}/2 \\
&\quad + \sum_{j\neq k\neq w} (-3a_{wk}^2 a_{wj}^2 - 2a_{wk}^2 a_{kj}^2 + 2a_{wk}a_{wj}a_{kj}^2)I_{wz}/2 + \\
&\quad + \sum_{j\neq k\neq w} (3a_{wk}^2 a_{wj}^2 + 2a_{wj}^2 a_{kj}^2 - 2a_{wk}a_{wj}a_{kj}^2)I_{jz}/2 + \\
&\quad + \text{other non observable terms}
\end{aligned}
$$

Table 3.3.I ρ^n represents the n-th order term of the series expansion as defined in the text. To simplify the notation a_{ij} is used instead of $2\pi J_{ij}t$ (a_{ii} is assumed equal 0) and a shorthand is used to collect operators: Π_{ij} and Δ_{ij} stand for $(I_{ix}I_{jy} - I_{iy}I_{jx})$ and $(I_{iz} - I_{jz})/2$, respectively.

Other zero–quantum coherences, evolving in antiphase observable magnetization during t_2, which develop as well are not considered since their overall net intensity is zero. As can be gleaned by Table 3.3.I the first observable coherences (apart for the trivial starting magnetization) appear in the second order term. These represent the initial development of the transfer from spin w to the directly coupled

spins, unaffected at this level of the series expansion by the presence of the other spins in the system. In turn, each of these coherences gives rise, in the fourth order term of the series expansion, to other observable coherences of the directly coupled spins.

If all the coherence transfer were accounted for by these terms, which are collected in the first line of the fourth–order term in Table 3.3.I, the problem of the time development of the observable coherences would amount to solve the equations of motion of a set of coupled harmonic oscillators and the calculations would be significantly reduced. Unfortunately three-spin coherences in the second order term (Table 3.3.I), which do not give rise to any observable coherence in the next term of the expansion, being the Hamiltonian the sum of two spin Hamiltonians, can contribute to the observable transfers in the successive term (the fourth order term in Table 3.3.I). It is worth notice therefore that the term "collective modes"(Braunschweiler and Ernst, 1983; Müller and Ernst, 1979), proposed to describe the time evolution of the magnetization, does not refer in any way to a kind of "normal modes"in the sense mentioned above, except for very simple (two spins) or symmetrical systems.

This process is also different from NOESY second order transfer or "spin diffusion", that only proceeds through z–axis single spin magnetizations, e.g.:

$$I_{1z} \longrightarrow I_{2z} \longrightarrow I_{3z}$$

while in TOCSY we may have (for instance in a three spin system) a possible pathway like:

$$I_{1z} \longrightarrow (I_{1x}I_{2y} - I_{1y}I_{2x}) \longrightarrow I_{3z}\mathrm{I}_1\mathrm{I}_2 \longrightarrow (I_{3x}I_{2y} - I_{3y}I_{2x}) \longrightarrow I_{3z}$$

The third order term contains several unobservable multispin coherences, some of which (shown in Table 3.3.I) may be brought into single spin z–coherences in the next term of the expansion. The absence of observable coherences in the third order term of the expansion tells us that for short mixing times only directly coupled spins will exchange magnetization and, moreover, that the relative magnetization transferred to spin k will be $(2\pi J_{wk}t)^2/4$ to an accuracy of the order of $(2\pi Jt)^4$, being J a typical value for the coupling constants of the system.

This discussion constitutes the basis for the algorithm we have employed to derive coupling constants from the peak intensities of TOCSY or SQC–TOCSY spectra.

Before performing any quantitative analysis, the cross– and auto–peak intensities must be normalized in such a way that the sum of all the intensities along ω_1 equals 1. The normalization of the peaks is of fundamental importance since, due to the usually limited relaxation delay, only partially recovered magnetizations may be present at the beginning of the TOCSY mixing time, while, on the other hand, waiting for a complete recovery of the magnetization would enormously increase the duration of the experiments. In addition, the volume ratios one has to calculate to normalize connectivity amplitudes, should prove much less affected by errors due to insufficient data digitization. The normalization procedure may be prohibitive for crowded diagonals in homonuclear TOCSY spectra, where assumptions about the individual auto–peak intensities should be made when specific relaxation rates are not available.

In this context heteronuclear schemes, where auto–peaks are likely to be well resolved, may be very helpful, though difficulties can arise for inequivalent protons attached to the same heteronucleus because of the lack of resolution on the heteronuclear axis. For instance the auto– and cross–peaks of non equivalent methylene protons overlap in ^{13}C–^{1}H SQC–TOCSY spectra.

From the spectra recorded with short mixing time tentative values for the J coupling constants are put forward according to the relation:

$$J = \frac{(4 \times \text{normalized intensity})^{1/2}}{2\pi t} \tag{3.3.11}$$

Employing the set of J values thus obtained the exact spectrum is calculated and compared to the experimental one. A random variation of the J coupling constants is then performed, the exact spectrum recalculated and the sum of the squares of the deviations from the measured peaks ($\sum sd$ in the following formula) is estimated. If this is reduced the variation is kept and the entity of the random variation is decreased according to the rule:

$$\text{random variation} = \frac{(\sum sd)_{new}}{(\sum sd)_{old}} \times \exp(-i/n) \tag{3.3.12}$$

where i is the iteration number and n the maximum number of iterations. Reduction of the random variation is performed as the first improvements of the error

function are reached, or when these are too small. The procedure is repeated until $\sum sd$ is less than a threshold value or when the maximum number of steps has been performed. The quality of the fit may be then judged by the residual mean square deviation.

Results and discussion

A well characterized dinucleotide adduct with a ruthenium complex, *trans*–$RuCl(DMSO)_2(H_2O)\{d(GpG)\}$ (Esposito et al., 1992) was used to test the proposed method. The two sugar spin systems are a good test model, because their conformations are quite different and close to standard conformations of A– and B–DNA sugar rings. Indeed, when complexed with ruthenium, the dinucleotide 5' terminal guanine residue, named hereafter G1, adopts a pure C2'–endo conformation, while the other, more flexible, is mainly in C3'–endo conformation. The J coupling constants of the two sugar ring spin systems have been characterized by simulation of the 1D experimental pattern with the standard Bruker software (PANIC) and are reported in Table 3.3.II along with the assignment list.

A preliminary check of the reliability of the mixing sequence efficiency, in this case WALTZ16, was performed. Though this sequence has been demonstrated both from theoretical (Shaka et al., 1983; Griesinger and Ernst, 1988) and experimental (Rance, 1987) point of view to achieve very efficiently the isotropic mixing condition, we wanted to make sure that spurious effects due to pulse imperfections or resonance offset, i. e. generally speaking the extent of coherent transfers arising from imperfect isotropic mixing, could not undermine the outcome and the very prerequisites of the experiment. The measured intensities vs the calculated ones are reported in Figure 3.3.1 and a fairly good agreement may be appreciated.

The largest deviations observed are related to peaks involving 5'5"and 2'2" connectivities, not enough resolved for an accurate quantitation (Figure 3.3.2). Moreover inherent strong coupling effects may alter the pattern of the peaks and, as a consequence, the apparent overall intensity (Kay et al., 1986b, Esposito et al., in press), so that also a very careful quantitation could lead to discrepancies

Proton	Chemical shifts			
	G1	G2		
1'	6.251	6.330		
2'	2.542	2.602		
2"	2.812	2.480		
3'	4.924	4.633		
4'	4.122	4.207		
5'	3.772	4.064		
5"	3.834	4.114		
Couple	Coupling constants			
	G1	G1 (t_m=12.1 msec)	G2	G2(t_m=12.1 msec)
1' 2'	0.9	1.4	9.0	8.1
1' 2"	7.6	7.1	5.4	5.0
2' 2"	-14.0	-13.5	-13.6	-15.6
2' 3'	7.4	7.1	6.7	6.1
2" 3'	10.8	10.2	2.9	3.2
3' 4'	8.0	8.1	3.6	3.2
4' 5'	2.8	2.7	2.0	5.1
4' 5"	2.6	2.6	3.8	5.5
5' 5"	-13.1	-18.2	-11.7	non resolved

Table 3.3.II Chemical shifts (ppm) and J couplings (Hz) of the deoxyribose spin systems of trans–$RuCl(DMSO)_2(H_2O)\{d(GpG)\}$ in D_2O at 298 K (referenced to internal free DMSO resonance at 2.73 ppm). The tentative J values calculated according to eq. (3.3.11) from the TOCSY spectra with short mixing time (t_m=12.1 msec) are listed correspondingly aside the values obtained from 1D spectrum simulation.

with theoretical predictions which do not take into account such effects.

We have retained also the points exhibiting large scattering in Figure 3.3.1 to give a hint of possible errors inherent to the method. However the algorithm, which is working simultaneously on all the experimental amplitudes, is rather efficient in reducing the detrimental effects of both inaccurate quantitation and strong coupling effects. We have not taken into account incoherent transfer which may also occurr during the mixing time, since efficient schemes to remove its effect have been proposed (Griesinger et al. 1988), at least for large molecules

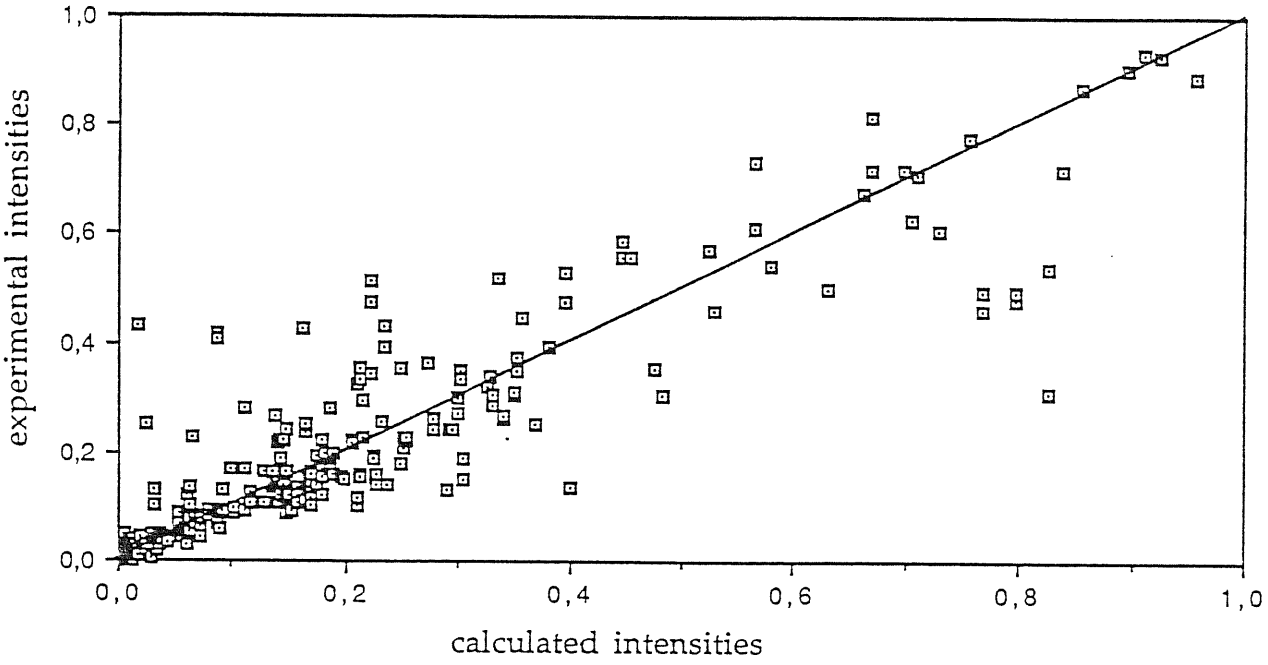

Figure 3.3.1 Experimental versus calculated normalized cross-peak intensities in TOCSY spectra, recorded with different mixing times (12, 24, 46 and 92 msec), for trans-$RuCl(DMSO)_2(H_2O)$\{d(GpG)\}.

($\omega\tau_c > 1.12$), whereas for small molecules like d(GpG)-ruthenium complex, at short mixing times, it should be negligible. According to the approximation described above, tentative J couplings have been estimated from the spectra recorded at the shortest mixing times using eq. . The resulting values are shown in Table 3.3.II together with those obtained from 1D pattern simulation. A negative sign has been imposed to geminal couplings. As can be appreciated, the latters appear sometimes unexpectedly large so that in subsequent simulations we have reset their initial guess to a lower bound of -15 Hz (De Marco et al., 1978). From inspection of Table 3.3.II it is clearly seen that the deviations observed for geminal couplings increase with increasing degree of inherent strong coupling. Notwithstanding all the inaccuracy sources originating from inherent limits (strong coupling, resolution, integration routine) and experimental errors, most of the deviations are less than 1 Hz, and are sufficient to distinguish, for instance, the sugar puckering. The fitting procedure extended to all the sets of experimental amplitudes available (i. e. including longer mixing times) led to the results depicted in Figure 3.3.3.

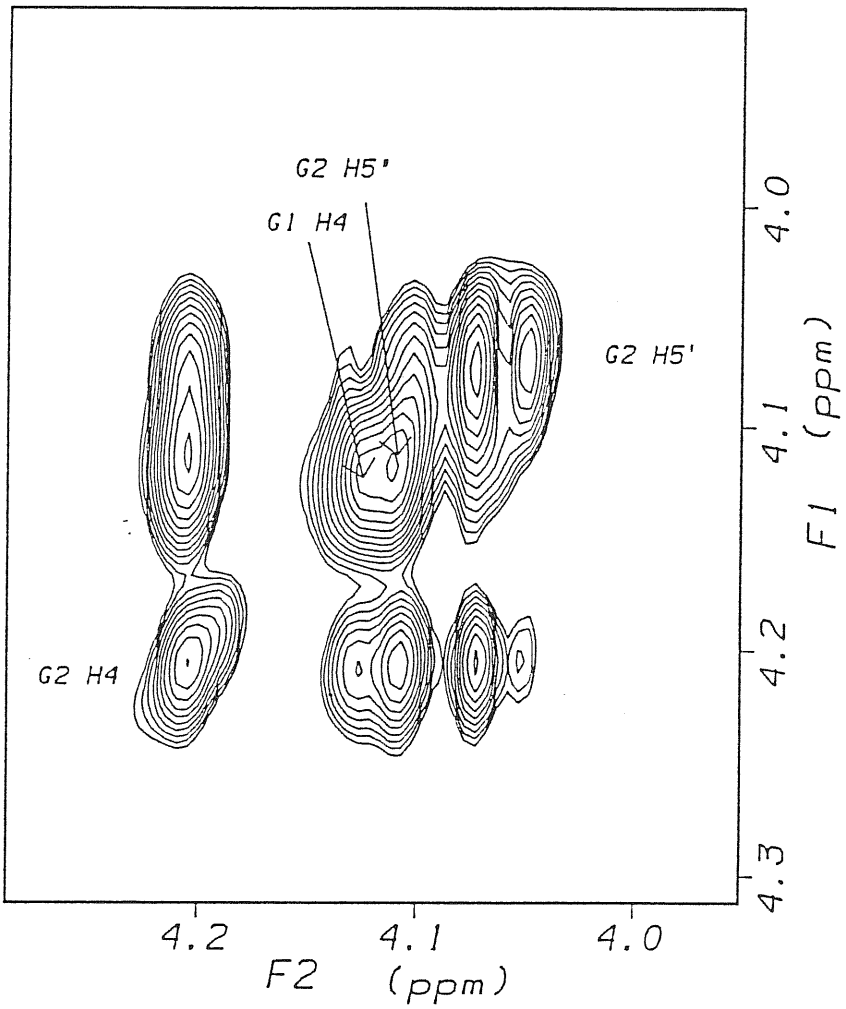

Figure 3.3.2 A detail of the TOCSY spectrum (mixing time 46 msec) of trans–$RuCl(DMSO)_2(H_2O)\{d(GpG)\}$ illustrating limitations to peak quantitation. The resonance attributions are explicitly indicated.

Zero coupling constants were not allowed to vary throughout the calculations while a starting maximum random variation of 1Hz was applied to the others. The residual root mean square deviation of calculated versus experimental intensities was always very small (0.01 – 0.04 per normalized peak) within the limits imposed by the asymmetry of the experimental matrices. The CPU time required for an iteration on such large spin system (seven $\frac{1}{2}$–spin nuclei per sugar ring) is $\sim$ 40 seconds with a Silicon Graphics VGX 4D320 computer, and increases approxi-

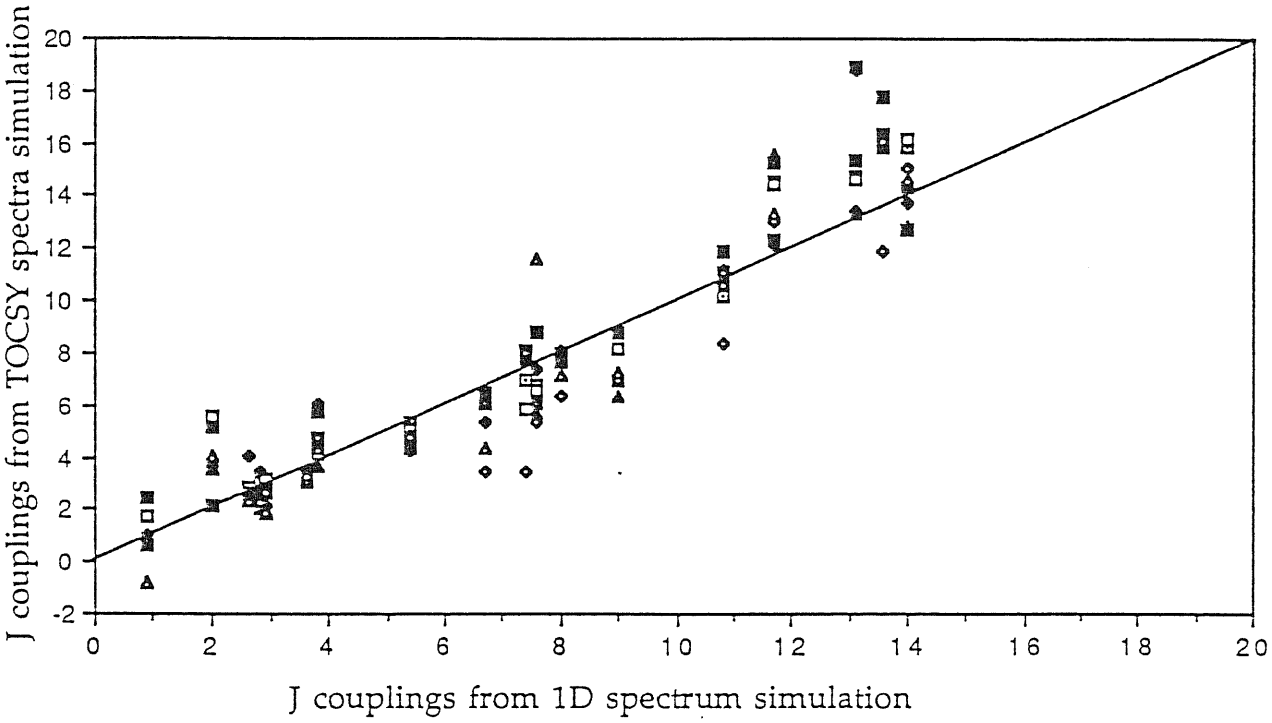

Figure 3.3.3 J couplings obtained by means of the presented algorithm versus those obtained by simulation of 1D proton spectrum for trans–$RuCl(DMSO)_2(H_2O)\{d(GpG)\}$ Different symbols correspond to J values obtained from simulations (2 for each spectrum) for data acquired with different mixing times (see text).

mately with 2^{3N} being N the number of spins in the system, with 70% of the time spent calculating the theoretical spectrum and 20% spent in diagonalization of the Hamiltonian matrix with the Jacobi algorithm (Press at al., 1990). The model considered so far is not too much representative of real life situations. Most often diagonal peaks can not in fact be easily quantitated, forcing one to make arbitrary assumptions on the intensity of the individual auto–peaks. An alternative solution, recently applied to NOESY spectra of proteins (Molinari et al. 1992), is to resort to heteronuclear correlated relayed TOCSY spectra where the auto–peaks, corresponding to diagonal peaks of ordinary homonuclear TOCSY maps, are likely to be better resolved. In order to test this alternative route, we have studied in detail the spectrum of biotin, a coenzyme involved in carboxylation processes. The chemical structure and numbering scheme of biotin are shown in Figure 3.3.4.

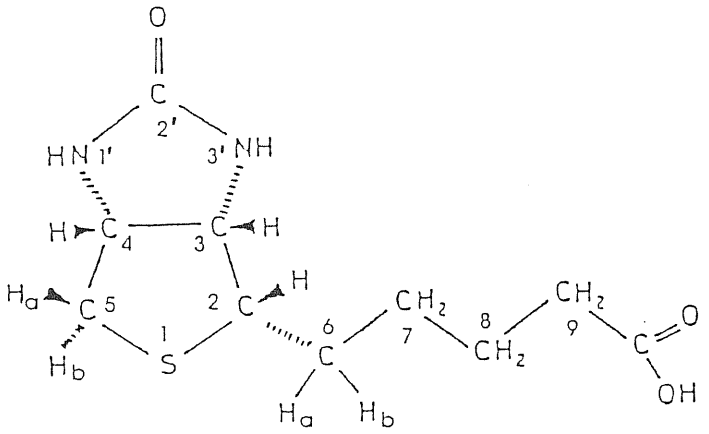

Figure 3.3.4 Chemical structure and numbering scheme of biotin.

A reduced set of J coupling constants (i. e. involving only 9 protons out of 15), as obtained from simulations of the 1D ^{1}H spectrum with PANIC, is reported in Table 3.3.III along with the list of ^{1}H and ^{13}C assignment.

The very large spin system of biotin cannot be simulated with our algorithm.

However we can apply the procedure above described to extract the J coupling values from the spectra recorded at the shortest possible mixing times, to essentially select only transfers between directly coupled spins (when possible as will be discussed later). A MLEV17 mixing train was employed in ^{13}C–^{1}H SQC–TOCSY (Figure 3.3.5) to use the simplest and shortest isotropic mixing scheme.

Indeed the selection of heteronuclear SQC coherences, to limit F_1 broadening (Bax et al., 1990), entails a quite long pulse protocol, which conflicts with the requirement of achieving a proper S/N ratio in reasonable experimental times. MLEV17 and WALTZ16 mixing schemes were also employed to acquire homonuclear TOCSY spectra, in order to compare homo and heteronuclear response and to ascertain that the performance difference, expected for the two spin lock trains (Griesinger and Ernst, 1988), was ininfluent for our purposes. The resulting J coupling constants are reported in Table 3.3.III. It was not possible to employ exactly the same mixing time in all three experiments due to different durations of a complete mixing step cycle.

There are some differences among the set of values obtained from 1D spec-

Proton	Chemical shift	Carbon	Chemical shift
1'	6.328	2	55.5
3'	6.402	3	61.2
2	3.082	4	59.3
3	4.111	5	40.0
4	4.278	6	28.2
5a	2.801	7	28.2
5b	2.555	8	24.6
6a	1.61	9	33.6
6b	1.47		
7	1.49		
8	1.32		
9	2.179		

Couple	Coupling constants			
	Simulated	MLEV17-^{1}H-^{1}H	WALTZ16-^{1}H-^{1}H	MLEV17-^{13}C-^{1}H
1' 4	0.5	observed	1.9	0.4
3' 3	2.0	observed	2.2	1.3
2 3	4.8	5.3	3.3	5.7
2 6a	5.7	7.0	5.7	6.1
2 6b	8.7	8.9	7.7	8.9
3 4	7.8	9.9	9.7	10.8
4 5a	5.0	6.0	4.2	5.6
4 5b	0.0	observed	2.5	observed

Table 3.3.III Chemical shifts (ppm) (referenced to the solvent resonance at 2.48 and 43.5 ppm for ^{1}H and ^{13}C, respectively) and coupling constants (Hz) of biotin (Figure 3.3.4) in DMSO at 298 K. The J values were obtained from simulation of 1D spectrum (first column) and calculated from homonuclear 2D TOCSY, with MLEV17 (t_m=11.4 msec) and WALTZ16 (t_m=13.7 msec) isotropic mixing sequence (second and third column, respectively), and from ^{13}C–^{1}H SQC–TOCSY spectrum (last column) employing MLEV17 (t_m=12.4 msec). The term "observed"means that the corresponding cross–peak was detected, but no reliable quantitation could be performed due to an intensity level just above the noise threshold.

trum simulation and those extracted from TOCSY or SQC–TOCSY amplitudes. In addition some discrepancies occurr also among the sets calculated from TOCSY's performed with different experimental schemes. Though in most situations these discrepancies range within quite narrow limits, it is worth noticing that when low intensity cross–peaks cannot be safely distinguished from the background

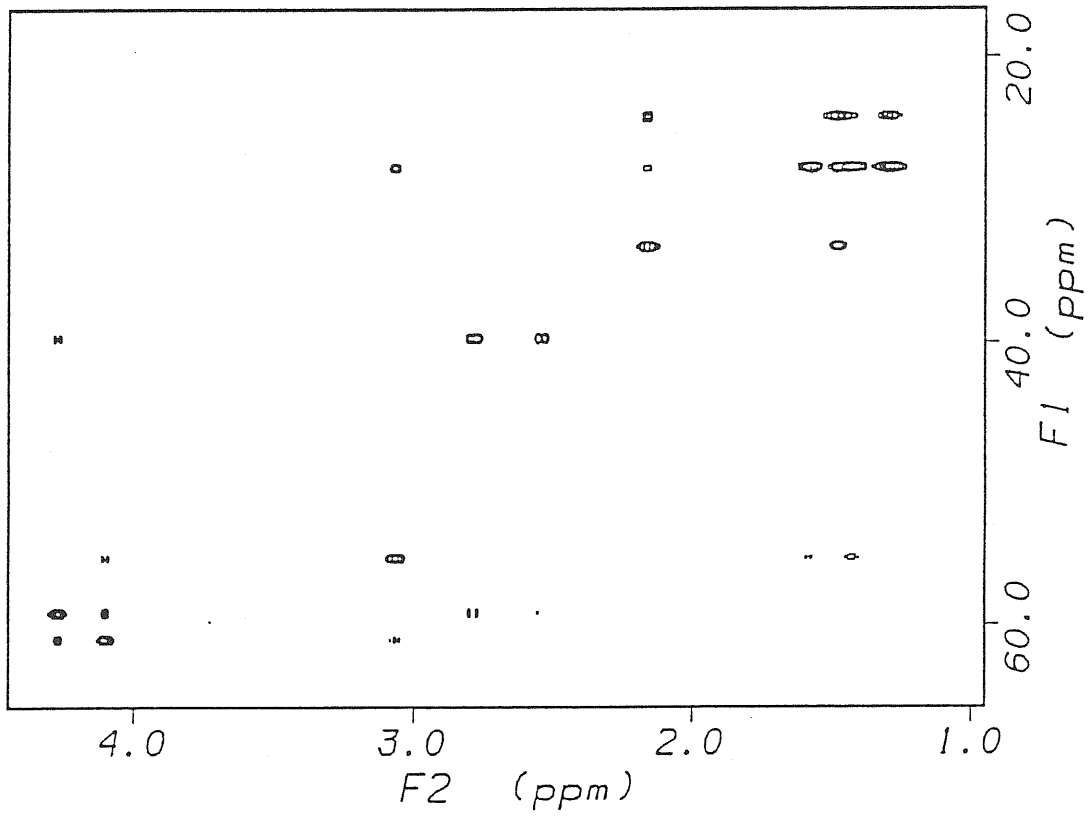

Figure 3.3.5 ^{13}C–^{1}H SQC–TOCSY spectrum of biotin (mixing time 12.4 msec).

noise, the estimate of the scalar couplings is rather inaccurate or absolutely impossible, as for $J_{1'4}$ and $J_{3'3}$. This is a very general feature of the method: small coupling constants can be evaluated only if the signal to noise ratio is good enough to allow for precise quantitation of the cross–peak intensity. Other discrepancies are observed for J_{34} and J_{45b}, which illustrate very well the effects of strong coupling. The issue is very similar to that already discussed for the overestimated geminal couplings in *trans*–$RuCl(DMSO)_2(H_2O)\{d(GpG)\}$ at least for J_{34} since H3 and H4 are near the condition of inherent strong coupling (Kay et al., 1986b, Esposito et al., in press), whereas for J_{45b} we must invoke the breakdown of the approximation underlying eq. (3.3.11).

Differently from the previous case, the refinement minimization fitting is not performed because of the impossibility of simulating the whole spin system (15 protons with 3 pairs of nearly equivalent nuclei and virtually uninterrupted

network of J couplings). The consequences are heavy when a proton (H4) has a very weak or zero coupling with only one spin (H5b) of a strongly coupled pair (H5a, H5b). In fact J_{5a5b} coupling is so efficient in transferring magnetization from 5a to 5b that also the extent of transfer from H4 to H5a will be partially exchanged to H5b resulting in a fake J_{45b}. For a three spin system ABC with J_{AB} = 5.0 Hz, J_{BC} = -15.0 Hz and J_{AC} = 0.0 Hz, the normalized crosspeak intensity for AC, even for such a short mixing time as 12.4 msec, would be 0.003, resulting in an estimated J_{AC} of 1.4 Hz, and in a correspondingly underestimated J_{AB} value of 4.6 Hz. Such situations are to be kept well in mind for accurate quantitation, when the considered spin configuration is too extended to permit simulation. For biotin homonuclear TOCSY spectra, even if the difference in offset effects of MLEV17 and WALTZ16 (Griesinger and Ernst, 1988) is really irrelevant in the chosen experimental conditions ($\gamma B_2/SW$ = 2.5), small differences in the overall mixing duration (10%) and reduced spin lock quality of the trim pulses flanking the MLEV17 trains result in appreciable effects on the experimental intensities just because of the extension of the scalar coupling network, poorly reproduced by calculations based only on approximation (3.3.11).

In general however, provided non–negligible offset effects are avoided, moderate spin system complexity should not represent a real problem because proper corrections can be applied by simulation of the specific spin subsystem (e.g. compare results in Figure 3.3.3 and Table 3.3.II). While the differences between the two biotin proton spectra may be ascribed to differences in the mixing schemes employed, the homo and heteronuclear experiments which use the same mixing pulse sequence (MLEV17) should give, at least in principle, the same results (neglecting the small t_m increase of SQC–TOCSY). We reckon that for most of the cases this is true within the experimental accuracy, as shown in Table 3.3.III. Obviously differences in the evolution of the magnetization before the mixing time, and in particular during t_1, may also play a role in this respect (Esposito et al., in press; Molinari et al., 1992). However, far from limiting instances, the deviations should not be so large as to impair the usefulness of the method.

Conclusions

The determination of scalar coupling constants can be tackled successfully by means of TOCSY auto– and cross–peak amplitudes, exploiting the net transfer character of isotropic mixing and some approximations of the theoretical model describing the process. We are confident that the proposed method may be helpful in many practical situations, in particular when ordinary 1D spectrum simulations are bound to fail due to resolution limits.

For complex spectra, direct measurement of antiphase splittings in pure phase 2D scalar correlation maps has been established as the method for extracting J coupling information (Marion and Wüthrich, 1983), but very large data matrices are necessary to achieve a meaningful resolution and avoid substantial distortion of the antiphase lineshape (Neuhaus et al., 1985). These strict experimental digitization requirements are no longer necessary when using TOCSY data because amplitude ratios and not frequency differences are now evaluated. Therefore underdigitization errors affecting the individual amplitude values should partially cancel out when the ratio of cross–peaks and parent auto–peaks is considered.

When auto–peaks cannot be resolved in homonuclear spectra, the TOCSY experiment can be run using heteronuclear resolution in F_1 like in SQC–TOCSY, which enables the application of the presented method also to complex molecules. In many cases an estimation of the coupling constants from spectra that would be anyway recorded because necessary for the assignment procedure, may provide information about the conformation of the molecules under study. The test reported on two model compounds are supporting this conclusion. The application to large molecules is still underway, but heteronuclear experiments seem rather promising in this respect.

3.4 A 3D EXPERIMENT TO OBSERVE "COLLECTIVE MODES"

Since its first proposal (Müller and Ernst, 1979; Braunschweiler and Ernst, 1983) total correlated spectroscopy (TOCSY) has become a very widely used tool in the NMR molecular characterization. The peculiarities of coherence transfer under the isotropic mixing Hamiltonian have been analysed theoretically as well as numerically in recent years (Chandrakumar and Subramanian, 1985; Visalakshi and Chandrakumar, 1987; Chandrakumar, 1987; Cavanagh et al., 1990). Attention has been drawn on the evolution of single spin magnetization, while the oscillatory evolution of the eigenoperators of the isotropic mixing superoperator have been referred to as "collective modes". No experimental attempt to observe these modes has been done yet to our knowledge.

The frequencies of the modes are obviously dependent on the strength and the topology of the coupling network and, in some cases, analytical formulas for them can be worked out. Though ways to extract J couplings (Fogolari et al., in press) and topology (Chung and Keeler, 1992) information from TOCSY transfer have been recently proposed the collective modes frequencies could, in principle, be also exploited to gain this information. However one may also think to use the spread of the frequencies related to different spin systems to resolve them on a proper frequency axis.

In the following a novel 3D experimental scheme (proposed recently by M. Pfuhl in the group of A. Pastore at EMBL, Heidelberg (Germany)), which is able to detect collective modes on the third axis by simply Fourier transforming a series of 2D TOCSY spectra recorded with increasing mixing times, is analysed. Strictly speaking, the idea of recording TOCSY at different mixing times is, obviously, not new, being indeed common experimental practice. Also the idea of transforming, employing a Taylor transformation, a series of spectra with different mixing times has been already proposed (Hyberts and Wagner, 1989). A systematic approach to the coherence transfer during TOCSY mixing time has been put forward recently by Chung and Keeler (1992) who proposed to use a Taylor transformation of the mixing time to separate spin couples connected by a different number of relayed transfer steps.

The present scheme, instead, treats the mixing time as any other time dimension, in an attempt to fully exploit the large number of frequencies contributing to the time development of the signal in the third axis.

Some preliminary investigation on the expected appearance of the spectrum should be done before proceeding further. Indeed we should consider the range and the number of frequencies one expects to observe together with the expected intensities. For a n $\frac{1}{2}$–spin system, in principle the Hamiltonian superoperator possesses 2^{2n} eigenvalues, however, the high degree of symmetry of the isotropic mixing Hamiltonian (H) drastically reduces this number. Due to rotational invariance, the eigenvalues of H depend only on the global angular momentum J, and not on the single axis projections J_x, J_y or J_z.

For a n $\frac{1}{2}$–spin system there are $\frac{n}{2}$ (or $\frac{n+1}{2}$) possible values for J. Each corresponding eigenspace of the operator **J** may be further split, according to its degeneracy, in order to obtain m rotationally invariant eigenspaces of the Hamiltonian.

Since m is also the number of the possible different eigenvalues of the Hamiltonian, the number of possible "collective modes"is equal $2(m!)+1$. (m can be easily computed according to standard coupling formalism. m is 1, 2, 3, 6, 10, 20, 35,... for 1, 2, 3,.... $\frac{1}{2}$–spin system.)

Though for common biopolymer spin systems this number may be exceedingly large, it should be remembered that not all the intensities are large enough to be observed. Problems may arise when standard Fourier transform is performed since the linewidth may be very large compared to the frequency range, so that mutual cancellation of peaks may occurr in the 3D spectrum.

TOCSY transfer may be expressed according to eq. (3.1.29); when the eigenbasis of the Hamiltonian $\{|J,\tau>\}$ is chosen we may write:

$$< I_{zj} >= \sum_{J,\tau,J',\tau'} < J,\tau|I_{zj}|J',\tau' >< J',\tau'|I_{zi}|J,\tau > \exp -i(\omega_m - \omega'_m)t_m \quad (3.4.1)$$

After Fourier Transform in t_m we get a peak at $(\omega_i, \omega_j, (\omega_m - \omega_{m'}))$ of intensity $\sum_{J,\tau,J',\tau'} < J,\tau|I_{zj}|J',\tau' >< J',\tau'|I_{zi}|J,\tau >$.

Generally speaking we can summarize the features of the resulting spectrum:

1) as already mentioned the third axis frequencies are not single spin, but

spin sytem properties, which makes them attractive in order to solve otherwise overlapping resonances;

2) though a large signal is expected at zero frequency, which is actually responsible for the commonly observed positive sign of TOCSY cross-peaks, collective modes span a range of frequencies approximately of the same order of the sum of all the J couplings in the system;

3) the third axis planes are repeating the same pattern of a common 2D TOCSY spectrum, except for the presence of both positive and negative peaks, instead of the most common positive peaks, being the normalized sum along the third axis equal 1 on the diagonal and 0 off the diagonal;

4) higher frequencies which should be readily used to distinguish larger size spin systems have also lower intensities as a consequence of the limited degeneracy of high J energy levels.

For the sake of clarity a 3 $\frac{1}{2}$–spin system (A, B, C) with couplings $J_{AB} = 8.2$ and $J_{BC} = 2.1$ will be considered in the following. The series of peak intensities (in the absence of relaxation is reported in Table 3.4.I corresponding to each "collective mode"frequency. From the figures in the table it can be easily seen how commonly observed linewidths can lead to mutual cancellation of opposite signed lobes and alter the apparent frequencies in the spectrum.

Since the transfer should be strongly damped oscillatory, a Fourier Transform might be not the best way to process the signal, since it results in large linewidths. Indeed preliminary results obtained by M. Pfuhl using just a plain FT, without the use of any filter function, fully confirm all the above predictions.

The combined use of a suitable window function and filtering in the third axis, should make the data amenable to the use of maximum entropy method (Press et al., 1990), possibly reducing significantly the linewidth. Maximum entropy method was alredy applied onto selected columns in the third axis and the resulting linewidths are strikingly reduced. Work in this direction is still going on in Heidelberg, mainly devoted, due to the lack of specific routines in available processing software, to solve computational problems. It should be kept in mind that such methods are demanding in computer power and memory, therefore optimization of the routines, and proper interface with graphical software is mandatory.

```
frequency:      -8.838834
        0.141232        -0.163238       0.022006
        -0.163238       0.188672        -0.025435
        0.022006        -0.025435       0.003429

frequency:      -7.377668
        0.102946        -0.076582       -0.026364
        -0.076582       0.056969        0.019612
        -0.026364       0.019612        0.006752

frequency:      -1.461165
        0.080990        0.052127        -0.133117
        0.052127        0.033550        -0.085676
        -0.133117       -0.085676       0.218793

frequency:      0.000001
        0.349664        0.375385        0.274951
        0.375385        0.441617        0.182998
        0.274951        0.182998        0.542052

frequency:      1.461166
        0.080990        0.052127        -0.133117
        0.052127        0.033550        -0.085676
        -0.133117       -0.085676       0.218793

frequency:      7.377669
        0.102946        -0.076582       -0.026364
        -0.076582       0.056969        0.019612
        -0.026364       0.019612        0.006752

frequency:      8.838835
        0.141232        -0.163238       0.022006
        -0.163238       0.188672        -0.025435
        0.022006        -0.025435       0.003429
```

Table 3.4.I Calculated intensities in the 3D spectrum for a 3 $\frac{1}{2}$ spin system with J_{AB}=8.2 and J_{BC}=2.1. The collective mode frequency is reported on top of the matrix of intensities expected in the corresponding (ω_1,ω_2) plane. First, second and third position in rows and columns indicate ω_A, ω_B and ω_C frequencies, respectively.

Chapter 4

STRUCTURAL CHARACTERIZATION OF THE REACTION PRODUCT BETWEEN d(GpG) AND THE OCTAHEDRAL ANTITUMOR COMPLEX trans–$RuCl_2(DMSO)_4$

In recent years metal–based antitumor drugs have been playing a relevant role in antiblastic chemotherapy; especially *cis*–diamminedichloroplatinum (cisplatin or *cis*–DDP) is regarded as one of the most effective anticancer drugs used in clinics (Loehrer and Einhorn, 1984; Muggia, 1991). In the design of new anticancer agents different complexes of Pt(II) (square planar) and of Pt(IV) (octahedral) were tested (Sherman and Lippard, 1987; Johnson et al., 1989; Chaney et al., 1991) and some of them are currently used in clinical applications (Twelves et al., 1991; Weiss et al., 1991). Among non platinum transition metal anticancer compounds, ruthenium complexes (Clarke, 1989; Garzon et al., 1987) have raised great interest. In particular ruthenium (II) (Alessio et al., 1987; Sava et al., 1989) and ruthenium (III) (Pacor et al., 1991) complexes, with dimethylsulfoxide (DMSO) as ligand, exhibit antiblastic activity comparable to that of cisplatin at equitoxic dosage in animal models of metastasizing tumors, but with less severe side effects and prolonged host survival times.

The mechanism of antitumor action of metal compounds is not fully understood, but in the case of the square planar cisplatin a lot of experimental evidences point to DNA binding as the crucial lesion (Sherman and Lippard, 1987; Johnson et al., 1989). The bifunctional binding to adjacent purine bases d(GpG) or d(ApG), which represent 65% and 25% of total platinum binding (Fichtinger–Schepman et al., 1985), respectively, is widely accepted as the critical interaction with DNA, inhibiting replication and trascription processes (Sherman and Lippard, 1987; Johnson et al., 1989).

NMR (Sherman and Lippard, 1987; Girault et al., 1982; Reedijk, 1987; Mukundan et al., 1991) and X ray investigations (Sherman et al., 1985; Admiraal et al., 1987) have been carried out in the last decade to elucidate the structural

features of the interaction. The purine N7 bifunctional binding determines the loss of stacking in coordinated bases and leads to a bending of the double helical DNA (Sherman and Lippard, 1987; Reedijk, 1987) associated to some extent of unwinding (Bellon et al., 1991).

The nature of DNA interaction with octahedral metal complexes has been much less explored. Attention has been focused on a ruthenium (II) complex (*trans*–$RuCl_2(DMSO)_4$) which exhibits interesting antiblastic activity and reacts in vitro and in vivo with DNA (Alessio et al., 1987; Mestroni et al., 1989; Cauci, 1990). This octahedral transition metal complex shows a mechanism of reaction similar to that of cisplatin, in spite of the different geometry, being N7 of guanine bases the preferential site of attack on DNA (Mestroni et al., 1989; Cauci, 1990). The reaction of *trans*–$RuCl_2(DMSO)_4$ with 5'dGMP leads to the formation of two diastereoisomeric monoadducts in which the guanine moiety and the α–phosphate group form a chelate to the metal center with opposite chirality (Alessio et al., 1989). In the case of the reaction with 2'dGuo an equilibrium state is achieved, two diastereoisomeric monoadducts and a biadduct being present in the reaction mixture. In all the cases the purine moiety is coordinated via N7 (Cauci et al., 1991). NMR evidences support a head to tail arrangement of guanine moieties in the biadduct in analogy with corresponding adducts of square planar Pt (II) (Bau and Gellert, 1978) and Pt(IV) (Choi et al., 1988) compounds.

The reversibility of monofunctional N7 purine coordination is in contrast with the irreversibility of binding to polymeric DNA (Cauci, 1990), strongly suggesting that a bifunctional binding occurs in the latter case. Therefore the dinucleotide d(GpG) was chosen as a better model to study the interaction of *trans*–$RuCl_2(DMSO)_4$ with nucleic acids. To our knowledge, this is the first structural characterization of a covalent bifunctional coordination of an antitumor octahedral complex to d(GpG).

Experimental procedures

trans–$RuCl_2(DMSO)_4$ and *trans*–$RuBr_2(DMSO)_4$ were synthesized as previously reported (Alessio et al., 1988). d(GpG) sodium salt and other reagents were purchased from Sigma, and used without further purification. A freshly

prepared stock solution of the ruthenium complex in D_2O, typically 30mM, was diluted to the desired final concentration. When necessary, the monohalogenated species was obtained incubating the stock ruthenium solution for 8 h at 37°C, in the dark, with equimolar $AgNO_3$ and then centrifuging to eliminate the AgCl formed.

HPLC analyses were performed on a Waters liquid chromatograph (the latter was equipped with mod. 680 automated gradient controller) on a μBondapack C_{18} reverse–phase column, with UV detection at 253 nm, using an aqueous 10 mM KCl solution as eluant A, and CH_3OH as eluant B; the separation of the reaction products was achieved with a linear gradient from 0% to 20% B, at a flow rate of 1mL/min.

CD spectra were acquired with a Jasco J600 dichrograph, equipped with a thermostatted cell holder. UV spectra were recorded on the same samples with a Cary 2200 spectrophotometer whose cell holder was also thermostatted.

NMR spectra were obtained at 500.13 MHz with a Bruker AM500 spectrometer. The temperature was adjusted at 23°C in all the experiments except for the kinetic measurements (40°C). Stoichiometric amounts of *trans*–$RuCl_2(DMSO)_4$ or *trans*–$RuBr_2(DMSO)_4$ were added, directly in the NMR tube, to d(GpG) solutions in D_2O (99.99% from Cambridge Isotope Laboratories, U. K.). Typically the final concentration was 3.5 mM. In the titration experiments the pH (uncorrected reading) was adjusted by DCl or NaOD microadditions directly in the NMR samples. Twenty–four hours at 40°C were sufficient to reach a nearly stationary composition of the reaction mixture. The final reaction product (A) was successively purified by HPLC and liophylized, before being redissolved in D_2O at 23°C for further NMR studies (at a concentration typically $\approx$ 1 mM). In these conditions the samples were stable for over two weeks, before oxidative degradation products could be detected.

All chemical shifts were referred to the free dimethylsulfoxide resonance (2.73 ppm). Typical 1D spectra acquisition parameters were: 5000 Hz sweep width; 1.64–3.28 s acquisition time; 1–2 s relaxation delay. The map of the scalar coupling connectivities was obtained from the 2D TOCSY spectrum (Müller and Ernst, 1979) acquired using the pulse scheme proposed by Rance (1987) with a WALTZ 16 (Shaka et al., 1983) spin lock lasting 62.2 ms, at $\gamma B_2 = 7.7$ kHz. Choosing

the same spectral width in both dimensions (i. e. 5000 Hz), the acquisition times were 0.205 s and 0.04 s in t_2 and t_1, respectively, i. e. a matrix $410 \times 2K$ with 64 scans each t_1 increment. Zero filling to 2K was performed in t_1 prior to Fourier transformation. A square sine–bell function, shifted by $\frac{\pi}{3}$, was applied in both dimensions.

The high–resolution 2D scalar correlation map was obtained from a 2D DQF–COSY experiment (Piantini et al., 1982), acquired over a sweep width of 3205 Hz in both dimensions. This spectral window was selected to observe deoxyribose resonances unaffected by the folding in the spectrum of H8 lines. The acquisition times were 0.479 and 0.087 s, corresponding to a resolution of 2.1 Hz and 11.4 Hz in t_2 and t_1, respectively. The experimental matrix ($560 \times 3K$ with 128 scans per t_1 increment) was zero filled to $4K \times 4K$, to achieve a final digital resolution of 1.6 Hz in both frequency domains, enough to allow for a detailed pattern attribution of the high–resolution (0.3 Hz) 1D spectrum employed for spin system simulation. A square cosine bell was used to condition the experimental data, in order to avoid spurious negative tails of the crosspeak patterns. No ^{31}P decoupling was performed. The simulations of the 1D patterns were performed separately for systems including non labile protons of each nucleoside moiety as well as the phosphorus nucleus. By means of the standard Bruker software program PANIC a satisfactory fitting of the experimental spectrum was obtained, in the worst conditions the probable parameter errors were 0.02–0.04 Hz, i. e. well below the experimental resolution.

Through space connectivities were obtained by 2D NOESY experiment (Jeener et al., 1979), recorded at three different mixing times (t_m) (200.4, 419.3 and 858.7 ms), randomly varied ($\pm 5\%$) to minimize coherent transfers due to J couplings. 2D NOESY matrices were acquired with 128 scans for each of the 600 t_1 increments, over a sweep width of 5000 Hz in both dimensions (i. e. with a resolution of 4.9 and 16.7 Hz in t_2 and t_1, respectively). Zero filling to 2K was performed in t_1 and a square cosine–bell function was employed in both dimensions prior to 2D FT.

All 2D spectra were obtained with pure phase lineshapes using TPPI (Drobny et al., 1979) to achieve quadrature detection in t_1. The residual HOD resonance was always attenuated by coherent prolonged selective excitation (Esposito et al.,

1987) with a DANTE scheme (Morris and Freeman, 1978) during the relaxation delay (typically 1.5–2.0 s) and the mixing time too in NOESY experiments.

A modified version of AMBER forcefield (Weiner et al., 1984), see Table 4.I, was used throghout the calculations. All the parameters employed were estimated on the basis of the literature (Mercer and Trotter, 1975; Alessio et al., 1988; Seddon and Seddon, 1984; Henn et al., 1991; Alessio et al., in press) on analogous compounds. As to the charges, these were calculated with the algorithm of Gasteiger and Marsili (1980) on a model compound including Ru, 2 DMSO, Cl, H_2O and the two N7's in order not to modify too heavily AMBER parameters. Starting charges of $+1$, -1 and $+.5$ were assigned to Ru, Cl and N7, respectively. The final charges on the N7's were finally added to the original AMBER charges. The set of parameters involving the N7's and the sulphur atoms was duplicated and modified in order to parametrize differently *cis*– and *trans*– location relationships among the metal attached atoms. No energy barrier was set for rotation about the bonds involving ruthenium.

The dynamic simulations were run for 1 ns in steps of 1 fs. Vacuum ($\epsilon = 1$), water ($\epsilon = 80$) and distance dependent ($\epsilon = 4r$ with r in Å) dielectric constants were used for separate runs.

The conformational space was searched for global minima using a constrained simulated annealing procedure (Kirkpatrick et al., 1983) starting dynamics at 930°C and progressively reducing the temperature down to -73°C and finally minimizing the energy of the resulting structures. A force constant of 100 Kcal/(mol rad^2) was used in the constrained simulations.

Results

The octahedral complex *trans*–$RuCl_2(DMSO)_4$ dissolved in water shows the dissociation mechanism reported in Scheme 4.1.

Two dimethylsulfoxide molecules are released immediately after dissolution. The loss of the first chloride ion is observed after 6 hours at 37°C, whereas there is no evidence of release of the second chloride ion (Cauci et al., 1991). An enhancement of Cl^- release is induced by guanine moiety coordination to the metal center when *trans*–$RuCl_2(DMSO)_4$ is reacted with 2'deoxyguanosine (Cauci et al., 1991).

AMBER forcefield modifications following the notation of Weiner et al., (1984). The following charges (expressed in protonic charges) were used: Ru(+0.969), S(+0.115), O_{DMSO}(-0.258), C (+0.015), H_{methyl}(+0.036), H_{water}(+0.223), O_{water}(-0.509), Cl(-0.626) and N7 (+0.257).

$$E_{tot} = \sum_{bonds} K_r (r - r_{eq})^2 + \sum_{angles} K_\theta (\theta - \theta_{eq})^2 + \sum_{dihedrals} \frac{V_\phi}{2} [1 + \cos(n\Phi - \gamma)] +$$

$$+ \sum_{i>j} \varepsilon_{ij} [(\frac{r_{ij,eq}}{r_{ij}})^{12} - 2(\frac{r_{ij,eq}}{r_{ij}})^{6}] + \sum_{H\text{-bonds}} [\frac{C_{ij}}{r_{ij}^{12}} - \frac{D_{ij}}{r_{ij}^{10}}] + \sum_{i>j} \frac{q_i q_j}{\varepsilon r_{ij}}$$

Bonds	K_r (Kcal/mol Å^2)	r_{eq} (Å)
S-O	528.0	1.48
Ru-S	400.0	2.30
Ru-O	400.0	2.14
Ru-N7	400.0	2.15
Ru-Cl	400.0	2.40

Angles	K_θ (Kcal/mol deg^2)	θ_{eq} (degrees)
Ru-C-S	70.0	112.0°
Ru-S-O	70.0	119.0°
- Ru-	100.0	90° or 180°
Ru-N7-C8	100.0	128.1°
Ru-N7-C4	100.0	128.1°
Ru-O-H	100.0	109.5° (125°)

Dihedrals	$V_\phi/2$ (Kcal)	θ_{eq} (degrees)	n
-Ru--*	0.0	0.0°	0
Ru-C4-N7-C8	10.0	128.1°	2

Atoms	R(Å)	ε (Kcal/mol)
Ru	2.0	.200
Cl	2.0	.200

Table 4.I AMBER Force–Field modified parameters.

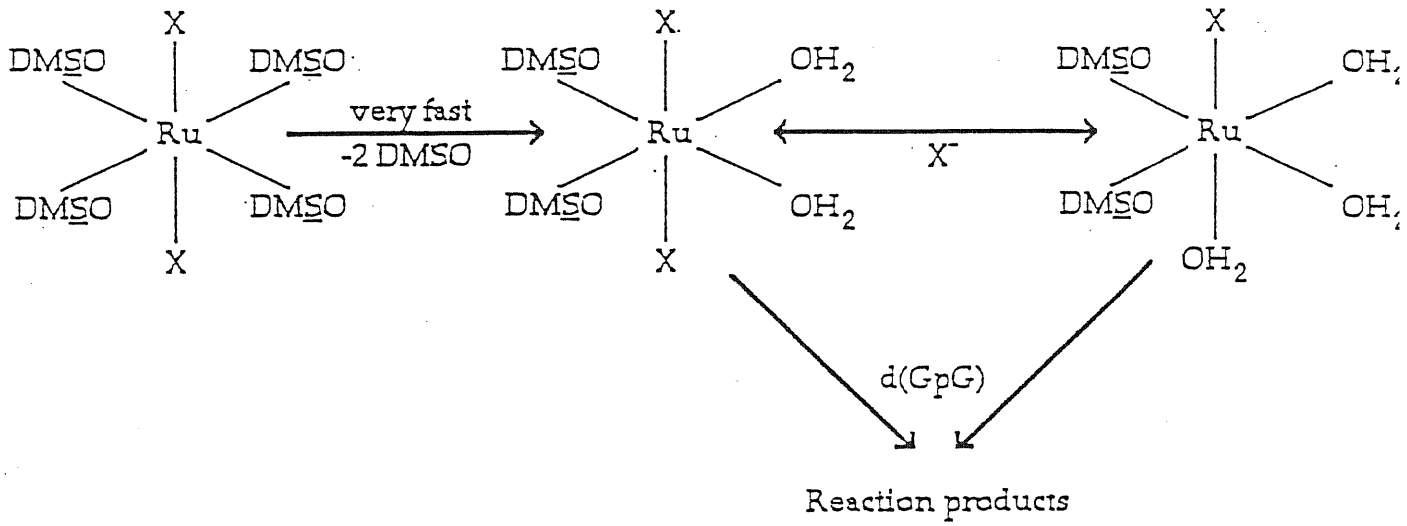

Scheme 4.1 Mechanism of the reaction between trans–$RuX_2(DMSO)_4$ and d(GpG) in unbuffered water; N7 = N7–coordinated guanine; DMSO = S–coordinated dimethylsulfoxide; X = Cl, Br.

When *trans*–$RuCl_2(DMSO)_4$ is incubated with d(GpG) at equimolar ratio (3.5 mM) in water at 40°C (final pH = 5.9) two different reaction products (A and B) are observed. The product B is an intermediate, which slowly disappears in about one day as shown in the kinetic pattern reported in Figure 4.1.
At low temperature ($\approx$ 5°C) the conversion of the intermediate into the final product is strongly slowed down, thus allowing the HPLC separation and spectroscopic characterization of the compounds.

The product B exhibits dichroic bands much more intense than A (Figure 4.2). On the contrary the final product A shows a negligible CD spectrum at pH 6 and a weak negative band (centered at about 280 nm) at alkaline pH values very similar to that exhibited by the corresponding complexes with cisplatin (Girault et al., 1982).

The aromatic region of the ^{1}H–NMR, including the guanine H8 resonances, recorded on the reaction mixture at 4 hours is reported in Figure 4.3. The large downfield shifts of the resonances arising from the final reaction product A (δ = 8.723 ppm and δ = 8.682 ppm) are typical of N7 coordination of guanine moieties to a transition metal center (Miller and Marzilli, 1985) and have been previously

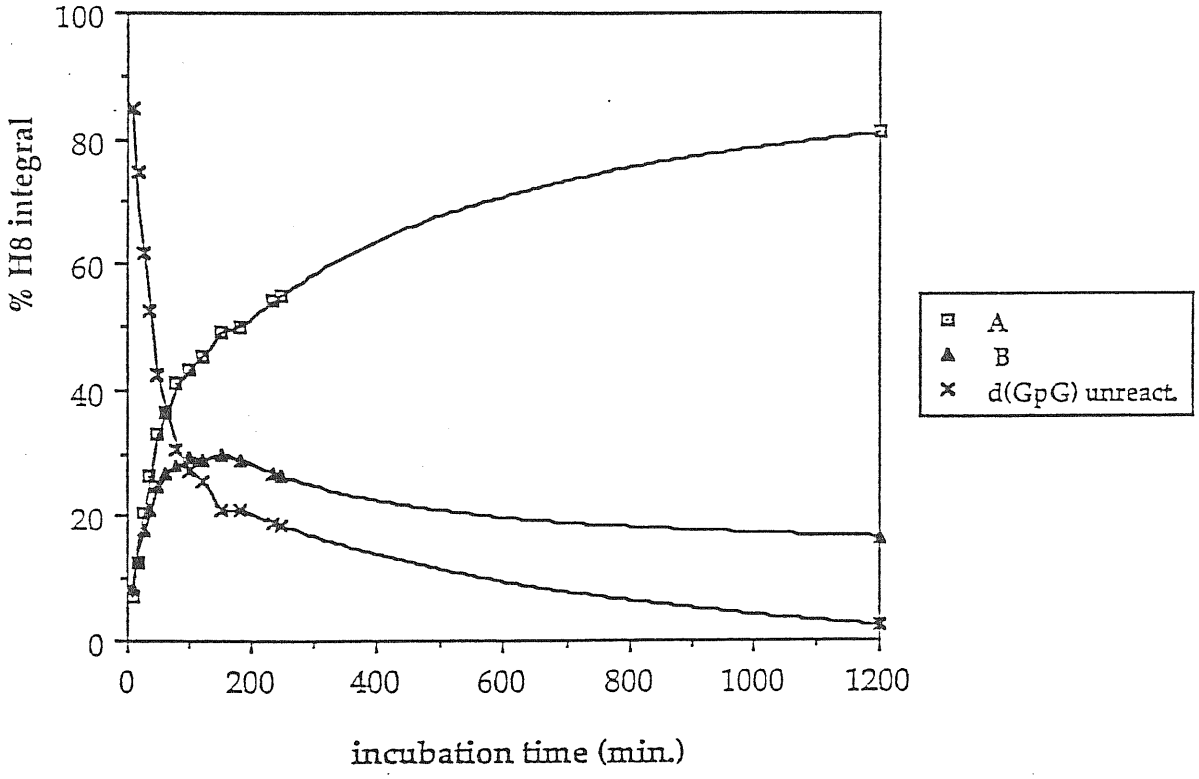

Figure 4.1 Time dependence of the concentration of different d(GpG) species in the reaction mixture: complex A (squares); complex B (triangles); unreacted dinucleotide (crosses) (d(GpG) dissolved in unbuffered water at equimolecular ratio with 3.5 mM trans-$RuCl_2(DMSO)_4$ at 40°C). The concentrations were determined by integration of the peak areas of the aromatic region (H8 of d(GpG)) in the ^1H NMR spectra.

observed in the reaction of *trans*-$RuCl_2(DMSO)_4$ with 2'dGuo (Cauci et al., 1991) and 5'dGMP (Alessio et al., 1989).

The two resonances at $\delta = 8.914$ ppm and $\delta = 7.792$ ppm, belonging to the intermediate product (B), can not be attributed to a complex in which only one guanine is coordinated via N7 (vide infra). No detectable monoadduct complex has been indeed observed in the investigated reaction.

A kinetic pattern similar to that of Figure 4.1 was observed when the reaction was carried out in buffered solution (30 mM PIPES, pH=7.5), all the other features being substantially unchanged except for the onset of a short lived intermediate that disappears in the first 30 minutes. The nature of this intermediate has not been further investigated.

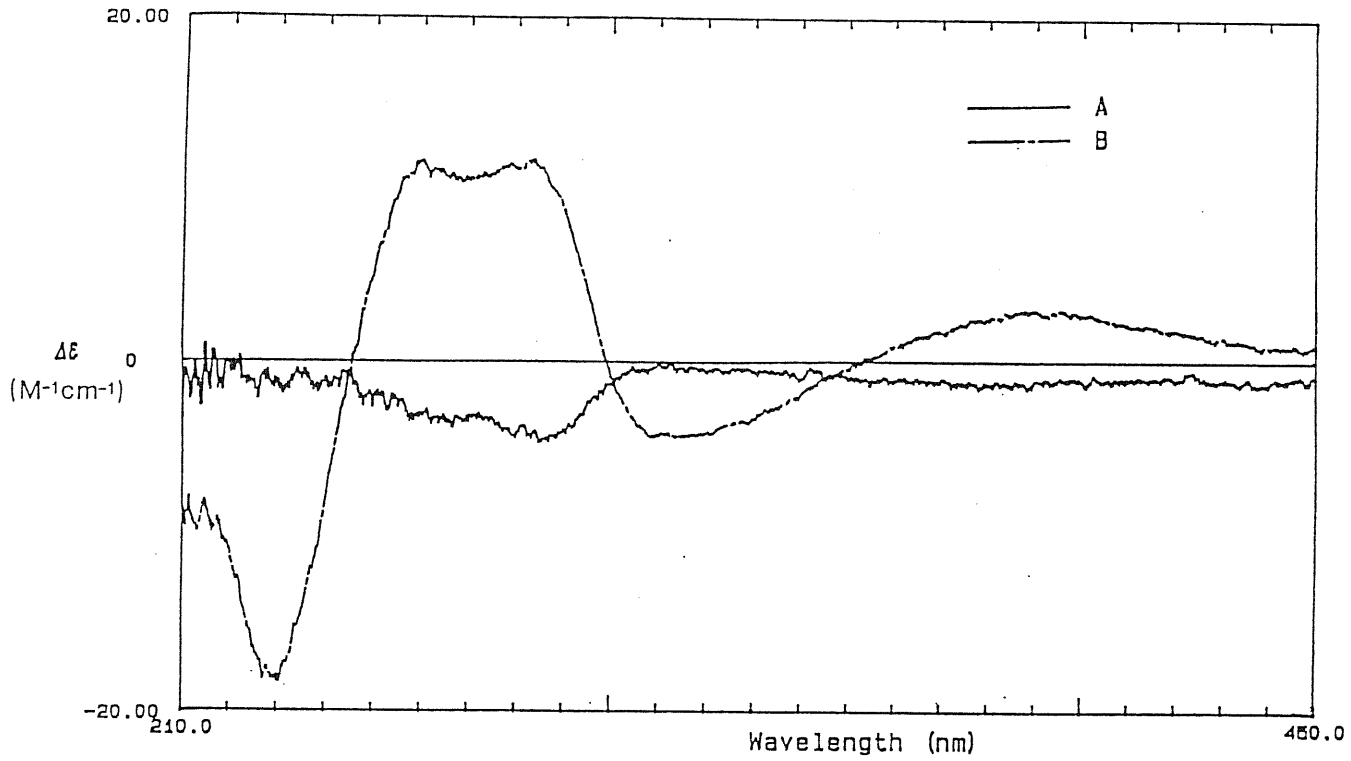

Figure 4.2 CD spectra of HPLC purified A and B reaction products in D_2O, pH 6.5, T= 23°C.

The pH titration of the reaction mixture in unbuffered water (Figure 4.4) clearly shows that in both the intermediate B and the final product A the ruthenium atom is coordinated via N7 atoms to two guanine moieties.

In fact all the chemical shifts of the H8 are unaffected by lowering the pH below 4, contrary to what expected for a free guanine N7 group (Girault et al., 1982), while at basic pH the relevant chemical shift changes observed are related to the decrease of the N1H pK_a, as previously found for the ruthenium dGuo complexes (Cauci et al., 1991) and N7 platinum complexes (Girault et al., 1982). On this basis we estabilished that an N7, N7 chelated structure occurs also for the intermediate B. Moreover the possibility of a phosphate coordination can be easily excluded by analysing the ^{31}P spectra, where the characteristic shift for a phosphate coordination at ruthenium, (Alessio et al., 1989) was not observed.

From Figure 4.4 it can be seen that the H8 resonances of the intermediate B are shifted upfield at increasing pH values, as generally observed for the platinum complexes (Girault et al., 1982), while for the final product A the downmost

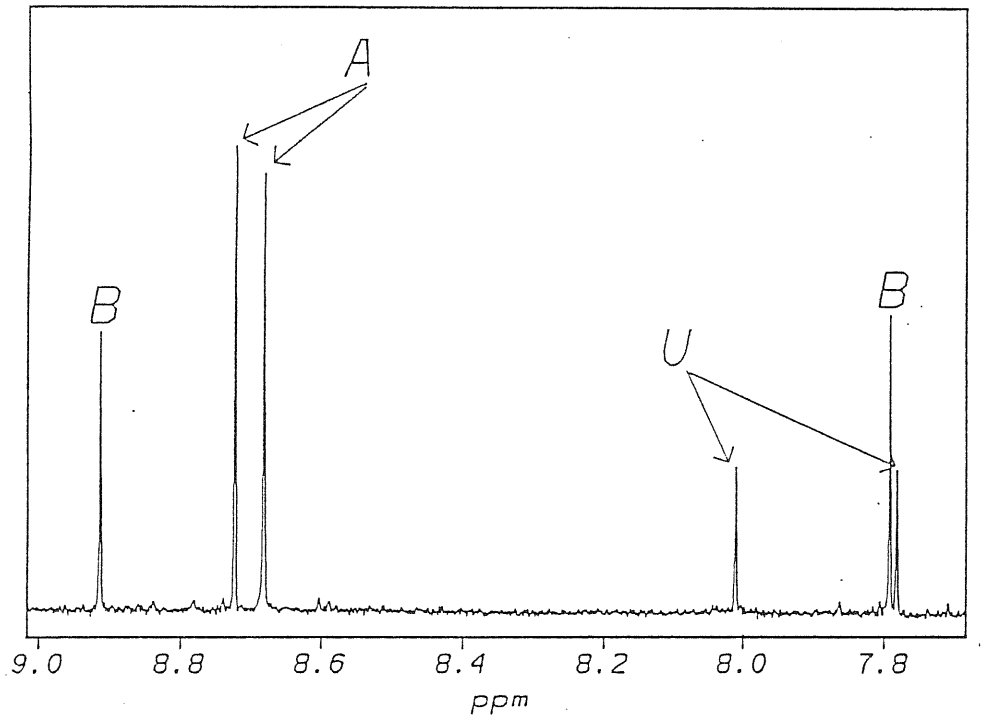

Figure 4.3 ^{1}H NMR spectrum low–field region of the reaction mixture four hours after dissolution of d(GpG) and trans–$RuCl_2(DMSO)_4$ in D_2O, at 40° C. Guanine H8 resonances of the final (A), intermediate (B) and unreacted (U) are identified.

resonance is shifted to lower field, probably due to ring current effects between the guanine residues.

The region of the 1H–NMR spectrum corresponding to DMSO methyl groups recorded on the reaction mixture shows up to 8 resonances (depending on the pH value, see Figure 4.5) which can be assigned, on the basis of the kinetic profile, to the intermediate B and to the final product A.

These assignments have been further confirmed by the NMR spectra of the HPLC isolated compounds. The number of resonances suggests a very low conformational mobility for DMSO ligands in the ruthenium complexes.

The pH dependence of the DMSO methyl chemical shifts is shown in Figure 4.5. The main feature of this profile is the coalescence at pH > 10 of two methyl pairs of the final product A. This effect has not been observed for the intermediate product B, confirming the more asymmetric configuration of the latter compound. Parallel titration of the final product A by UV absorption indicates that the titra-

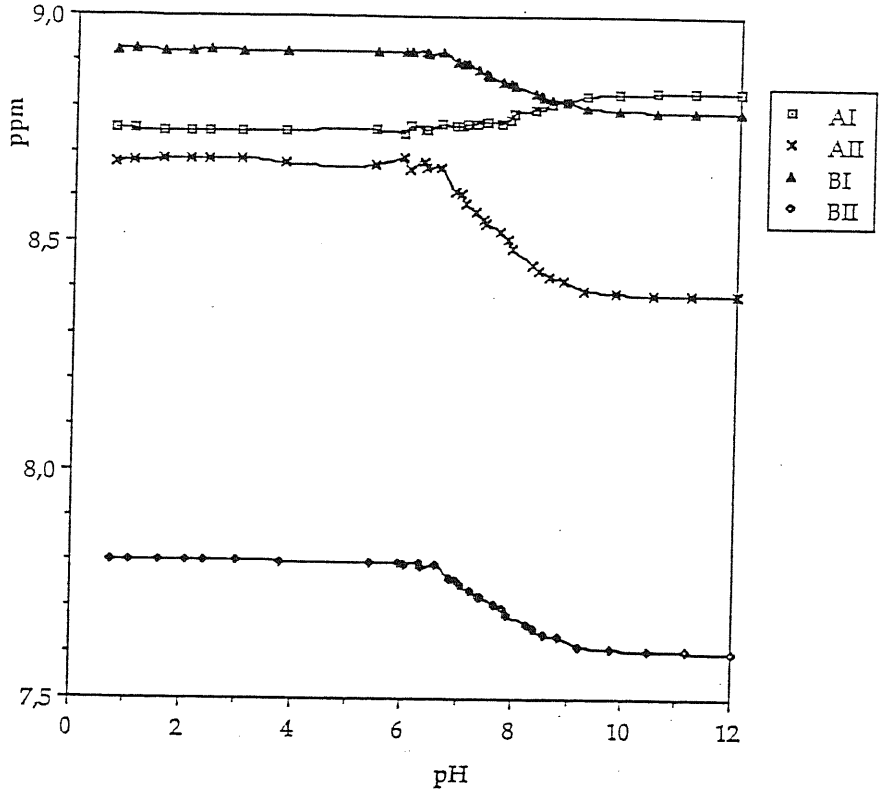

Figure 4.4 pH dependence of H8 chemical shifts of the products of the reaction between d(GpG) and trans-$RuCl_2(DMSO)_4$.

tion of N1H groups of guanine moieties is spread over the range 6 – 10 of pH values (data not shown).

In order to verify the possible release of the Cl^- coordinated at the metal center, both during the incubation and the titration procedure, we incubated d(GpG) with *trans*-$RuBr_2(DMSO)_4$ whose behaviour in water and with polymeric DNA is very similar to that of the corresponding chloride complex (Cauci, 1990). The kinetic pattern of the reaction in water at 40°C proved to be very similar to that described for the *trans*-$RuCl_2(DMSO)_4$. However the H8 chemical shifts in the intermediate B' (δ = 9.134 ppm and δ = 7.959 ppm) and the final product A' (δ = 8.953 ppm and δ = 8.855 ppm) were slightly different compared to the corresponding values of products B and A. Both the titration patterns of CH8 and DMSO methyls resonances show a shift similar to that observed with the chloride analogous but the individual values are different at each pH value, indicating that A, B, A' and B' are different compounds in the full pH range explored. This fact

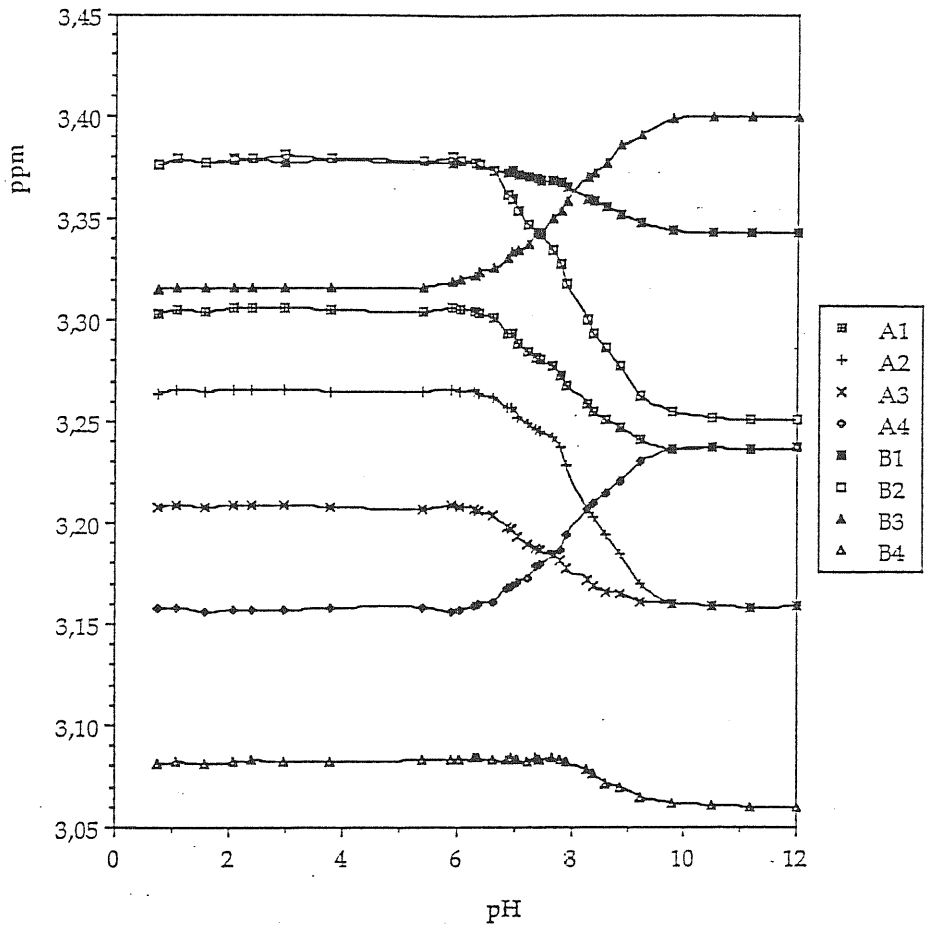

Figure 4.5 pH dependence of the chemical shifts of the DMSO methyl groups of the products of the reaction between d(GpG) and trans-$RuCl_2(DMSO)_4$. Employed symbols are indicated.

excludes, for all the compounds, the possibility of loosing the second halogen ligand also at high pH values (in fact the loss of the second halogen would render A=A' and B=B'). Moreover the absence of coalescence of the DMSO methyl pairs of A' (Figure 4.6) seems to indicate a more constrained structure for the bromo derivative as expected because of the larger steric hindrance of the bromide ion.

On the contrary the release of the first halogen ligand was confirmed by the reaction pattern obtained incubating the dinucleotide with monohalogenated ruthenium species, which gave exactly the same reaction products.

The purified final reaction product A has been extensively studied by means of 1D and 2D NMR in order to elucidate its structure.

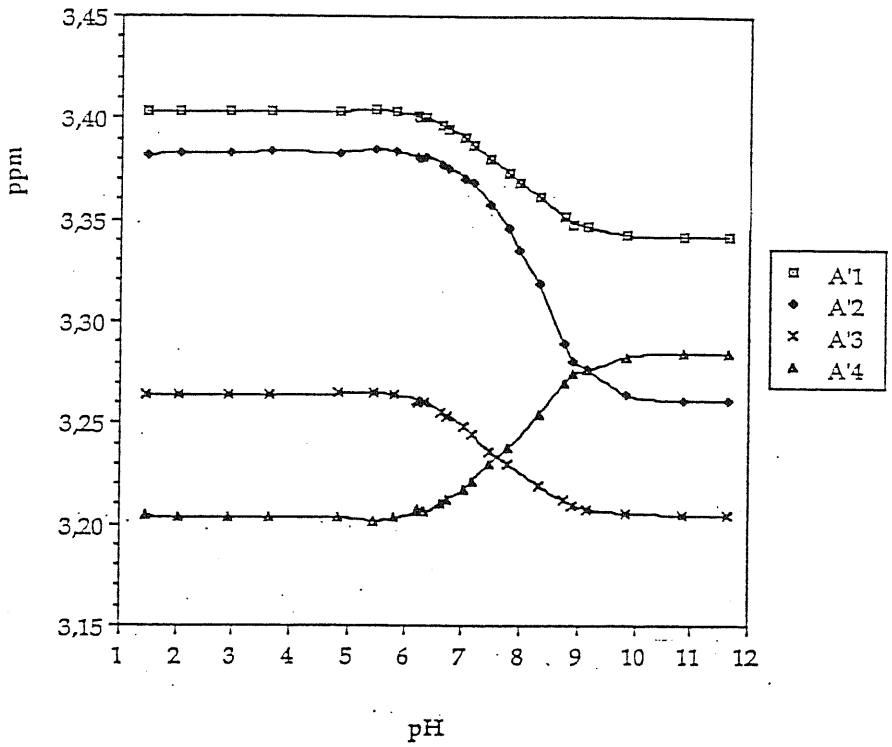

Figure 4.6 pH dependence of the chemical shifts of the DMSO methyl groups of the product A' from the reaction between d(GpG) and trans-$RuBr_2(DMSO)_4$.

NMR assignments

The examination of 2D TOCSY maps provided the connectivities within each deoxyribose spin system. The scalar networks were further confirmed by 2D DQF COSY spectrum that, in addition, allowed a proper attribution of the coupling pattern fine structure, for subsequent 1D simulations (vide infra). Each sugar ring spin system was connected to the attached guanine via the H8 NOESY crosspeaks to H2' and H3' resonances (Wuthrich, 1986). Additional base–sugar connectivities were consistent with the chosen attribution.

The detection of sequential contacts between the downmost H8 resonance and the deoxyribose H1', H2' and H2" of the adjacent residue, while further supporting the attribution based on the intraresidue contacts, also gives the relative position of each residue in the sequence. Namely, the system with the downfield H8 resonance is the 3' terminal residue and will henceforth be referred to as G_2. Consistently, the 5' terminal residue will be indicated as G_1. These conclusions are

also in line with the chemical shifts of the sugar spin systems, that are expected to exhibit a detectable difference for C5' protons (esteric in G_2 and alcoholic in G_1). The assignment list is given in Table 4.II.

Combined 2D NOESY and J coupling analysis

The qualitative interpretation of the intraresidue NOESY correlations allows to restrict the conformational space for both residues. The intranucleotide very weak H8–H1' contacts along with the stronger H8–H2', H8–H2" and H8–H3' connectivities agree with a χ angle in the anti range ($-90° \div -170°$) for both residues (Wuthrich, 1986). The latter contacts may also be indicative of the sugar puckering (Wuthrich, 1986). Indeed the strong H8–H3' crosspeak observed for G_1 suggests a N–type conformation of the corresponding deoxyribose. For G_2 conflicting NOE's are observed, between H8 and C2' and C3' protons, that may arise from fluctuation of the sugar puckering phase angle and/or χ torsion angle, as well as from higher order effects affecting the intensity of dipolar connectivities (Kumar et al., 1981; Macura et al., 1981; Borgias and James, 1988). Indeed the unfavourable value of the molecular tumbling rate (≈ 0.2 ns) required the use of long mixing times in order to achieve a signal to noise ratio amenable to quantitation. Thus any approximate NOESY quantitative analysis, based on the isolated spin pair and/or the initial linear buildup regime approximations (Kumar et al., 1981) proves affected by systematic underestimation of the interproton distances (Borgias and James, 1988). Nor would a complete relaxation matrix treatment of the NOESY data remove ambiguities in the presence of conformational equilibria not characterized in independent investigations.

The examination of the deoxyribose spin system coupling constants may help to remove ambiguity about G_2 conformation and is expected also to add further quantitative details to the conformational features of G_1 (Altona, 1982). Simulation of the coupling pattern in 1D NMR spectrum for both sugar spin systems, including the heteronuclear couplings, led to the results listed in Table 4.II. Qualitative inspection of the fine structure in 2D DQF COSY crosspeaks was sufficient for a detailed attribution of 1D splitting pattern (Figure 4.7).

Proton	Chemical shifts			
	G1 (A)	G2 (A)	G1 (*cis*-DDP)	G2(*cis*-DDP)
1'	6.251	6.330	6.186	6.222
2'	2.542	2.602	2.618	2.712
2"	2.812	2.480	2.735	2.556
3'	4.924	4.633	4.623	4.724
4'	4.122	4.207	4.073	4.229
5'	3.772	4.064	3.801	4.042
5"	3.834	4.114	3.520	4.042
8	8.659	8.753	8.267	8.572

Couple	Coupling constants			
	G1(A)	G2(A)	G1(*cis*-DDP)	G2(*cis*-DDP)
1'2'	0.9	9.0	0.6	8.1
1'2"	7.6	5.4	7.3	6.0
2'2"	-14.0	-13.6	-13.9	-13.6
2'3'	7.4	6.7	6.8	6.1
2"3'	10.8	2.9	10.7	2.9
3'4'	8.0	3.6	8.1	3.2
3'P	7.7	-	7.0	-
4'5'	2.8	2.0	2.7	2.9[a]
4'5"	2.6	3.8	3.4	2.9[a]
4'P	-	1.8	-	2.8
5'5"	-13.1	-11.7	-12.8	-
5'P	-	2.3	-	3.2[a]
5"P	-	3.5	-	3.2[a]

a) in *cis*-DDP only the sum of the coupling constants 4'5'+4'5" and 5'P+5"P was obtained (den Hartog et al., 1982).

Table 4.II Comparison between chemical shifts (ppm) and coupling constants of compound A (present thesis) and of d(GpG) with cis-DDP (den Hartog et al., 1982)(T = 23°C, pH =6.5).

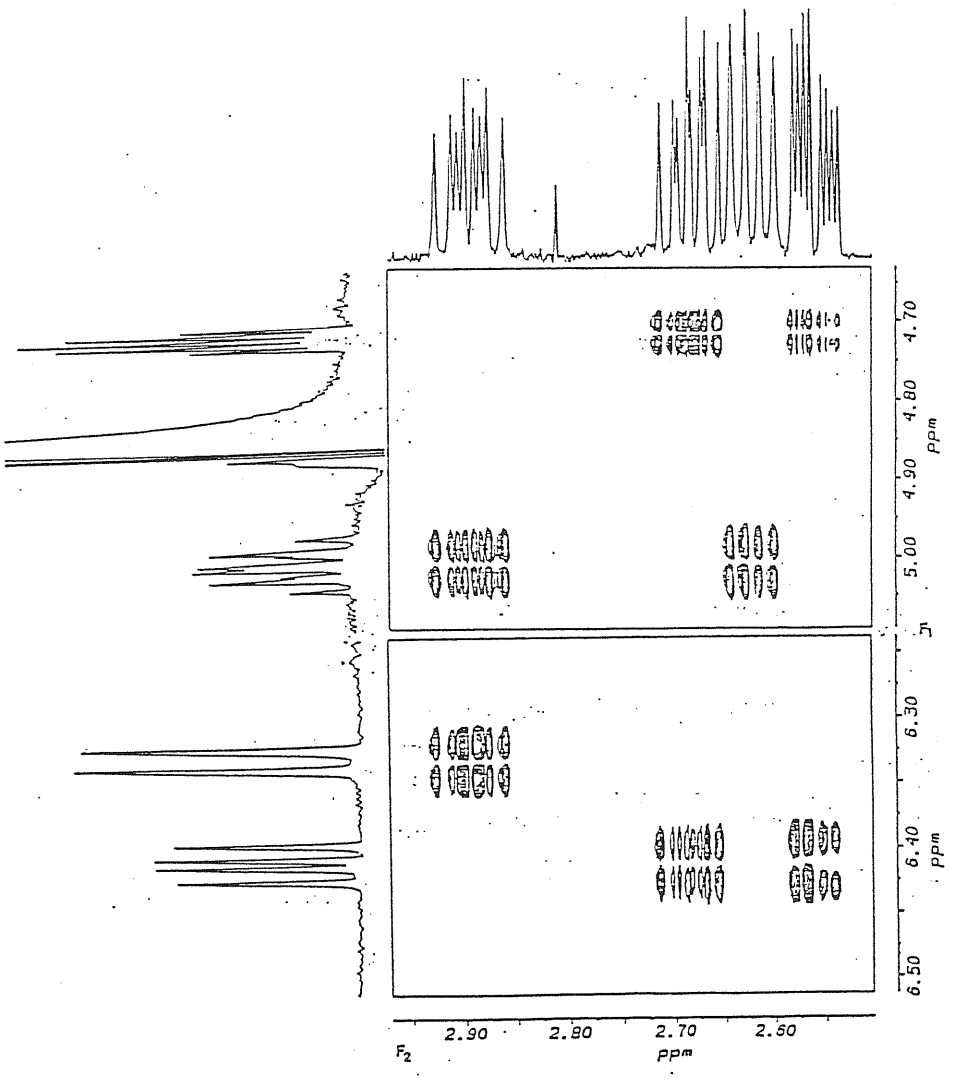

Figure 4.7 500 MHz 1H NMR 2D DQF–COSY spectrum of the final compound A as obtained, after purification, from the reaction between d(GpG) and trans–$RuCl_2(DMSO)_4$. The connectivities of deoxyribose 2' and 2" protons to 3' (upper panel) and 1' protons (lower panel) are shown. Positive and negative contour level are plotted without distinction. The corresponding 1D spectrum traces are also reported. Inspection of the cross–peak antiphase pattern enables the detailed interpretation of the corresponding 1D multiplet fine structure, for subsequent quantitative refinements via least squares fitting of the simulated and experimental 1D pattern.

The J values are consistent with a pure N type conformation for the G_1 residue, whose P and ϕ_M, the pseudorotation angle and puckering amplitude (Saenger, 1984), were estimated to be ≈ 0 and 35°, respectively, according to the tables giv-

en by Rinkel and Altona (1987). At variance, no single conformation accounts for the observed J couplings in residue G_2. The experimental values are therefore interpreted in terms of the equilibrium between the two most stable limit conformers N and S (Altona, 1982; Rinkel and Altona, 1987).

According to the equation reported by Altona (1982):

$$p(S) = \frac{[17.8 - (J_{1'2''} + J_{3'2''})]}{10.9} \tag{4.1}$$

the percentage of G_2 S–conformer (p(S)) was 85% entailing some 15% in N–conformation (as opposed to 100% N–conformation evaluated for G_1 with the same equation). The analysis of the J coupling values of the H4' with C5' proton pair and the heteronuclear couplings ($J_{3'P}$ for G_1 , $J_{4'P}$, $J_{5'P}$ and $J_{5''P}$ for G_2) may be exploited to estimate the single γ_1 , γ_2, ϵ_1 and β_2 (Altona, 1982). The J constants of G_1 C5' protons with the vicinal H4' (Tab. 4.II) are small and approximately equal (2.8 and 2.6 Hz). Based on the generalized Karplus equation (Karplus, 1959; Haasnot et al., 1980), one can argue that these values do not correspond to a single conformation, but rather to a restricted family of rotamers centered around $\gamma_1 \approx +60°(\gamma^+)$. An interpretation in terms of the three classical rotamers ($\gamma_1 = +60°$, 180°, $-60°$), using limit proper J values (Haasnot et al., 1980) leads to physically inconsistent results. This may be not unexpected when the rotational distribution is confined within a rather narrow width. Moreover, the asymmetry of the C4'H–C5'H2 ethanoid fragment should be considered, before choosing the "idealized"staggered rotamers. As suggested by Altona (1982), a reasonable assumption is to rely on the most commonly occurring γ values in oligonucleotides ($\gamma^+ = 53°$, $\gamma^- = 70°$, $\gamma^t = 180°$).

In spite of this "judicious"choice, the idealized ternary model appears however unsatisfactory for describing the γ distribution in double helix structure with strong preference for γ^+ conformations. A rotational restriction imposed because of the very low occurrence of the γ^- conformation in DNA leads to (Altona, 1982):

$$p(\gamma^+) = \frac{[13.3 - (J_{4'5'} + J_{4'5''})]}{9.7} \tag{4.2}$$

to estimate the amount of γ^+ rotamer. For our dinucleotide–ruthenium complex the rotational restraints acceptable for the DNA duplexes cannot be adopted tout

court. First, even with the very small J constants of G_1 C5' protons, the bias for the rotational distribution of γ cannot be safely assessed without a preliminary stereospecific assignment of the 5' geminal pair. In addition, the choice of the limit rotamers, i. e. the width of the rotational fluctuation, appears to drive the result of the calculation towards completely different distribution independent of the stereospecific assignment because of the very close values of $J_{4'5'}$ and $J_{4'5''}$. Namely, using the limit rotamers with $\gamma = +53°, 180°$ and $-70°$, one obtains $p(\gamma^+) = 83\%$, $p(\gamma^t) = 13\text{-}15\%$, $p(\gamma^-) = 4\text{-}2\%$, while for $\gamma = 43°, 180°$ and $-64°$ one obtains $p(\gamma^+) = 90\%$, $p(\gamma^t) = 0\%$, $p(\gamma^-) = 10\%$ (the sum relationship of equation 4.2 would give $p(\gamma^+) = 82\%$). Apparently even more intriguing results are obtained for G_2. Here the small $J_{4'5}$ values (2.0 and 3.8 Hz) again indicate the predominance of the γ^+ rotamers ($\gamma_2 \approx 60°$), but the extraction of physically meaningful distribution depends on the stereospecific assignment for different sets of limit rotamers (Altona, 1982). The consideration of C5' protons NOE's may provide some clue for their stereospecific identification. In both the deoxyribose moieties the closest 3'–5' contact is exhibited by the downfield C5' proton. Unfortunately the reliability of these NOE's is partially reduced by strong coupling effects, expected because of the limited chemical shift difference of C5' geminal pairs (≈ 0.05 ppm) (Kay et al., 1986, Esposito et al., in press). Thus, when both C5' hydrogens are involved in NOE connectivities, as observed for G_1, the relative intensities should be regarded with some care. Hence no firm conclusion can be reached for G_1. On the contrary the observation of a single intraresidue 3'–5' contact in G_2 suffices to assign stereospecifically the lowfield C5' proton resonance as pro–R and allows to conclude that γ_2 rotational distribution entails mainly γ^+ (82%) and γ^t (16%) conformers, choosing limit rotamers with $\gamma = 43, 180, -64$ (Altona, 1982) according to the commonly occurring distribution in oligonucleotides.

Incidentally, we also notice that the relative chemical shifts of pro–R and pro–S resonances do not agree with the usual occurrence reported for C5' hydrogens (Remin and Shugar, 1972).

The stereospecific identification of G_2 C5' protons also enables an unambiguos evaluation of β_2 torsion angle, using the $J_{5'P}$ and $J_{5''P}$ values (Tab. 4.II) in the Lankorst et al. equation (Lankorst et al., 1984):

$$J_{HCOP} = 15.3\cos^2(\phi) - 6.1\cos(\phi) + 1.6 \qquad (4.3)$$

where $\phi = \phi^R$ or ϕ^S i.e. the H5"–C5'–O–P and H5'–C5'–O–P dihedral angles, being $\beta = \phi^R - 120° = \phi^S + 120°$. Calculations yield $\phi^S = \pm 60°, \pm 95°$ and $\phi^R = \pm 53°, \pm 102°$, that are compatible only for $\phi^S \approx +60°$ and $\phi^R \approx -53°$, i. e. $\beta_2 = -177° \pm 3°$. Overall a limited deviation from $\gamma^+\beta^t$ conformation seems to emerge for G_2, which apparently conflicts with the value of the G_2 long range $J_{4'P}$ (1.8 Hz). Although no reliable parametrisation of $J_{4'P}$ (γ, β) has been established yet, an average experimental value of 3.3 Hz has in fact been suggested by Altona (1982) for typical $\gamma^+\beta^t$. It is rather hard to evaluate the effect of a γ_2 fluctation on the value of $J_{4'P}$, without accounting for the accompanying β_2 rearrangement (the two torsion angles are interdependent). It seems interesting to notice, however, that the amount of G_2 γ^t rotamer (16%) is similar to the amount of G_2 N–type conformer (15%) suggesting that γ_2 fluctations may be viewed within a molecular framework involving concerted rearrengement. Equation 4.3 can be employed also for evaluating ϵ_1 exploiting the γ_1 $J_{3'P}$ coupling constant (Tab. 4.II) and the relationship $\epsilon = \phi_{3'P} - 120°$. Among the four possibilities calculated from equation , only two are acceptable after ruling out the unfavorable ϵ^- conformers, i. e. $\epsilon_1 = -151°$ or $\epsilon_1 = +63°$. Inspection of a NOE restrained model leads to retain only the former value i. e. $\epsilon_1 = -151°$, a conformation commonly encountered in RNA oligomers (Saenger, 1984), but reported also in alternating N–S oligodeoxyribonucleotides (Altona, 1982).

Once combined all together these structural elements can provide a model for the coordination complex of d(GpG) to ruthenium, which accounts also for the G_1 H8 - G_2 H8 proximity inferred from the corresponding connectivities, observed in NOESY spectra. The presence of this contact clearly indicates a head to head arrangement of the two bases, coordinated at the central metal via N7,N7 chelation. Moreover the low asymmetry of the metal center as suggested by the CD spectrum (Figure 4.2) and the coalescence at basic pH of the DMSO methyl resonances (Figure 4.5), indicate that N7, N7 cis chelation of d(GpG) to ruthenium is accommodated in equatorial synclinal position, opposite to DMSO ligands, with the axial positions still engaged in water and chloride coordination.

Molecular modelling

Starting from the structural restraints discussed above a preliminary investigation over the possible conformations of compound A was undertaken. As a starting model a complex between the two isolated nucleosides, i. e. without phosphate groups connecting the deoxyribose moieties and $Ru(DMSO)_2$ via the N7's was chosen. The phosphate group, the Ru coordinated water and the chloride atom were added later. In this first step the charges on Ru and the DMSO's were taken equal 0 while the AMBER parameters were left unchanged for the two nucleosides. The torsional angles were frozen at the following values:

$$\chi_1 = -154 \qquad \gamma_1 = 45.5 \qquad \delta_1 = 84.3$$

$$\chi_2 = -97.8 \qquad \gamma_2 = 53.0 \qquad \delta_2 = 156.4$$

which are close to the standard values for single strand A– and B–DNA (Saenger, 1984) (entailing pure N and S deoxyribose ring puckering respectively) and are in agreement with the experimental restraints. The two torsional angles defined by the sequence C8–N7–Ru–S, θ_1 and θ_2 for the respective residues, were then rotated in steps of 18° in order to get an energy map. The low energy regions were further examined to check if the distance between the O5' and the O3' atoms was sufficiently short to accommodate a phosphate group with no major changes in the structural parameters. We were rather tolerant in this step since unfreezing the remaining degrees of freedom could reduce this distance. Such a procedure, while not expected to give a realistic energy quantitation can nevertheless monitor steric hindrance which energies are by far overcoming the inaccuracy of both the model and the forcefield. The only two regions that could match the above requirements were those centred around (−108, 108) and (108, −108) in the (θ_1, θ_2) plane, corresponding to head to head conformations which also fit well the experimentally observed proximity of the H8 protons.

Starting from these two conformations the angles θ_1, θ_2, χ_1 and χ_2 were roughly adjusted in order to add the phosphate group. We choose to add the water molecule on the side where hydrogen bond could be possible with the O6 atoms of the base; the opposite choice would have brought the chloride atom in close contact with the same atoms. Once the satisfactory initial conformation

was obtained, a preliminary constrained energy minimization in vacuo, to remove high energy spots introduced in the previous step, was run using the complete modified AMBER forcefield. The following values were assumed to represent the experimental data:

$$\gamma_1 = 45.5^\circ \qquad \delta_1 = 84.3^\circ \qquad \epsilon_1 = -151^\circ$$

$$\beta_2 = 180^\circ \qquad \gamma_2 = 53.0^\circ \qquad \delta_2 = 156.4^\circ$$

In this way two starting structures for subsequent analysis were obtained. Since all the simulations do not take into account the solvent and a dielectric constant of 1 was used throughout, the energy differences between them at this level are not very significant.

For the structure corrresponding to $\theta_1 \approx 108^\circ$ and $\theta_2 \approx -108^\circ$, (which will be called hereafter model 2, as opposed to the other called model 1 (Figure 4.8a) with $\theta_1 \approx -108^\circ$ and $\theta_2 \approx 108^\circ$) the addition of the phosphate group and the subsequent minimization led invariably to a loss of the anti conformation in one or both residues (in addition the final conformer was also the one at higher energy).

In order to sample the conformational space around the two structures obtained, possibly overcoming energy barriers, we run restrained simulated annealing for both conformations assuming alternatively $\epsilon = 1$ and $\epsilon = 80$. For both starting structures the choice of $\epsilon = 1$ led to results inconsistent with the experimental findings, due to the overestimated electrostatic interactions. The choice of $\epsilon = 80$, unrealistically reducing the electrostatic interactions, increases the accessibility of the conformational space sampling, which is highly desirable when the model does not include all the features of the system under investigation (like the interactions with the solvent). The results obtained in this case are different for the two starting structures. In none of the runs the simultaneous presence of χ_1 and χ_2 in anti conformation was found for model 2, thus confirming the probable inconsistency of this model with the experimental data. At variance for model 1 χ_1 is preserved in the anti range (close to -150°) in most of the runs while χ_2 varies within a large range of values including also anti conformations. The structural restraints, however, introduce a strong correlation among χ_2 and the backbone angles ζ and α which determine the orientation of the phosphate group relative

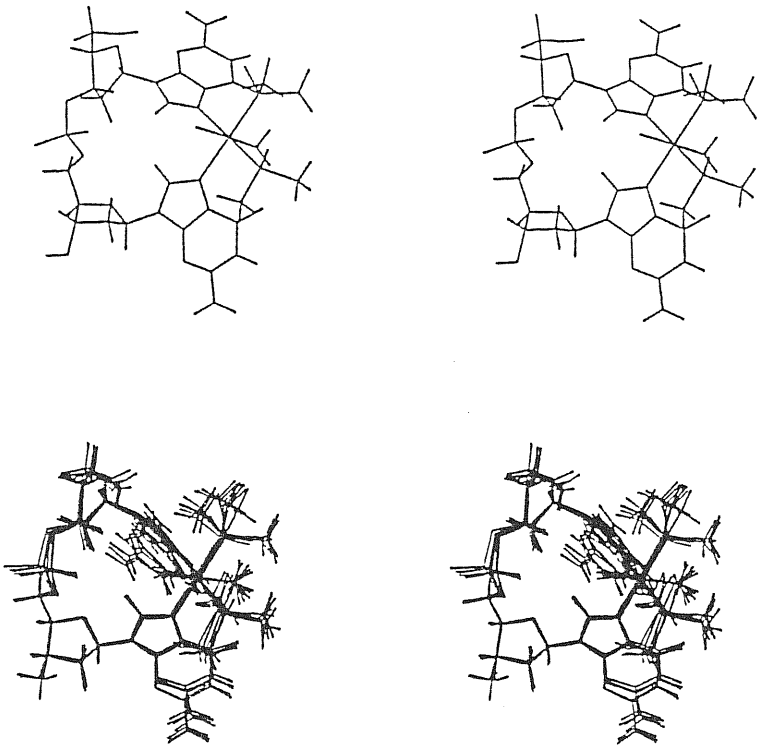

Figure 4.8 a) Stereodrawing of the starting model of compound A (model 1); b) Superimposed stereodrawing of 8 structures of compound A as obtained after simulated annealing.

to the complex (provided that the other angles are forced to their experimental values). Whenever the angle χ_2 is in the anti range, which happens in 20% of the runs, ζ and α both assume values close to $-60°$, forcing the phosphate oxygens outwards with respect to the metal center, presumably toward the solvent. This arrangement is expected to occur in solution where the phosphate group can be involved in hydrogen bonds with the water molecules. Incidentally the values of ζ and α are those commonly occurring in X–ray structure of nucleic acids. A stereo view of some of the superimposed final structures obtained is given in Figure 4.8b.

The variability of χ_2 can be ascribed to the very poor solvent representativity in conjunction with the type of restraints inferred from experimental data for residue γ_2 , whose increased mobility should ultimately reflect a rather broad minimum in the conformational energy map.

The reliability of the class of structures originating from model 1 was further investigated. In particular an MD simulation was run at 27°C, imposing a distance

dependent dielectric constant $\epsilon = 4r$ (r in Å). The results were rather striking since the overall features were maintained also removing the experimental restraints. The angles ϵ_1, β_2 and γ_2 stayed close to their experimental values. The endocyclic angles δ_1 and δ_2 are interesting since they should be sensitive to the sugar puckering and mobility. The results nicely agree with the picture of G_1 sugar ring fixed in N–conformation (δ_1 = 84.3) and G_2 moving between N– and S– conformer (δ_2 = 156.4), in agreement with the NMR analysis. The values of δ_2 were found to scatter between the two limit values showing no preference for either of the two conformers.

The 5' terminal CH_2OH is found, as expected from model inspection, completely free to rotate thus contraddicting the experimental data. Even accounting for an imperfect parametrization of the Karplus relationship in 5' free terminals, the NMR inequivalence of G_1 H5' and H5" (significantly increased on complexation) along with their small coupling constants to H4' can hardly be reconciled with a free rotating 5' terminal. According to the model a hydrogen bond might be formed with an oxygen of the phosphate group (G_1 O5 – OP separation 3.0). Water bridges with phosphate oxygen may also be responsible for blocking rotation around C4–C5 bond.

In simulations with distance dependent dielectric constant χ_1 and χ_2 depart from their initial values and both vary around 180° in a range of approximately 40° so that they do not completely agree with the data. This behaviour parallels the rearrangement of the angles ζ_1 and α_2, close, most of the time, to 60° and 180° respectively. These values maintain, however, the phosphate group pointing outwards.

In conclusion the fair agreement between the simulations and the experimental findings strongly points to model 1 as the structure adopted by d(GpG)–$RuCl(DMSO)_2(H2O)$ in solution.

Comparison of d(GpG) conformation in ruthenium and platinum complexes

In summary the data discussed so far suggest that the spatial arrangement of d(GpG) complexed with ruthenium is closely related to the conformation it

adopts in the *cis*–DDP complex, obtained via NMR studies (den Hartog et al., 1982) and successively confirmed by the X–ray structure of cisplatin d(pGpG) complex (Sherman et al., 1985). In the ruthenium complex the deoxyribose skeleton is rigid in G_1, with a nearly pure N–conformation, and more flexible in G_2, with some 85% S–type and 15% N–type puckering equilibrium, as inferred from J coupling analysis. The base–sugar relative orientations exhibit the same mobility difference, being anti in both nucleoside moieties, but with a much more reduced fluctuation amplitude in G_1. The latter conclusion rests mainly on 2D NOESY evidence and on subsequent molecular dynamics simulations. Despite the systematic deviation expected in NOESY quantitative analysis from the assumption of the isolated spin pair model, approximate distance restraints for G_1 are compatible with only a limited range of χ_1 values, i. e. a limited class of closely related anti structures. At variance a much broader family of χ_2 conformations is obtained for G_2, even constraining its sugar part in the most populated S–conformer. No attempt was performed to simulate the simultaneous fluctuation of G_2 χ angle and deoxyribose puckering because of the inherent accuracy limits of our NOE quantitative determinations. An analogous G_2 conformational freedom has been reported in *cis*–DDP complex too and was regarded as surprising by den Hartog and co–workers (1982), in view of the expectedly strict stereochemical requirements of a chelating dinucleotide. In both ruthenium and platinum adducts, the complexation of d(GpG) occurs via N7, N7 chelation with a head to head arrangement of the bases (den Hartog et al., 1982, Sherman et al., 1985). In a head to tail geometry G_1 and/or G_2 O6 are intuitively expected to engage unfavourable steric and electrostatic interactions with the axial chloride, whilst both may be involved in hydrogen bonds with the opposite axial water molecule when one of the head to head arrangement is selected. This feature is further confirmed by the results of our simulations shown in Figure 4.8 where the distances H_{water}–O6 and O_{water}–O6 range between 1.83 and 3.09, and 2.61 and 2.78 respectively. Thus no steric hindrance is found between guanine O6 and axial water. Whether and to what extent these interactions are actually responsible for the stabilization of a single diastereoisomer out of four possible it is hard to predict because of lack of information about the orientation of the bulky DMSO molecules.

As a matter of fact, in the chosen head to head geometry the values of θ_1 and

θ_2 are very close to the corresponding angles derived from the X–ray structure of d(pGpG)–Pt (Sherman et al., 1985) using the definitions and the figures reported. The dihedral angle between the oriented planes of the bases, which is found around 100° in our starting model, varies within a large range (60°–100°) in the structures obtained by simulated annealing. A similar unstacking of the bases has been reported for the cisplatin analog (76°–87°) (Sherman et al., 1985).

As far as the remaining conformational features are concerned, ϵ_1 and β_2 dihedral angles are quite similar in the ruthenium and platinum complexes of d(GpG). In fact for the *cis*–DDP complex a $\epsilon_1 = -162$ has been evaluated (den Hartog et al., 1982, Sherman et al., 1985) in good agreement with the $\epsilon_1 = -151$ of the ruthenium complex. The β_2 value in the cisplatin analog could not be safely assessed because of chemical shift equivalence of G_2 C5' protons (den Hartog et al., 1982). The sum of their coupling constants to phosphorus was therefore employed to calculate the relative population of β_t conformer (93%). Complexation with ruthenium removes the chemical shift degeneracy of G_2 C5' protons and their stereospecific assignment allows a precise estimate of β_2 ($-177°$). This value corresponds to 96% bt conformer, if stereospecific assignments are disregarded and limit rotameric populations are calculated, i.e. a conformational distribution very close to that observed with platinum.

Slightly different rotational distributions are observed for γ_1 and γ_2. In the d(GpG) cisplatin complex at 23°C γ_1 and γ_2 exhibit an approximately equal population of most abundant γ^+ (77% and 79% respectively), while with ruthenium the two distributions appear to be different (γ^+ = 83–90% for γ_1 and 82% for γ_2).

Discussion

The octahedral antitumor complex *trans*–$RuCl_2(DMSO)_4$ is able to form a 1,2 intrastrand cross–link with d(GpG); preliminary measurements on a tetramer (d(TpGpGpT)) indicate that a similar behavior can be extrapolated to higher molecular weight DNA. Moreover the presence of two N7–coordinated guanine moieties, two dimethyl sulfoxide molecules and one halogen atom in the coordination sphere of the metal was demonstrated in both the intermediate and final

reaction products.

The final reaction product shows structural features which are surprisingly similar to those exhibited by the corresponding cisplatin complex, indicating that such a way of interaction with DNA is not exclusive to Pt or to metals with square planar coordination geometry, as previously suggested (Lippard, 1987), but is probably a common motif in the interaction of transition metal complex which possess two ligand positions in cis available for covalent binding. If one assume that the 1,2 intrastrand cross–link lesion on DNA is the crucial damage responsible of the antitumor effect, our findings can give the rationale to the design of octahedral metal based anticancer compounds.

NMR and molecular modelling studies led to depict a structure very similar to that described for *cis*–DDP, in which the bases have a head to head disposition, with the glycosidic χ angles essentially in the anti range, the sugar puckering of 5'G is 3'–endo, whereas that of the 3'G is less constrained, but mainly 2'–endo. The two guanine bases result strongly destacked, suggesting that, if this feature is maintained in double stranded DNA, a relevant distortion of the duplex, mainly consisting of bending, should occur (as in the case of cisplatin complexes).

The nature of the intermediate reaction product B was not studied in detail. The main features of this complex appeared to be an highly asymmetric disposition of the ligands around the metal center (see CD spectrum, relative position of the CH8 resonances, absence of coalescence of DMSO methyl resonances at basic pH). At variance with the final compound A, the H1' coupling constants of both the N7 coordinated guanines indicated a sugar puckering mainly 2'–endo. A structure in which one guanine is trans to the halogen ligand and one is trans to a DMSO ligand is proposed, and could be derived from the kinetic trans effect of the halogen atom.

Finally the irreversible binding of *trans*–$RuX_2(DMSO)_4$ (X=Cl, Br) is likely to be responsible of the DNA damage and antitumor action of these complexes. On the other hand the reversibility of the N7 monofuctional binding may justify the low host toxicity and also give a rationale for the administration route.

REFERENCES

Abragam, A., (1961) Principles of Nuclear Magnetism, Oxford University Press, London.

Admiraal, G., van der Veer, J. L., de Graff, R. A. G., den Hartog, J. H. J., Reedijk, J. (1987) J. Am. Chem. Soc. **109**, 592.

Alessio, E., Attia, W. M., Calligaris, M., Cauci, S., Dolzani, L., Mestroni, G., Monti-Bragadin, C., Nardin, G., Quadrifoglio, F., Sava, G., Tamaro, M., Zorzet, S. (1987) in Platinum and Other Metal Coordination Compounds in Cancer Chemotherapy Nicolini, M., ed., Martinus Nijhoff Publishing, Boston, 617.

Alessio, E., Mestroni, G., Nardin, G., Attia, W. M., Calligaris, M., Sava , G., and Zorzet, S. (1988) Inorg. Chem. **27**, 4099.

Alessio, E., Xu, Y., Cauci, S., Mestroni, G., Quadrifoglio, F., Viglino, P., and Marzilli, L. G. (1989) J. Am. Chem. Soc. **111**, 7068.

Alessio, E., Balducci, G., Calligaris, M., Costa, G., Attia, W. M., and Mestroni, G. (1991) Inorg. Chem. **30**, 609.

Alfrey, T., Berg, P. W., and Morawetz, H. (1951) J. Polym. Sci. **7**, 543.

Altona, C. (1982) Recl. Trav. Chim. Pays Bas **101**, 413.

Anderson, C. F., and Record, T. M. Jr., (1982) Ann. Rev. Phys. Chem. **33**, 191.

Aue, W. P., Bartholdi, E., and Ernst, R. R. (1976) J. Chem. Phys. **64**, 229.

Bain, A. D., (1984) J. Magn. Reson. **56**, 418.

Bax, A., Davis, G. (1985) J. Magn. Reson. **65**, 355.

Bax, A., Ikura, M., Kay, L. E., Torchia, D. E., and Tschudin, R. (1990) J. Magn. Reson. **86**, 304.

Bau, R., and Gellert, R. W. (1978) Biochimie **60**, 1040.

Bellon, S. F., Coleman, J. H., and Lippard, S. J. (1991) Biochemistry **30**, 8026.

Bleam, M. L., Anderson, M. T., and Record, C. F. (1983) Biochem. **22**, 5418.

Bodenhausen, G., and Ernst, R. R., (1982) J. Am. Chem. Soc. **104**, 1304.

Bodenhausen, G., Kogler, H., and Ernst, R. R., (1982) J. Magn. Reson. **58**, 370.

Bodenhausen, G., and Ruben, D. J. (1980) Chem. Phys. Lett. **69**, 185.

Bolton, P. H., and Bodenhausen, G. (1979) J. Am. Chem. Soc.**101**, 1080.

Bolton, P. H., and Bodenhausen, G. (1982) Chem. Phys. Lett. **89**, 139.

Borgias, B. A., and James, T. (1988) J. Magn. Reson. **79**, 493.

Braunlin, W. H., Drakenberg, T., and Nordenskiöld, L. (1987) Biopol. **26**, 1047.

Braunschweiler, L., and Ernst, R. R., (1983) J. Magn. Reson. **53**, 521.

Cantor, C. R., and Schimmel, P. R. (1980) Biophysical Chemistry (vol. 3), W. H. Freeman and Company, San Francisco.

Cauci, S., (1990) PhD Thesis, University of Trieste, Trieste (Italy).

Cauci, S., Viglino, P., Esposito, G., and Quadrifoglio, F. (1991) J. Inorg. Biochem. **43**, 735.

Cavanagh, J., Chazin, W. J., and Rance, M. (1990) J. Magn. Reson. **87**, 110.

Cesàro, A., Delben, F., Flaibani, A., and Paoletti, S., (1986) Carbohydr. Res. **161**, 355.

Chandrakumar, N., and Subramanian, S. (1985) J. Magn. Reson. **62**, 346.

Chandrakumar, N. (1987) J. Magn. Reson. **71**, 322.

Chaney, S. G., Gibbons, G. R., Wyrick, S.D., Podhasky, P. (1991) Cancer Res. **51**, 969.

Choi, H.-K., Huang, S. K.-S., and Bau, R. (1988) Biochem. Biophys. Res. Commun. **156**, 1125.

Chung, C. W., and Keeler, J. (1992) Book of Abstracts 11^th EENC, Lisboa, Portugal.

Clarke, M. J. (1989) Prog. Clin. Biochem. Med. **10**, 25.

De Marco, A., Llinas, M., and Wüthrich, K. (1978) Biopol. **17**, 617.

De Vita, V. T., Hellmann, S. Jr., and Rosenberg, S. A., (1985) Cancer. Principles and practice of oncology. J. B. Lippincott Company (Philadelphia).

den Hartog, J. M. J., Altona, C., Chottard, J. C., Girault, J. P., Lallemand, J. Y., de Leeuw, F. A. A. M., Marcelis, A. T. M. and Reedijk, J. (1982) Nucleic Acids Res. **10**, 4715.

Drobny, G., Pines, A., Sinton, S., Weitekamp, D., and Wemmer, D. (1979) Faraday Div. Chem. Soc. Symp. **13**, 49.

Eich, G. W., Bodenhausen, G., and Ernst, R. R. (1982) J. Am. Chem. Soc. **104**, 3731.

Ernst, R. R., Bodenhausen, G., and Wokaun, A. (1990) Principles of Nuclear Magnetic Resonance in one and two dimensions (paperback ed.), Oxford University Press, Oxford.

Esposito, G., Fogolari, F., Molinari, H., Pegna, M., and Zetta, L., J. Magn. Reson. in press.

Esposito, G., Cauci, S., Fogolari, F., Alessio, E., Scocchi, M., Quadrifoglio, F., and Viglino, P. (1992) Biochemistry **31**, 7094.

Esposito, G., Gibbons, W. A., and Bazzo, R., (1987) J. Magn. Reson. **80**, 523.

Esposito, G., and Pastore, A. (1988) J. Magn. Reson. **76**, 331.

Fano, U. (1957) Rev. Mod. Phys. **29**, 74.

Fichtinger-Schepman, A. M. J., van der Veer, J. L., den Hartog, J. H. J., Lohman, P. H. M., and Reedijk, J. (1985) Biochemistry **24**, 707.

Fixman, M. (1979) J. Chem. Phys. **70**, 4995.

Fogolari, F., Esposito, G., Cauci, and Viglino, P. J. Magn. Reson., in press.

Friedman, R. A. G., and Manning, G. S., (1984) Biopol. **23**, 2671.

Fuoss, R. M., Katchalsky, A., and Lifson, S. (1951) Proc. Natl. Acad. Sci. USA **37**, 579.

Garbow, J. R., Weitekamp, D. P., and Pines, A., (1982) Chem. Phys. Lett. **93**, 504.

Garzon, F. T., Berger, M. R., Keppler, B. K., Schmahl, D. (1987) Cancer Chemother. Pharmacol. **19**, 347.

Gasteiger, J., and Marsili, M. (1980) Tetrahedron **36**, 3219.

Girault, J. P., Chottard, G., Lallemand, J. Y., and Chottard J. C. (1982) Biochemistry **21**, 1352.

Griesinger, C., and Ernst, R. R., (1988) Chem. Phys Lett. **152**, 239.

Griesinger, C., Otting, G., and Wüthrich, K., and Ernst, R. R., (1988) J. Am. Chem. Soc. **110**, 7870.

Gueron, M., and Weisbuch, G. (1980) Biopol. **19**, 353.

Haasnot, C. A. G., de Leeuw, F. A. A. M., and Altona, C. (1980) Tetrahedron **36**, 2783.

Haeberlen, U., and Waugh, J. S. (1968) Phys. Rev. **175**, 2.

Henn, M., Alessio, E., Mestroni, G., Calligaris, M., and Attia, W.M. (1991) Inorg. Chim. Acta, **187**, 39.

Hikura, M., and Hikichi, K. (1987) Org. Magn. Reson. **20**, 266.

Hyberts, S. G., and Wagner, G. (1989) J. Magn. Reson. **81**, 418.

IUPAC-IUB Commission on Biochemical Nomenclature (1970) Eur. J. Biochem. **17**, 193.

Iwasa, K., (1977) J. Phys. Chem. **91**, 1829.

Jeener, J., Meier, B. H., Bachmann, P. and Ernst, R. R. (1979) J. Chem. Phys. **71**, 4546.

Johnson, N. P., Butour, J.-L., Villani G., Wimmer, F. L., Defais, M., Pierson, V., and Brabec, V. (1989) Prog. Clin. Biochem. Med. **10**, 1.

Karplus, M. (1959) J. Chem. Phys. **30**, 11.

Katchalsky, A., (1971) Pure Appl. Chem. **26**, 327.

Kay, L. E., Holak, T. A., Johnson, B. A., Armitage, L. M., and Prestegard, J. H. (1986a) J. Am. Chem. Soc. **108**, 4242.

Kay, L. E., Scarsdale, J. N., Hare, D. R., and Prestegard, J. H. (1986b) J. Magn. Reson. **68**, 515.

Keepers, J. W., and James, T. L. (1984) J. Magn. Reson. **57**, 404.

Kirkpatrick, S., Gelatt, C. D. Jr, and Vecchi, M. P. (1983) Science **220**, 671.

Kövér, K., and Batta, G. (1987) J. Magn. Reson. **74**, 397 (1987)

Kreyszig E. (1972) Advanced Engeneering Mathematics, John Wiley and Sons, New York.

Kumar, A., Wagner, G., Ernst, R. R., and Wütrich, K. (1981) J. Am. Chem. Soc. **103**, 3654.

Lankorst, P. P., Haasnot, C. A. G., Erkelens, C. and Altona, C. (1984) J. Biomol. Struct. Dyn. **1**, 1387.

Lippard, S. J. (1987) Pure Appl. Chem. **59**, 731.

Loehrer, P. J., and Einhorn, L. H. (1984) Ann. Intern. Med. **100**, 704.

Mc Ghee, J. D., and Von Hippel, P. H., (1974) J. Mol. Biol. **86**, 469.

Macura, S., Farmer, B. T.,and Brown, L. R., (1986) J. Magn. Reson. 70, 493.

Macura, S., Huang, Y., Suter, D., Ernst, R. R. (1981) J. Magn. Reson. **43**, 259.

Manning, G. S., (1969) J. Chem. Phys. **51**, 924.

Manning, G. S., (1977) Biophys. Chem. **7**, 95.

Manning, G. S., (1978) Q. Rev. Biophys. **11**, 179.

Manning, G. S., (1984) J. Chem. Phys. **88**, 6654.

Manzini, G., Xodo, L. E., Fogolari, F., and Quadrifoglio, F., (1990) Biopol. **30**, 325.

Marion, D., and Bax, A. (1989) J. Magn. Reson. **83**, 205.

Marion, D., and Wüthrich, K. (1983) Biochem Biophys. Res. Commun. **113**, 967.

Mercer, A., and Trotter, J. (1975) J. Chem. Soc. Dalton, 2480-2483.

Mestroni, G., Alessio, E., Calligaris, M., Attia, W. M., Quadrifoglio, F., Cauci, S., Sava, G., Zorzet, S., Pacor, S., Monti-Bragadin, C., Tamaro, M., and Dolzani L. (1989) Prog. Clin. Biochem. Med. **10**, 71.

Miller, S. K., and Marzilli, L. G. (1985) Inorg. Chem. **24**, 2421.

Molinari, H., Esposito, G., Pegna, M., Consonni, R., and Zetta, L. (1992) J. Biomolec. NMR **2**, 289.

Morris, G. A., and Freeman, R. (1978) J. Magn. Reson. **29**, 433.

Morris G. A., and Freeman, R. (1979) J. Am. Chem. Soc. **101**, 760.

Muhandiram, D. R., and McClung, R. E. D. (1988) J. Magn. Reson. **80**, 539.

Muggia, F. M. (1991) Semin. Oncol. **18**, 1.

Mukundan, S. Jr., Xu, Y., Zon, G., and Marzilli, L. (1991) J. Am. Chem. Soc. **113**, 3021.

Müller, L. and Ernst, R. R. (1979) Mol. Phys. **38**, 963.

Neuhaus, D., Wagner, G., Vasak, M., Kagi, J. H. R., and Wüthrich, K. (1985) Eur. J. Biochem. **151**, 257.

Neuhaus D., and M. P. Williamson, M. P. (1989) The Nuclear Overhauser Effect in Structural and Conformational Analysis, VCH publishers, New York.

Norwood, T. J., Boyd, J., Heritage, J. E., Soffe, N.,and Campbell, I. D. (1990) J. Magn. Reson.**87**, 488.

Orbell, J. D., Marzilli, L. G., and Kistenmaker, T. J. (1981) J. Am. Chem. Soc. **103**, 5126.

Otting, G., and Wüthrich, K. (1988) J. Magn. Reson. **76**, 569.

Pacor, S., Sava, G., Ceschia, V., Bregant, F., Mestroni, G., and Alessio, E. (1991) Chem.-Biol. Interact. **78**, 223.

Paulsen, M. D., Anderson, C. F., and Record, T. M. Jr., (1988) Biopol. **27**, 1249.

Piantini, U., Sorensen, O. W., and Ernst, R. R. (1982) J. Am. Chem. Soc. **104**, 6800.

Press, W. H., Flannery, B. P., Teukolsky, S. A. and Vetterling, W. T. (1990) Numerical Recipes in C, Cambridge University Press, New York.

Ramanathan, G. V., and Woodbury, C. P. Jr. (1982) J. Chem. Phys. **77**, 4133.

Rance, M. (1987) J. Magn. Reson. **74**, 557.

Record, M. T., Anderson, C. F., and Lohman, T. M. (1978) Q. Rev. Biophys. **11**, 103.

Reedijk, J. (1987) Pure Appl. Chem. **59**, 181.

Reisenhofer, E., Cesàro, A., Delben, F., Manzini, G., and Paoletti, S., (1984) Bioelectrochem. Bioenerg. **12**, 455.

Remin, M., and Shugar, D. (1972) Biochim. Biophys. Res. Commun. **48**, 636.

Riedl, C., Qian, C., Savitsky, G. B., Spencer, H. G., and Moss, W. F., (1989) Macromolecules **22**, 3983.

Rinkel, L. J., and Altona, C. (1987) J. Biomol. Struct. Dyn. **4**, 621.

Ruggiero, J., Manzini, G., and Quadrifoglio, F. (1987) Biopol. **26**, 1975.

Saenger, W., (1984) in Principles of Nucleic Acid Structure, chps. 2 and 4, Springer-Verlag, New York.

Satoh, M., Kawashima, T., and Komijama, J., (1988) Biophys. Chem. **31**, 209.

Sava, G., Pacor, S., Zorzet, S., Alessio, E., Mestroni, G. (1989) Pharmacol. Res. **21**, 617.

Seddon, E. A., and Seddon, K. R. (1984) in The chemistry of Ruthenium, Elsevier, Amsterdam.

Shaka, A. J., Barker, P. B., and Freeman, R. (1985) J. Magn. Reson. **64**, 547.

Shaka, A. J., Keeler, J. and Freeman, R. (1983) J. Magn. Reson. **53**, 313.

Sharp, K. A., and Honig, B. (1990) J. Phys. Chem. **94**, 7984.

Sherman, S. E., Gibson, D., Wang, A. H.-J., Lippard, S. J. (1985) Science **230**, 412.

Sherman, S. E., and Lippard, S. J. (1987) Chem. Rev. **87**, 1153.

Shon, K., and Opella, S. J. (1989) J. Magn. Reson. **82**, 193.

Solomon, I. (1955), Phys. Rev. **99**, 559.

Tate, S., Masui, Y., and Inagaki, F., (1991) J. Magn. Reson. **94**, 394.

Twelves, C. J., Ash, C. M., Miles, D. W., Thomas, D. G. T., Souhami, R. L. (1991) Cancer Chemother. Pharmacol. **27**, 481.

Visalakshi, G. V., and Chandrakumar, N. (1987) J. Magn. Reson. **75**, 1.

Wagner, G.,(1990) Progr. NMR Spectr. **22**, 101.

Wagner, G., Brühwiler, D., and Wüthrich, K. (1987) J. Mol. Biol. **196**, 227.

Wagner, G., and Wüthrich, K. (1982) J. Mol. Biol. **155**, 347.

Weiner, J. S., Kollman, P. A., Case, D. A., Singh, U. C., Ghio, C., Alagona, G., Profeta, S., and Weiner, W. (1984) J. Am. Chem. Soc. **106**, 765.

Weiss, G., Green, S., Alberts, D. S., Thigpen, J. T., Hines, H. E., Hanson, K., Pierce, H. I., Baker, L. H., Goodwin, J. W. (1991) Eur. J. Cancer **27**, 135.

Wüthrich, K., (1986) NMR of Proteins and Nucleic Acids, Wiley-Interscience, New York.

Acknowledgemnts

I wish to thank here, in the first place, my family for invaluable support before and during all the time the work presented in this thesis has been done, Paola for sharing hopes, disillusions, successes, ups and downs during all this time and for constant confrontation, which built up a large part of my own way to understand my job. I have to thank as well all the people (students, pre–docs, post–docs, professors, admnistrative and technical personnell) I have met in the institutions I worked in. It would be really too long to mention all of them, so I want just to remember here the pleasant time I had in Trieste (Biophysics, Biochemistry and Macromolecular Chemistry at University and Biophysics Sector at S.I.S.S.A.), in Nijmegen (in the Department of Biophysical Chemistry), in Udine (Biomedical Science and Technology Department at University) and in Heidelberg (Structures and Biocomputing). I wish to thank the persons I worked closer with in these years, and whose methods, views and opinions have contributed to this work in many ways: prof. G. Manzini and prof. F. Quadrifoglio, who started me to the field of Biophysics and in particular to that of polyelectrolytes, Prof. C. W. Hilbers, who accepted me in his laboratory giving me the unique chance to learn 2D NMR in a very stimulating and active environment, Dr. F. Van de Ven, who taught me a lot about protein 2D NMR and current topics and methods of research in this field as well, Dr. G. Esposito whose knowledge and experience in 2D NMR is a continuing source of learning, Prof. P. Viglino, who started me to NMR, when I was still a student, for sharing his experience with me, Dr. S. Cattarinussi for useful discussions and helpful expertise in programming, Dr. A. Pastore for sharing with me her experience and understanding in the field of biomolecular modelling. I wish also to thank all the nice persons I had the luck to meet, in Italy and abroad, during this time, which made these four years really a good time.